In vivo investigation of deep cerebellar nuclei neurons plasticity and functional connection with the prefrontal cortex

Università degli Studi di Pavia

PhD School in Biomedical Sciences XXX Cycle

Coordinator: Prof. Egidio D'Angelo

Department of Brain and Behavioral Sciences

Doctoral Dissertation by Letizia Moscato

Supervisor: Prof. Egidio D'Angelo

Co-supervisor: Dr. Lisa Mapelli

Academic Year 2016-2017

Contents

1. Introduction

The cerebellum is a central nervous system structure traditionally considered involved in learning and storage of sensory-motor information. The cerebellum processes and integrates sensory inputs coming from different pathways, distributed along the spinal cord, the brain stem and other parts of the brain, thus fine-tuning the motor activity. Although its role in motor control has been assessed over the years, recent studies stand for a prominent involvement also in cognitive functions *(Gowen and Miall 2007; Kansal et al. 2017)*. The cerebellum is anatomically connected to both motor and cognitive areas of the brain, mainly through red nucleus and thalamus. Therefore, the cerebello-cerebral connection is reciprocal and feedback projections from the cerebral cortex reach the cerebellum through the pons *(Middleton and Strick 2001; 1997)*. Several experimental studies provide evidence of the interplay between associative brain regions and cerebellum *(Palesi et al. 2015; Watson et al. 2014; Watson et al. 2009)* and clinical reports link cerebellar abnormalities with different cognitive dysfunctions, such as the cerebellar cognitive affective syndrome (CCAS) reported in patients with cerebellar lesions *(Schmahmann and Sherman 1998)*. The anatomical connection between cerebellum and cortical areas involved in higher order processes has been well characterized in humans and nonhuman primates *(Middleton and Strick 2001)* but beside the general anatomical knowledge how this circuit functionally operates is still unknown. Damage of these circuits is involved in several brain pathologies, ranging from sensori-motor ataxia to autism spectrum disorders (ASD) and Alzheimer's disease (AD) *(D'Angelo and Casali 2012; Giza et al. 2010; Konarski et al. 2005)*. Moreover, it has been recently reported that the cerebellar output affects plasticity in some of its target regions, such as striatal and motor cortex, which are known to be the major nodes of the motor network, likely affecting motor performance and motor learning *(Caligiore et al. 2017; Kishore et al. 2014)*. From this perspective, impaired cerebellar synaptic plasticity might drive an altered interplay within and across the cerebello-cerebral network, eventually leading to cognitive dysfunctions. So, it would be interesting to understand the precise role of the cerebellum in these loops, which remains still a challenge for future investigations.

1.1 Cerebellar anatomy

The cerebellum lies in the posterior cranial fossa, below the occipital and temporal lobes, from which it is separated by the *tentorium cerebelli*. It is located dorsally to the pons to which it is connected through three peduncles: superior, middle and inferior (Fig.1.1). The superior cerebellar peduncle connects the cerebellum to the midbrain, and it contains manly efferent fibers directed to red nucleus (the cerebellorubral tract arises from the globose and emboliform nuclei and targets the contralateral red nucleus), thalamus (the cerebellothalamic tract arises from the dentate nucleus and targets the contralateral thalamus) and reticular formation (the fastigioreticular tract arises from the fastigial nucleus and targets the reticular formation of the midbrain, pons, and medulla oblongata); the afferent components include the anterior spinocerebellar and tectocerebellar tracts. The middle cerebellar peduncle connects the cerebellum to the pons, and it contains exclusively afferent fibers from the contralateral pontine nuclei; the inferior peduncle connects the cerebellum to the brain stem and spinal cord, it contains both afferent fibers (posterior spinocerebellar, cuneocerebellar, trigeminocerebellar tracts, olivocerebellar and vestibulocerebellar fibers) and efferent fibers from vestibulocerebellar Purkinje cells headed toward the vestibular nuclei *(Rand S. and Swenson 2006; Swenson et al. 1984)*.

The cerebellum is formed by two hemispheres separated by a median zone called *vermis*. It is composed by an outer layered mantle of gray substance called cerebellar cortex, which contains most of the cerebellar neurons, and an inner white matter in which the deep cerebellar nuclei are located. From medial to lateral, these nuclei are: the fastigial nucleus; globose and emboliform nuclei (in non-primate mammals, such as rodents, globose and emboliform nuclei are fused in a single nucleus called interposed nucleus) and the dentate nucleus (Fig. 1.2). The cerebellar cortex is connected to the deep nuclei by the Purkinje cells axons that represent the only output from the cerebellar cortex. The deep cerebellar nuclei represent the sole output of the cerebellum with the exception of the vestibulocerebellar Purkinje cells, which send projections directed to the vestibular nuclei located in the brain stem.

The cerebellum is organized in lobes: the anterior and posterior lobes are divided by the primary fissure; the posterolateral fissure separates the posterior and flocculonodular lobes. Functionally, the cerebellum may be divided in three subdivisions: the vestibulocerebellum (*archicerebellum*) includes the flocculonodular lobe and regulates balance and eye movements; the spinocerebellum (*paleocerebellum*) includes the vermis and paravermis-intermediate part of the hemispheres, as well as fastigial and interposed nuclei, and regulates body and limb movements; the neocerebellum (*pontocerebellum*) includes the lateral hemispheres and dentate nuclei and it is involved in planning movement and cognitive functions *(Rand S. and Swenson 2006)*.

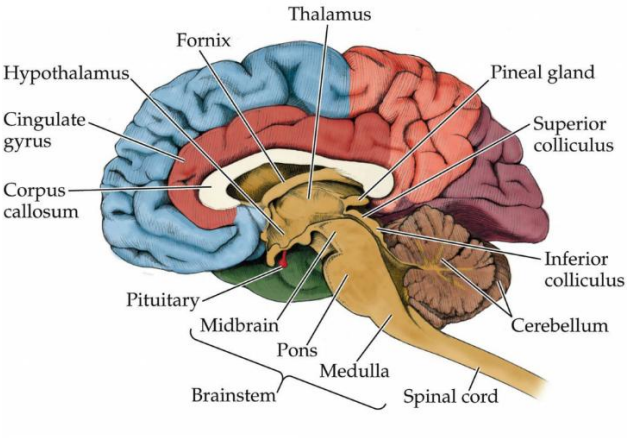

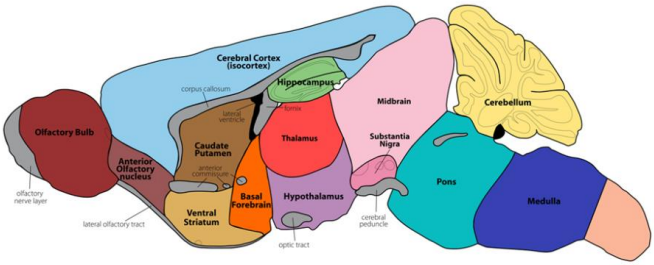

Figure 1.1| Cerebellar comparative anatomy. In the upper panel, a mediosagittal section of the human brain, including the cerebellum. In human, the cerebellum is located dorsally to the pons, below the occipital and temporal lobes and it is connected to the rest of the brain through the three cerebellar peduncles. The lower panel shows a rodent sagittal brain section. In rodents, the cerebellum is located behind the midbrain, on the dorsal surface of the pons to which is connected by the three cerebellar peduncles.

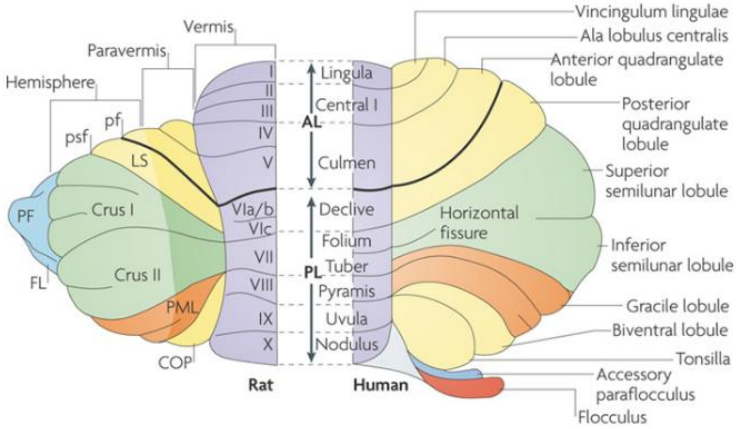

Figure 1.2| Comparative anatomy and nomenclature of the main cerebellar subdivisions. Simplified illustration of rat (on the left) and human (on the right) dorsal view of the cerebellum. Equivalent regions in rat and human cerebellum are indicated with the same color (Apps and Hawkes 2009). Anatomy and cytoarchitecture of the cerebellum are quite conserved between mouse and human. In rodents, the fastigial nucleus is located in the cerebellar vermis, the interposed nucleus (globose and emboliform nuclei in human) lies in the intermediate zone of the cerebellar hemisphere (paravermis) and the dentate nucleus is embedded in the lateral zone of the hemisphere. The cerebellar hemispheres are more extended laterally in humans, due to a greater length and number of folia and also the amount of corticopontocerebellar projections coming from higher brain areas is larger, whereas the parafloccular lobule is larger in rodents. Abbreviations: **Pf**, primary fissure; **AL**, anterior lobe; **COP**, copula pyramidis; **Crus I** and **Crus II**, ansiform lobule; **FL**, flocculus; **LS**, lobulus simplex; **PF**, paraflocculus; **PL**, posterior lobe; **PML**, paramedian lobule; **psf**, posterior superior fissure.

1.2 Cerebellar circuits

The cerebellum is formed by a mantle of superficial gray matter, the cerebellar cortex, containing several types of excitatory and inhibitory neurons, and an inner white substance in which the deep cerebellar nuclei are located (Fig. 1.3). The cerebellar cortex consists of three layers: the molecular layer is the outmost layer, it contains molecular layer interneurons (MLIs), such as stellate and basket cells (SCs and BCs, respectively), the dendritic trees of Golgi cells (GoCs) and Purkinje cells (PCs) and the ascending axons of the granule cells (GCs). GCs axons extend superficially into the molecular layer where they bifurcate in two branches, forming the parallel fibers (PFs) that make excitatory glutamatergic synaptic contacts with all the cells of the molecular layer. The Purkinje cells layer, underneath the molecular layer, contains mainly PCs. Their dendrites receive excitatory synaptic contacts from PFs whilst GABAergic inhibitory contacts from MLIs target the initial segment of their axon. Furthermore, each PC receives a single climbing fiber (CF), coming from the inferior olive (IO), that contacts the base of its dendritic arbor. The PCs axons represent the only output of the cerebellar cortex, they make inhibitory synapses with deep cerebellar nuclei (DCN) neurons and send recurrent collaterals to other PCs and MLIs *(Witter et al. 2016)*. The Granular layer is the innermost layer, containing mainly GCs and GoCs. Non-traditional large cells (NTc), such as unipolar brush cells (UBCs), Lugaro cells, synarmotic neurons, candelabrum neurons and the perivascular neurons have been also observed in the granular layer but their function is poorly explored *(Ambrosi et al. 2007)*. GCs receive glutamatergic excitatory inputs from MFs, arising from heterogeneous precerebellar pathways, and GABAergic inhibitory inputs from GoCs. The DCN are bilateral structures embedded into the white matter of the cerebellum. Except for the direct PCs vestibulocerebellar projections to the vestibular nuclei, the DCN neurons represent the sole output of the cerebellum. There are six types of neurons in the deep nuclei and their classification is mainly based on neurotransmitters phenotypes (glutamate, GABA and glycine), electrophysiological and morphological properties. There are four classes of projection neurons, such as glutamatergic, GABAergic and glycinergic extracerebellar projection neurons and two

classes of local GABAergic/glycinergic interneurons *(Uusisaari and Knöpfel 2012)*. Most of these neurons have been suggested to send projections back to the cerebellar cortex *(Houck and Person 2014)*. DCN neurons process and integrate excitatory synaptic inputs carried by MFs and CFs and inhibitory inputs from PCs, thus playing a crucial role in regulating the cerebellar output. Their projections, passing through red nucleus and thalamus, target premotor and associative brain areas. Since the cerebello-cerebral connection is reciprocal, feedback projections from the cerebral cortex reach the cerebellum through the pontine nuclei, forming a closed-loop network that control motor and cognitive functions.

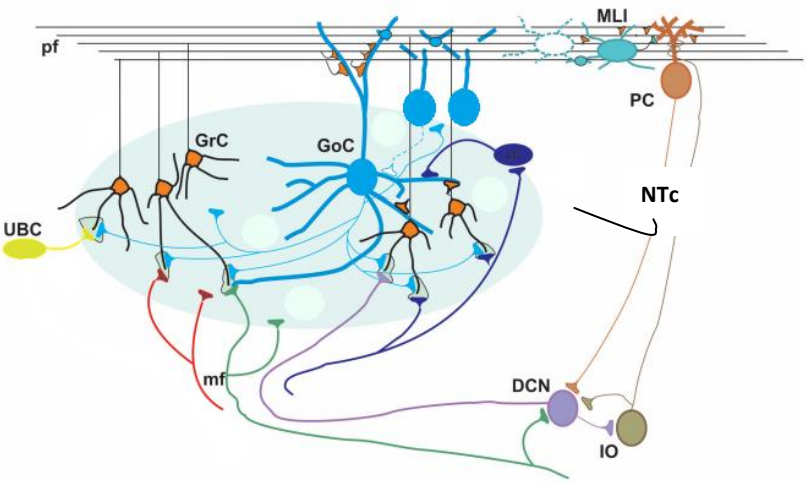

Figure 1.3| Schematic representation of the cerebellar circuit. The cerebellum receives two main afferents: MFs and CFs. MFs coming from precerebellar structures form synaptic contacts with GrCs and DCN neurons. CFs coming from the IO contact both DCN neurons and PCs. DCN neurons integrate excitatory synaptic inputs coming from MFs and CFs and inhibitory inputs coming from GrC-PC pathway regulating the cerebellar output. Abbreviations: **Pf**: parallel fiber; **MLI**: molecular layer interneuron; **PC**: Purkinje cell; **GrC**: granule cell; **GoC**: Golgi cell; **UBC**: unipolar brush cell; **NTc**: non-traditional cell; **mf**: mossy fiber; **DCN**: deep cerebellar nuclei; **IO**: inferior olive. *Figure modified from (D'Angelo et al. 2016b).*

1.3 Cerebellar connections with the prefrontal cortex

A considerable amount of studies provide evidence of the connection between the cerebellum and cerebral associative areas of the brain, such as the prefrontal cortex (PFC). Clinical reports also support this hypothesis linking cerebellar abnormalities with several cognitive dysfunctions. Recently, the integral tractographic reconstruction of the pathways passing through the superior cerebellar peduncle (SCP) provided a clearer picture of the nature of cerebello-cerebral communication in humans *(Palesi et al. 2015)*. It has been reported that the majority of the cerebellar projections passing through the SCP connect the cerebellum with contralateral cognitive areas, such as prefrontal and posterior parietal cortices. The cerebellar output reaches the prefrontal and parietal cortices through the posterior thalamic nuclei whilst the ventro-anterior (VA) and ventro-lateral (VL) nuclei of the thalamus relay cerebellar projections mainly to motor areas (Fig. 1.4). Surprisingly, the cerebellar connections with cerebral cortex areas involved in cognitive functions seem to be more extended than those involved in sensori-motor control (around 80% vs. 20%) *(Palesi et al. 2015)* (Fig. 1.5). *In vivo* electrophysiological experiments in rodents support this finding, providing evidence that cerebellar PCs exhibit prominent field potentials responses to the contralateral stimulation of medial prefrontal cortex (mPFC). Those responses were larger in the lobule VII of the contralateral vermis, a well-known cerebellar region involved in the control of eye movements, through projections arising from the fastigial nucleus *(Watson et al. 2009)* (Fig. 1.6). From this perspective, the logical assumption might be that the connection between cerebellum and higher order regions subserves the control of eye movements in goal-directed behaviour instead of cognitive information processing *per se (Watson et al. 2009)*. However**,** the consistent reports that link cerebellar abnormalities with different cognitive disorders, such as psychosis, depression, schizophrenia, autism and CCAS, strongly contradict this hypothesis *(Konarski et al. 2005; Pierce and Courchesne 2001; Schmahmann and Sherman 1998)*. Furthermore, the cerebello-cerebral communication is reciprocal and the stimulation of the DCN was proved able to elicit different response patterns in the mPFC neurons of rats *(Watson et al. 2014)* (Fig. 1.7 and Fig. 1.8). The heterogeneity of the response patterns

may be due to several factors, such as the different dopamine receptors expressed in PFC neurons and the different effect of the dopamine release on pyramidal cells and interneurons, which are also connected each other complicating the picture of the dopamine release impact onto PFC neurons *(Dembrow and Johnston 2014)* (Fig. 1.9). It has been reported that the stimulation of the dentate nucleus induced dopamine realise in the mPFC that might modulate cortical neurons responses *(Mittleman et al. 2008)*. The dopaminergic modulation is mediated by several types of dopamine receptors expressed in the mPFC neurons, belonging to the family of D1 and D2 receptors. D1 receptors comprise two receptors subtypes, D1 and D5, whilst D2 receptors are divided in D2, D3, D4 receptors subtypes *(Lidow et al. 2003; Rinaldi et al. 2007)*. Moreover, in rodents PFC the density of D1 receptors is higher than D2 *(Gaspar et al. 1995)* and their activation exerts a mixture of contrasting effects on pyramidal cells and local interneurons. The activation of D1 receptors has both excitatory and inhibitory effects on pyramidal cells, engaging NMDA and GABA-mediated synaptic responses whilst the recruitment of D2 receptors reduce the excitability of pyramidal neurons and their GABAergic transmission *(Floresco and Magyar 2006; Floresco et al. 2006)*. The pathways through which the cerebellum might affect the dopamine release have not been determined yet. The cerebello-cerebral communication might be mediated by glutamatergic projections via the thalamic nuclei *(Hoover and Vertes 2007)* that in turn induce dopamine release from the dopamine axon varicosities of PFC neurons *(Blaha et al. 1997)*. Alternatively, the release of dopamine might be induced via ventral tegmental area (VTA), through cerebello-VTA or cerebello-thalamo-VTA projections *(Kehr et al. 1976; Snider and Maiti 1976; Snider et al. 1976; Watson et al. 2014)*, via substantia nigra or basal ganglia *(Nieoullon et al. 1978)*.

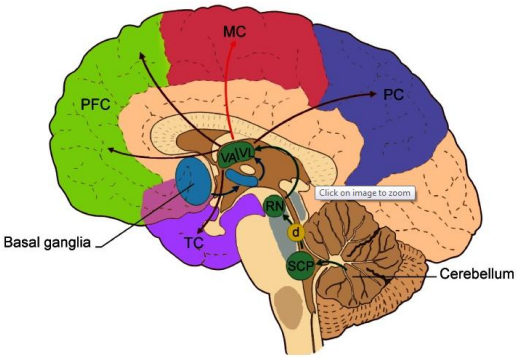

Figure 1.4| Cerebello-cortical pathways. The cerebellar projections passing through the PCS reach the contralateral motor cortex (MC), the prefrontal cortex (PFC), the parietal cortex (PC), and the temporal cortex (TC) via red nucleus (RN) and VA/VL of the thalamus. Basal ganglia project (through the subthalamic nucleus, STN) mainly to VA/VL. The decussation (d) of the cerebello-thalamo-cortical pathway is indicated by the *yellow circle (Palesi et al. 2015).*

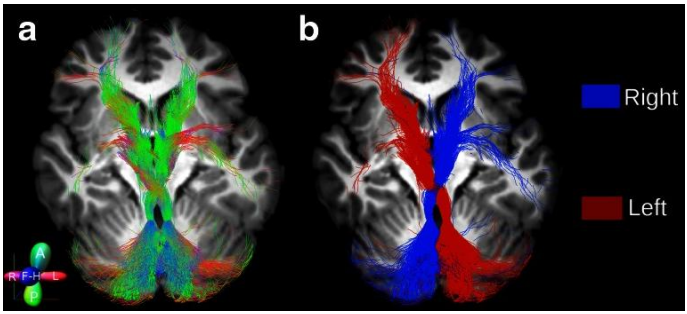

Figure 1.5| 2D rendering of cerebello-thalamo-cortical pathways of a representative subject. (**a)** The tracts are colour-coded by direction to represent their anatomy (**b)** A single solid colour has been used for each tract to distinguish the streamlines from the left (red) and right (blue) pathways *(Palesi et al. 2015).*

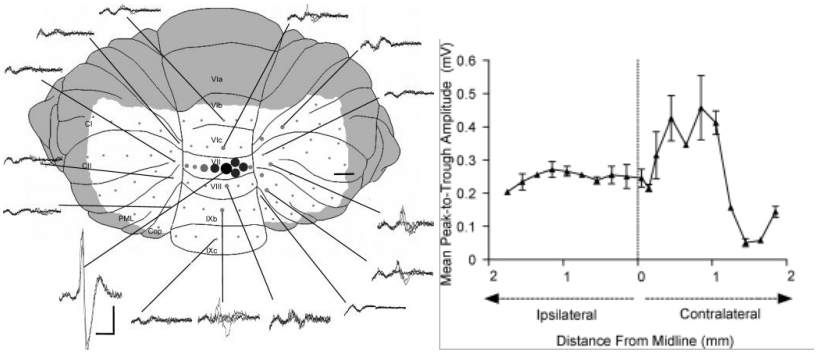

Figure 1.6| Prefrontal cortex projections to the contralateral cerebellar cortex of rat. On the right, a schematic representation of the dorsal view of the cerebellum reporting the distribution of local field potential (LFP) responses evoked by the stimulation of the prelimbic subdivision (PrL) of the mPFC. The amplitude of the LFP responses are approximately represented by example waveforms recorded within each cerebellar region and the size of circles. On the left, it is shown the field potential amplitude change as a function of the medio-lateral position along the vermal lobule VII. Data points are reported as mean of four responses ± SEM *(Watson et al. 2009).*

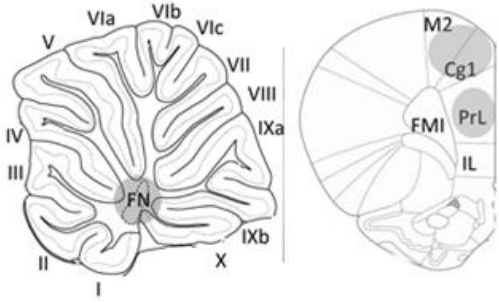

Figure 1.7| Schematic representation of the location of the sites involved in the FN-mPFC communication. On the right, a sagittal brain slide showing the position of the fastigial nucleus (FN). On the left, a transverse brain slide reporting the subdivisions of the mPFC showing prominet responses to the electrical stimulation of the FN. Abbreviations: **M2**, supplementary cortex; **Cg1**, cingulate

cortex; **IL**, infralimbic cortex; **FMI**, forceps minor of the corpus callosum *(Watson et al. 2014).*

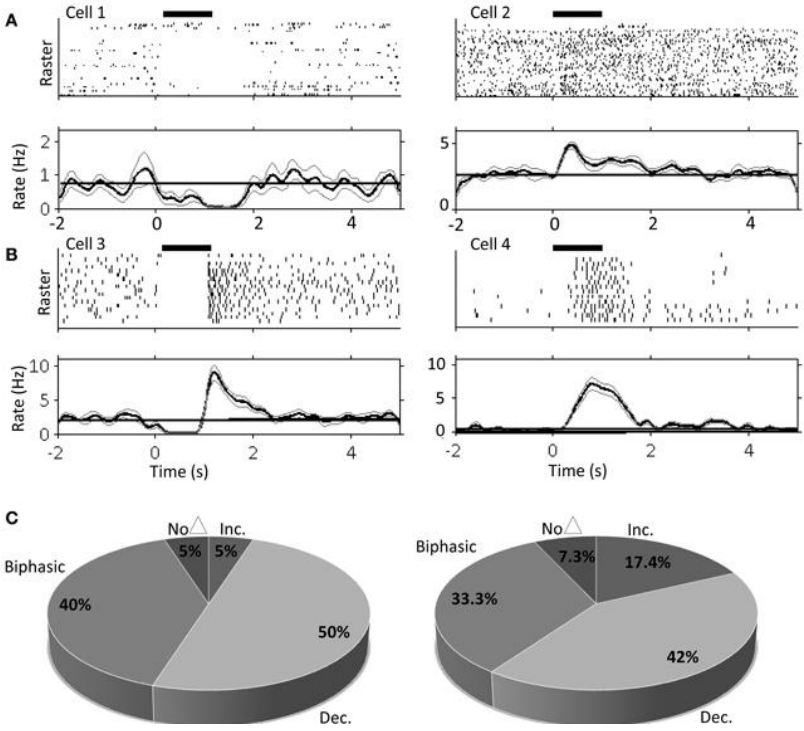

Figure 1.8| PrL neurons response patterns to the electrical stimulation of the contralateral FN. Raster plots and peri-stimulus time histograms of typical responsive neurons in the PrL of awake **(A)** and urethane-anesthetized rat **(B)**. High frequency FN stimulation (100 Hz, 100 stimuli, 1s duration, 100 µA) evokes 3 typical response patterns in both awake and anesthetized animals: decrease of firing rate compared to baseline activity (**cell 1** in Figure A); increase of spike discharge (**cell 2** in Figure A; **cell 4** in Figure B); biphasic response consisting in a decrease of firing rate followed by a rebound increase (**cell 3** in Figure B). In **(C)** are reported the response patterns percentages following FN stimulation in awake (n=20) and anesthetized (n=69) rats *(Watson et al. 2014).*

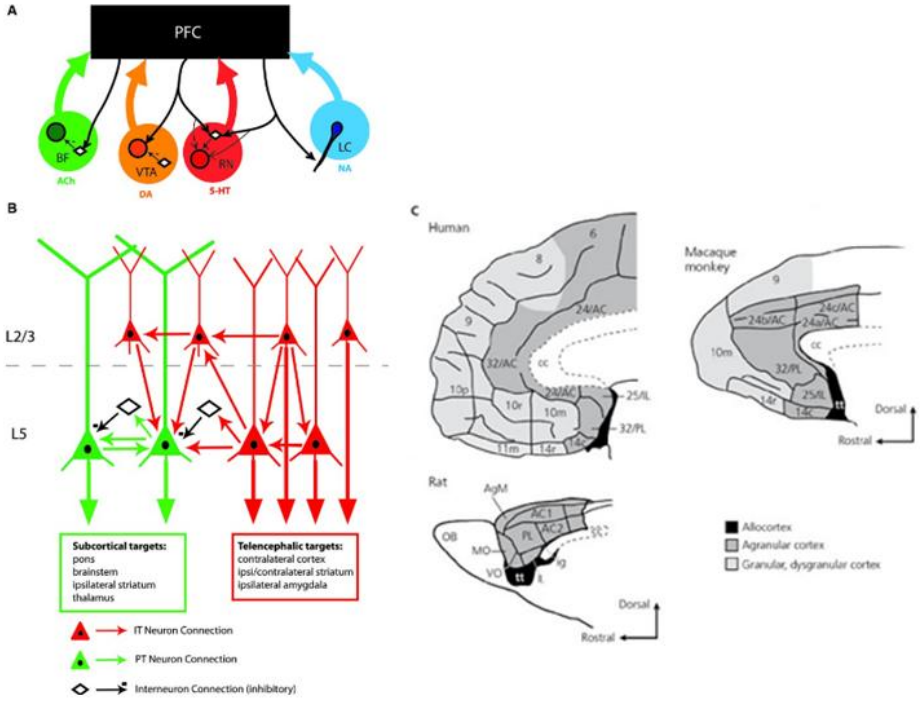

Figure 1.9| Schematic representation of anatomy and network connectivity within and across the rodent mPFC. (A) Schematic representation of ascending and discending projections to and from the PFC. Noradrenaline (NA) is realized from the locus coeruleus (LC) terminals; Acetylcholine (ACh) from the basal forebrain (BF); Serotonin (5-HT) from the medial and dorsal raphe nuclei (RN); Dopamine (DA) from the ventral tegmental area (VTA) and substantia nigra (SN). PFC neurons project to the neuromodulatory centers, contacting back the neuromodulator-synthesizing projection neurons (shaded circles), inhibitory interneurons (open diamonds), or both. In the case of locus coeruleus, PFC inputs contact the noradrenergic neurons dendrites. **(B)** Schematic representation of the connections within the mPFC. The pyramidal tract (PT, green) neurons are located in the layers 5/6 (L5/6); intratelencephalic (IT, red) neurons throughout L2-6. PT neurons receive input from other PT neurons, IT and inhibitory interneurons. IT neurons receive inputs only from other IT neurons *(Dembrow and Johnston 2014)*.

(C) Homologies among prefrontal areas: medial view of human, macaque monkey and rats PFC. In human, the PFC is located in the rostral part of the frontal lobe and as well as in non-human primate and rodents. The cytoarchitecture of human and primate PFC is relatively similar to rodents PCF, except for the presence of the granular layer IV. Indeed, in rodents the PFC is agranular and it contains two different classes of neurons: pyramidal neurons which project subcortically to ipsilateral striatum, thalamus and/or brainstem and interneurons which project mainly within the cortex *(Dembrow and Johnston 2014; Murray et al. 2017)*. Abbreviations: **AC**, anterior cingulate cortex; **AgM**, medial agranular motor area; **AON**, anterior olfactory nucleus; **cc**, corpus callosum; **G**, gustatory cortex; **Ia**, agranular insula cortex; **ig**, induseum griseum; **IL**, infralimbic cortex; **LO**, lateral orbitofrontal cortex; **MO**, medial orbitofrontal cortex; **OB**, olfactory bulb; **Pir**, piriform cortex; **PL**, prelimbic cortex; **tt**, tenia tecta; **VO**, ventral obitofrontal cortex; **c**, caudal; **i**, inferior; **l**, lateral; **m**, medial; **o**, orbital; **p**, posterios (as in Iapl) or polar (as in 10p); **r**, rostral; **v**, ventral *(Murray et al. 2017)*.

1.4 Cerebellar receptive field

The cerebellum can be portioned longitudinally into three parts: two lateral hemispheres separated by a median zone called vermis. Each part is folded into lobules, in turn subdivided into folia. It is composed by an outer layered mantle of gray substance called cerebellar cortex, which contains most of the cerebellar neurons and an inner white matter in which are located the DCN. Two major afferents convey information to the cerebellar cortex: CFs and MFs. CFs send direct projections to PCs whilst MFs contact indirectly PCs via GrC-PF and MLI. It has been suggested that the cerebellum can be divided in transverse zones, which are cerebellar cortex regions indentified by gene expression patterns *(Apps and Hawkes 2009)*. These transverse zones are: the anterior zone (lobules I-V, in mouse); the central zone (lobules VI and VII); the posterior zone (lobules VIII-IX) and the nodular zone (ventral lobule IX and lobule X). Each transverse zone can be further divided into stripes, identified by the expression of specific molecular markers. The molecular marker most extensively studied is zebrin II, expressed by a subset of PCs also known as zebrin II+. Conversely, PCs that do not express this marker are identified as zebrin II-, thus forming zebrin II+/- stripes which are differently distributed within the

transverse zones *(Apps and Hawkes 2009)* (Fig. 1.10). During the embryological development, PCs are the first neurons of the cerebellar cortex to be formed and their cellular identity is initially independent from other cerebellar neurons *(Apps and Hawkes 2009; Larouche et al. 2006)*. The PCs stripe patterns are also defined early in the development but the topographic organization of their afferents is secondary to the PCs formation. It has been suggested that PCs provide a template around which afferent topography is built. Indeed, it would seem that early in the development, during the period in which most of the GrCs are not formed yet, MFs terminals transiently contact embryonic cluster of PCs before establish mature connections with GrCs *(Apps and Hawkes 2009; Grishkat and Eisenman 1995; Mason and Gregory 1984; Takeda and Maekawa 1989)*. Moreover, several longitudinal zones that run perpendicularly to the axis of the lobules have been also identified in the cerebellar cortex, based on their topographically organized CFs inputs and PCs output *(Apps and Hawkes 2009)*. CFs originating from a specific subnucleus of the inferior olive target selectively one or two zones, whilst MFs arising from a specific area form several branches that terminate in multiple longitudinal zones (Fig. 1.11). The electrophysiological mapping of PCs and GrCs responses to sensory tactile stimulation of different parts of the body provided a clearer picture of the topographic organization of the cerebellar afferents. The cerebellar cortex seems to display a somatotopic organization of its afferents. It shows a “fractured somatotopy", evident primarily in the granular layer, in which receptive fields, responding to the stimulation of a specific body area, are represented several times, in non-contiguous patches of the cerebellar cortex *(Apps and Hawkes 2009)* (Fig. 1.12). Therefore, a single stimulus location is able to activate multiple patches distributed along both granular and Purkinje cells layers *(Bower and Woolston 1983)*. Conversely, DCN neurons show extended bilateral receptive fields and constant response patterns following the tactile stimulation of the body surface *(Rowland and Jaeger 2005)*. All the DCN present a similar somatotopic representation of the body areas, encompassing ipsilateral and contralateral facial regions and forepaws (Fig. 1.13).

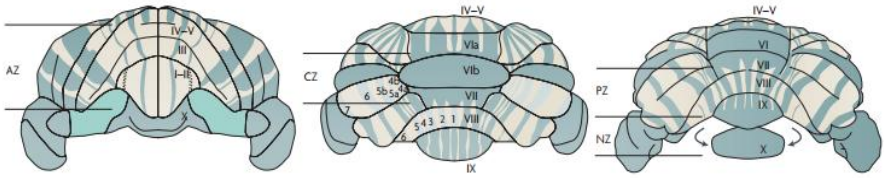

Figure 1.10| Anterior, dorsal and posterior views of transverse zones and stripes. The distribution of zebrin II+ PCs (green in the figure) reveals the presence of transverse zones. Each transverse zone can be further subdivided in stripes running along the rostrocaudal axis and defined by the expression of zebrin II molecular marker. Zebrin II- stripes are beige in the figure. Abbreviations: **AZ**, anterior zone; **CZ**, central zone; **PZ**, posterior zone; **NZ**, nodular zone *(Apps and Hawkes 2009).*

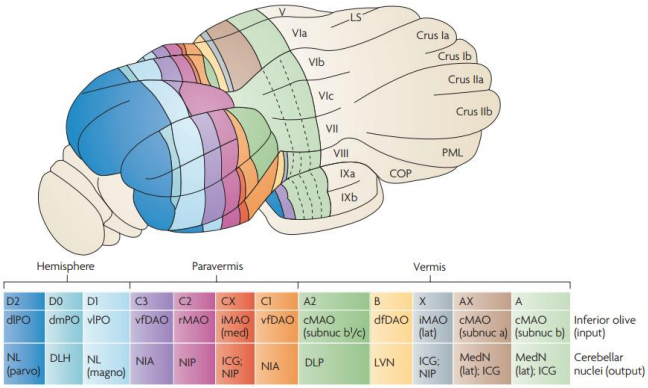

Figure 1.11| Dorso-posterior view of the rat cerebellum reporting the distribution of the longitudinal zones. Longitudinal zones have been identified in the cereberellar cortex, based on the topographically organized CFs inputs and PCs output. In the simplified diagram below are reported the sites of origin of CFs inputs direct toward the longitudinal zone of the cerebellar cortex and the PCs output to ipsilateral DCN and vestibular nuclei. Matching colours link the origin of the CFs inputs in the contralateral IO (reported in the simplified block diagram below) to their cerebellar cortex projection zones (showed in the illustration above). From the medial to the lateral plane are shown: the A, AX, X, B and A2 zones (in the vermis), the C1, CX, C2 and C3 zones (in the paravermis), and the D1, D0 and D2 zones (in the hemisphere). Abbreviations: **cMAO (subnuc a)**,

subnucleus a of caudal medial accessory olive; **cMAO (subnuc b)**, subnucleus b of caudal medial accessory olive; **cMAO** (**subnuc b1/c)**, subnucleus b1 and c of caudal medial accessory olive; **COP**, copula pyramidis; **dfDAO**, dorsal fold of dorsal accessory olive; **DLH**, dorsolateral hump; **DLP**, dorsolateral protuberance of medial nucleus; **dlPO**, dorsal lamella of the principal olive; **dmPO**, dorsomedial subnucleus of the principal olive; **ICG**, interstitial cell group; **iMAO** (lat), lateral part of intermediate medial accessory olive; **iMAO** (med), medial part of intermediate medial accessory olive; **LVN**, lateral vestibular nucleus; **LS**, lobulus simplex; **MedN** (lat), lateral part of medial nucleus; **MedN** (med), medial part of medial nucleus; **NIA**, nucleus interpositus anterior; **NIP**, nucleus interpositus posterior; **NL (magno)**, magnocellular part of lateral nucleus. **NL (parvo)**, parvocellular part of lateral nucleus; **PM**L, paramedian lobule; **rMAO**, rostral medial accessory olive; **vfDAO**, ventral fold of dorsal accessory olive; **vlPO**, ventral lamella of the principal olive *(Apps and Hawkes 2009).*

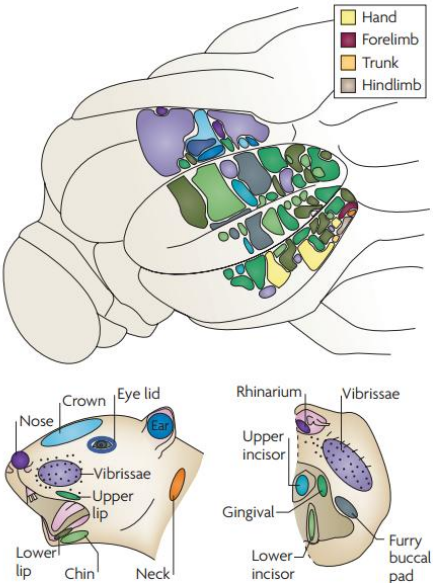

Figure 1.12| Spatial distribution of receptive fields in the granular layer of the rat cerebellum. The granular layer shows a "fractured somatotopy" in which the same part of the body is represented several times, in discontinuous patches along the layer. The image below shows the somatotopic representation of the body regions in the cerebellar granular layer. The colours of the body regions subjected

to tactile stimulation match with the colours of the corresponding cerebellar areas activated by the stimulation *(Apps and Hawkes 2009).*

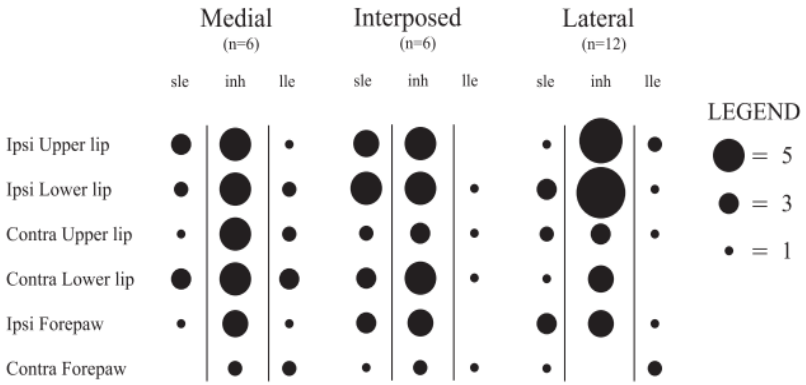

Figure 1.13| Distribution of the DCN neurons response patterns following the stimulation of different part of the body. The amount of neurons showing a particular response pattern following the stimulation of a given body area is represented by a proportioned size dot *(Rowland and Jaeger 2005).*

1.5 Sensory tactile input transmission from the mouse peri-oral region

The cerebellum is strategically located among sensory and motor pathways and it is notoriously involved in processing and integration of sensory motor information *(Bosman et al. 2010)*. Sensory tactile inputs from the mouse peri-oral region reach the cerebellum through several pathways: trigeminal nuclei, inferior olive and thalamo-cortical-pontine loop *(Bosman et al. 2010)* (Fig. 1.14). The afferent pathways to the cerebellum, MFs and CFs, contact both cortical and nuclear cerebellar neurons. The trigeminal MFs provide their amount of excitation to both GrCs in the cerebellar cortex and DCN neurons in the cerebellar white matter whilst olivary CFs terminate on both cerebellar PCs and DCN neurons. MF-GrC and CF pathways converging on PCs produce two different effects: the latter triggers complex spikes while PFs modulate their simple spike firing *(Bosman et al. 2010)*. The PCs represent the efference of the cerebellar

cortex, they project to the downstream nuclear neurons shaping their output, together with MFs and CFs. DCN neurons show typical response patterns following the sensory tactile stimulation of the orofacial region, reflecting the different combination of excitatory and inhibitory synaptic inputs they receive. The sensory-evoked responses combine three principal components: short-latency excitation, inhibition and long-latency rebound excitation *(Rowland and Jaeger 2005; 2008)*. The inhibitory component is likely elicited by the sensory stimuli-activated GrC-PC pathway. The short-latency excitation pattern probably reflect the activation of the trigeminal pathway whilst the long-latency rebound excitation following the inhibition likely emerges from the disinhibition of nuclear neurons discharge caused by a pause in Purkinje cells activity, which is reported to determine a rebound increase in DCN neurons firing *(Dykstra et al. 2016).*

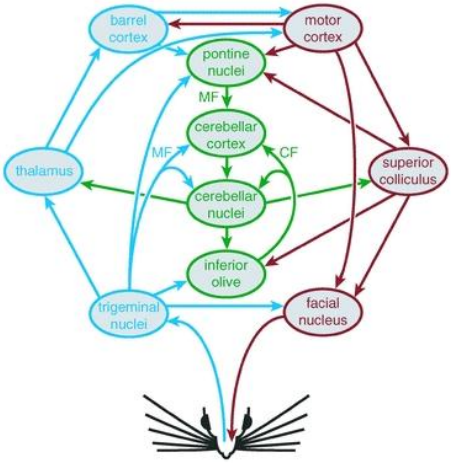

Figure 1.14| Pathways involved in the transmission of the sensory inputs from the mouse peri-oral region. Cerebellar neurons display typical response patterns resulting from the sensory activation of synaptic pathways converging on these neurons *(Bosman et al. 2010).*

1.6 Plasticity in the cerebellar network

Synaptic plasticity is the ability of neurons to modify the strength of their synaptic transmission in an activity-dependent manner. It is generally assumed that long-term modifications in the strength of the synaptic transmission, in form of potentiation (LTP) or depression (LTD), and neuronal intrinsic excitability provide the biological basis for learning in the neuronal circuits. Therefore, the main issue addressed by investigations on synaptic plasticity concerned which particular type of plasticity underlies the mechanism of learning. The LTD at the PF-PC synapse, under the control of CFs teaching signal, was initially suggested to provide the principal mechanism for cerebellar motor learning *(**Albus** 1971b; Marr 1969)*. However, it is unlikely that only one form of plasticity comes into play in a complex mechanism such as learning. Indeed, recent evidences have shown that many forms of synaptic and intrinsic plasticity at different sites are induced conjunctively during procedural memory formation in the cerebellum and the picture that emerges goes much beyond the classic concept that cerebellar-dependent learning is controlled solely by depression at the PF-PC synapse *(D'Angelo et al. 2016b)*.

Several forms of synaptic and non-synaptic plasticity have been described in the cerebellar cortex *in vitro* and *in vivo (Antonietti et al. 2016a; D'Angelo 2014; Gao et al. 2012; Hansel et al. 2001a; Mapelli et al. 2015a)*. However, multiple forms of plasticity distributed along the cerebellar cortex are still insufficient to explain the cerebellar motor learning which likely emerges from a more complex picture that includes various forms of plasticity not confined to the cerebellar cortex *(D'Angelo et al. 2016b)*. Indeed, consistently with experimental data, computational models embedding plasticity sites at the cerebellar nuclear level, showed faster and more stable learning capabilities compared to previous models with only cortical plasticity sites, providing a more realistic reproduction of human-like behavior during cerebellar learning of associative task *(Antonietti et al. 2016a)* and shedding light on the role of DCN plasticity previously poorly considered.

DCN receive excitatory input from MFs and CFs collaterals and inhibitory input from PCs. This strategic location allows DCN to process and

integrate excitatory and inhibitory synaptic inputs coming from different pathways, regulating the cerebellar output. Long-term modifications in the synaptic strength (both LTP and LTD) have been described in the inhibitory synapses between PCs and DCN neurons and in the excitatory synapses between MFs and DCN, in cerebellar slices *(Medina and Mauk 1999; Morishita and Sastry 1996; Ouardouz and Sastry 2000; Pugh and Raman 2009; Zhang and Linden 2006)*. Moreover, persistent changes of the intrinsic excitability have been also reported in nuclear neurons *(Zhang et al. 2004)*. During cerebellar learning of an associative task, as eyelid conditioning, the MFs convey the conditioned stimulus (CS, like a tone), while the unconditioned stimulus (US, like air puff or periorbital electrical stimulation) is carried by the CFs. In the cerebellar cortex, PCs simple spike firing increases as a consequence of MFs activation while they respond to the CFs activation with unaffected or facilitated complex spikes *(Rasmussen et al. 2008)*. When the conditioned and unconditioned stimuli are paired and repeated, the PCs respond with a brief pause in simple spike firing, consequent to the stimulus-evoked complex spike, which is known to determine a post-inhibitory rebound increase in the cerebellar nuclei firing that elicits an eye blink *(Jirenhed et al. 2007)*. Furthermore, it has been reported that conditioned responses persist after cerebellar cortex lesion, suggesting that DCN might have a role in the consolidation of learned movements *(Ohyama et al. 2003)*.

1.6.1 Theta patterned stimulation-induced plasticity

The theta-burst stimulation (TBS; 10 x 100 Hz bursts at 4 Hz) of MF projections to the cerebellar cortex has been proved able to induce long-term plasticity in cerebellar cortex neurons *in vitro (Armano et al. 2000; Gall et al. 2005; Mapelli and D'Angelo 2007)*. The same pattern of activity elicited in MFs through the TBS has been mimicked also in *in vivo* experiments. Sensory tactile stimuli organized in theta patterns (theta-sensory stimulation, TSS) are able to induce long-term changes in cerebellar cortex neurons *in vivo*. In *in vivo* urethane anesthetized rodents, the TSS evoked long-term plastic changes in the granular layer (LTD) *(Roggeri et al. 2008)*, Purkinje cells layer (LTP) and molecular layer

interneurons (LTD) *(Ramakrishnan et al. 2016; Roggeri et al. 2008)*. However, whether and how DCN are able to modify their discharges properties in response to patterned sensory stimulation, as the TSS, has not been studied yet. DCN neurons are known to respond to sensory stimulation through typical discharge patterns which reflect the different combinations of inhibitory and excitatory inputs converging onto these nuclei, provided by PCs and MFs respectively *(Rowland and Jaeger 2005; 2008)*. Despite plasticity in cerebellar nuclear neurons has been extensively studied *in vitro (Morishita and Sastry 1996; Ouardouz and Sastry 2000; Pugh and Raman 2008; 2009; 2006; Zhang and Linden 2006; Zheng and Raman 2010)* to date, whether and how DCN develop plasticity in response to patterned natural stimulation *in vivo* remains unexplored.

2. Materials and methods

Experiments were performed on 30-40 days old C57BL/6 mice. Mice were located in cages in which water and food were available *ad libitum*. The day-night cycle was 12 hours (12 hours light from 06.00 am - 06.00 pm, 12 hours dark from 06.00 pm - 06.00 am). All animals were head-fixed and deeply anesthetized during electrophysiological recordings.

2.1. Animal preparation

Single-units were recorded from the FN or PrL of mPFC in two independent set of experiments, requiring similar surgical procedures. In both experimental sets, C57BL/6 mice were deeply anesthetized with intraperitoneal injections of urethane (Sigma). Induction (1.3g/kg urethane dissolved in 0.9% NaCl) was followed by a booster injection (10% of the induction dose) 30 minutes later. 3-4 booster injections every 30 minutes were administered in order to stabilize deep anesthesia. The level of anesthesia was constantly monitored by evaluating the intensity of leg withdrawal after pinching and spontaneous whisking. The animal was placed on a stereotaxic table covered with a heating plate (HP-1M: RTD/157, Physitemp Instruments Inc, Clifton, NJ, USA) and the body temperature was monitored with a rectal probe and maintained at 36°C through a feedback temperature controller (TCAT-2LV controller, Physitemp Instruments Inc, Clifton, NJ, USA). The mouse head was fixed to a metal bar of the custom-built stereotaxis table through a pedestal implanted over the bregma. Cutaneous reflex were reduced by subcutaneous application of lidocaine (0.2ml; Astrazeneca), the skin and muscles were removed and a subsequent craniotomy was performed over the cerebellum and/or mPFC to expose the surface to the electrodes placement (FN stereotaxic coordinates: -7.8 AP, +0.50 ML, +2.4 DV; DN: -7.8 AP, +2.5 ML, +2.6 DV; PrL: +2.8 AP, 0.25 ML, +0.6 DV).

2.2 Electrophysiological extracellular recordings

Extracellular microelectrodes record action potential or "spike" produced by currents flowing in the extracellular space of an active neuron. The membrane potential (also known as transmembrane potential or membrane voltage) is the difference in electric potential between the intracellular and extracellular space. The neuronal resting membrane potential is usually around -70 mV, meaning that the inside of the cell is -70 mV more negative with respect to the outside. The volume conductor theory *(Heinricher 2004; LORENTE de NO 1947; RALL 1962)* allows to model the extracellular current flow around the axon of an active neuron, providing a clear picture of the extracellular signal genesis. In the simplest case, the axon is visualized as surrounded by an extracellular saline bath, known as "volume conductor". When the axon is at rest, no current flows and the membrane potential is uniform along is entire length (Fig. 2.1A). When an action potential is generated in the initial segment of the axon, that spot of the membrane is depolarized. The membrane produces a current flow inward at the depolarized region ("sink") and a microelectrode located close to the sink will record a negative potential with respect to a distant indifferent electrode. The other regions of the membrane adjacent or distant to the sink serve as a "source" of current for the active, depolarized, region. Since the current flows outward at the source, a microelectrode located near the source will record a positive potential, relative to a distant indifferent electrode (Fig. 2.1B).

According to the model of source and sink, a microelectrode adjacent to an axon that is conducting an action potential, will record a triphasic signal (+ - +): a small positive flexion, reflecting the positive potential of the membrane under the electrode, which is not affected by the depolarization; a prominent negative deflection, representing the negative potential observed when the action potential reaches the membrane underlying the electrode; a small positive flexion again when the action potential, which is propagating along the axon, overpasses the electrode and the membrane acts as a source again. Positive flexions are always smaller than the negative ones because the current density in the regions distal to the site of genesis of the action potential is lower *(Heinricher 2004)* (Fig.2.2). Moreover, simultaneous recordings of intracellular and extracellular

potentials during antidromic activation of a motoneuron in the ventral horn of cat revealed that the negative deflection of the extracellular spike corresponds to the depolarization seen by the electrode during intracellular recording whilst the late positive flexion coincides with the repolarization phase intracellularly recorded *(Heinricher 2004)* (Fig. 2.3).

Furthermore, spikes can be generated at the dendrites or soma. In both cases, the model predicts a biphasic signal with an initial negative component followed by a positive phase (Fig. 2.4). However, it should be taken into account that in real conditions, the morphology of the cells, the geometry of the dendrites and the distribution of conductances along the membrane vary among neurons; also the location of the electrode relative to the cell, influences several features of the recorded signal, complicating the picture of the simplified model deriving from the volume conductor theory.

The *in vivo* extracellular recording technique allows to derive the extracellular action potential generated by currents that flow through the neuronal membrane into the extracellular space. Extracellular recordings of single neurons (single-unit; SU) or neighboring neurons potentials (local field potential; LFP) allows the study of the neuronal physiology and connectivity in a functional context. In chronic preparations, neuronal activity may be recorded for hours or even days, allowing the correlation with behaviors or physiological events. In this perspective, the extracellular recording technique is the method of choice to study neuronal spike discharge properties and network connectivity within and across brain structures, exploiting the fact that neurons use action potentials as a code to provide information. Indeed, neurons transmit information using two different strategies: the "rate coding" in which frequency-encoded information is transferred and the neuron firing rate is the key to decode the incoming information; or "time coding" in which the temporal occurrence of individual spikes represents the key to decode the information. However, as every technique, extracellular recordings bear limitations, such as the inability to unravel electrophysiological properties at the cellular level, or subthreshold physiological events that influence cellular intrinsic excitability.

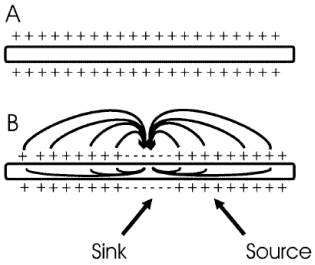

Figure 2.1| Volume conductor theory. (A) Schematic representation of the extracellular currents flow around an axon at rest, surrounded by a low resistance volume conductor. **(B)** Schematic representation of the extracellular currents flow around an axon of an active neuron. Figure from *(Heinricher 2004).*

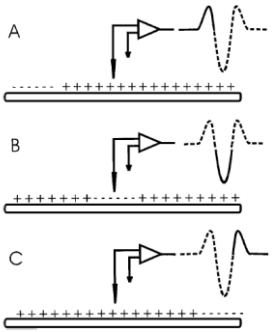

Figure 2.2| Triphasic extracellular signal recorded by a microelectrode adjacent to an axon that is conducting an action potential, according to the model of source and sink based on the volume conductor theory. (A) Small positive flexion, reflecting the positive potential of the membrane under the electrode, which is not affected by the depolarization; **(B)** prominent negative deflection, representing the negative potential observed when the action potential reaches the membrane underlying the electrode; **(C)** small positive flexion when the action potential, which is propagating along the axon, overpasses the electrode and the membrane act as a source again. Figure from *(Heinricher 2004).*

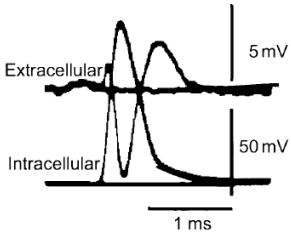

Figure 2.3| Simultaneous recordings of intracellular and extracellular potentials during antidromic activation of a motoneuron in the ventral horn of cat. The negative deflection of the extracellular spike corresponds to the depolarization seen by the electrode during intracellular recording whilst the late positive flexion coincides with the repolarization phase intracellularly recorded. Figure from *(Heinricher 2004).*

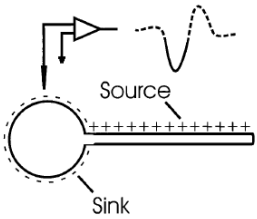

Figure 2.4| Spikes generated at the soma. The model predicts a biphasic signal with an initial negative component corresponding to the sink followed by a positive late phase reflecting the source. Figure from *(Heinricher 2004).*

2.3 In vivo extracellular recordings from FN and PrL in mice

Several types of microelectrodes for extracellular recordings are commercially available, depending on the experimental needs, and they ensure a good signal-to-noise ratio. Quartz-coated platinum/tungsten fiber microelectrodes (1-5MΩ; Thomas Recording, GmbH, Germany) were used in this work for neuronal recordings. The electrodes were suited to be placed in a 16-channel multielectrode array (MEA) system (system Eckhorn microdrive, Thomas Recording GmbH, Germany; Fig. 2.5A). The 4x4 matrix with an inter-electrode distance of 100 µm allowed the

simultaneous and independent insertion of microelectrodes into the exposed brain surface (Fig. 2.5B). The electrophysiological signals, acquired using OpenEx software suite (Tucker-Davis Technologies, Alachua, FL, USA), were then digitalized at 25 kHz, using a 300-5000 Hz band-pass filter, amplified and stored using a RZ5D processor multi-channel workstation (Tucker-Davis Technologies, Alachua, FL, USA).

Single-units were recorded from the FN or PrL of mPFC in two independent set of experiments:

1. FN neurons received a sensory tactile stimulation protocol. The sensory stimulation was performed using air-puffs delivered to the mouse orofacial region. Following 5 minutes of FN spontaneous activity recording, low frequency air-puffs stimuli (0.5 Hz- 30 ms-30-60 psi) were delivered to the mouse upper lip, lower lip or whisker pad to activate the corresponding receptive fields and evoke the neuronal responses. FN neurons responses were revealed in real-time by making peri-stimulus time histograms (PSTHs) triggered by air-puffs during the on-going experiment. Once a responsive neuron was detected, control stimuli at 0.5 Hz were delivered for 20 minutes. Then, a theta sensory stimulation (TSS) entrainment pattern (a burst of 100 air-puffs delivered at 4 Hz) was delivered to induce plasticity, followed by post-induction recordings at 0.5 Hz for at least 40 minutes.

2. PrL neurons received an electrical stimulation protocol. The electrical stimulation was performed using a co-axial platinum bi-polar tungsten electrode placed into the FN or DN. Following 5 minutes of PrL neurons spontaneous activity recording, electrical stimuli (21 pulses, 100 Hz, 100 µA) were delivered every 5 sec to evoke neuronal responses.
   In a subset of experiments, dopaminergic receptor antagonists (SCH23390 hydrochloride, selective D1-like antagonist; (S)-(-)-Sulpiride, selective D2-like antagonist) were perfused onto the exposed mPFC surface, in order to study the dopaminergic contribution to the observed responses. In this case, after 5 minutes

of mPFC neurons spontaneous activity recording, electrical stimuli were delivered every 5 sec as control period and the drugs were applied immediately after the control period and maintained throughout the recording.

2.4 Data analysis

Recordings were analyzed offline using SpikeTrain (Neurasmus B.V., Rotterdam the Netherlands) running under MATLAB (mathworks, MA, USA) and Excel, in both individual experimental sets. The recorded waveforms from each electrode were sorted into "spikes" and "noise" using SpikeTrain software tools. The spike sorting consisted of three steps:

1. Thresholding: a manually positioned threshold detected the events and assigned a marker to each event, without discriminating between spikes and noise.

2. Clustering: through the principal component analysis (PCA), color-coded marker were automatically assigned to each event, based on their waveforms, thus color-coded waveforms were clustered into groups.

3. Wave sorting: color-coded waveforms of each cluster were visualized and single event form each cluster were selected for further manual discrimination of events.

Concerning experiments in which the sensory tactile stimulation protocol was applied, Openscope (from OpenEx suite) was used to construct online peri-stimulus time histograms (PSTHs) triggered by the air-puffs, in order to identify responsive neurons. PSTHs constructed with 5 or 15 ms bin widths and raster plots of 300 trials were used for an accurate analysis of FN neurons responses offline. Changes of the neuronal responses after TSS delivery were evaluated from the corresponding PSTHs made offline, comparing PSTHs peaks and pauses amplitude after TSS to those of the pre-induction period. To identify statistically significant responses to air-

puff stimuli, the post-stimulus excursions of the mean basal frequency that exceeded twice the value of the mean standard deviation of the pre-stimulus period was considered. Statistical comparisons were carried out using the paired or unpaired Student's t-test, or one-way ANOVA in Origin software. Clustering analysis was conducted using MATLAB routine for *k*-means clustering, providing responses latency and duration or frequency and magnitude resulting from autocorrelation analysis, as input parameters. Autocorrelation analysis on post-stimulus PSTHs was conducted using MATLAB routine *xcorr*, with the feature of oscillation peaks normalization to 1. The analysis was applied to all single-unit recordings. A further *k-means* analysis was applied to the autocorrelation results, unraveling two distinct clusters of units characterized by low frequency - high magnitude and high frequency - low magnitude oscillations.

Concerning experiments in which the electrical stimulation protocol was applied, PSTHs constructed with 100 ms bin widths were used for the analysis of PrL neurons responses. For PrL neurons firing frequency analyses, the spontaneous firing rate of individual cells was compared to that measured during their correspondent stimulation period, as a measure of changes in the in neuronal spike discharge. For the analysis of the coefficient of variation of the inter-spike interval (CV2), which was considered as a measure of the regularity of the spike firing, CV2 measured during spontaneous activity of individual cells was compared to that obtained from their correspondent stimulation period.

In the subset of experiments in which the dopaminergic receptor antagonists were applied, amplitude changes of the neuronal responses after drugs perfusion were evaluated from the corresponding PSTHs of 100 ms bin widths, comparing PSTHs amplitude changes after drugs perfusion to those of the control period. To identify statistically significant amplitude changes of the neuronal responses, the post-stimulus excursions of the mean basal frequency that exceeded once the value of the mean standard deviation of the pre-stimulus period was considered.

Statistical comparisons were carried out using paired or unpaired Student's *t*-test. Data in the text are reported as mean ± SEM.

Fitting to the data was performed using routines written in OriginPro8 (OriginLac co., MA, USA).

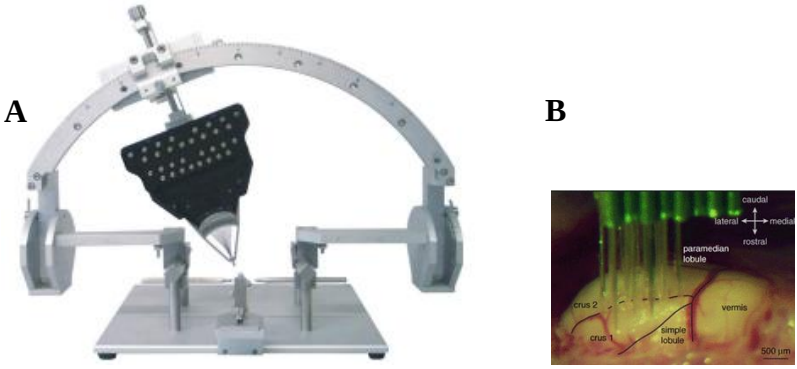

Figure 2.5| Multielectrode Array (MEA). The recording microelectrodes were placed in a 16-channel multielectrode array system **(A)**. The 4x4 matrix with an interelectrode distance of 100 µm allowed the simultaneous and independent insertion of microelectrodes into the exposed brain surface **(B)**. Figure **B** from *(Bosman et al. 2010).*

3. Scope of the thesis

This thesis focuses on two brain regions, the cerebellum and the prefrontal cortex, two structures functionally and anatomically interconnected (a detailed description has been provided in **chapter 1**), and it tries to address two key points related to cerebellar functions.

The first point is tightly related to the role of the cerebellum in learning and storage of sensory information. In particular, the attention has been focused on deep cerebellar neurons, which represent the "relay station" of the cerebellum. Nuclear neurons process and integrate sensory inputs coming from several pathways and they play fundamental role in shaping cerebellar output. In this scenario, particular attention has been given to the theta-frequency stimulation pattern. Indeed, coherent theta frequency oscillations, generated through complex set of mechanisms, have been observed in several brain regions, including the cerebellum, during certain behavioral states such as active motion and cognition. It is therefore reliable that the theta band may represent the frequency band in which neurons are entrained during learning. The cerebellar network is itself resonant in the theta band frequency and it exhibits a theta frequency oscillatory state that may control the plastic changes underlying the cerebellar learning. In this perspective, **chapters 4 and 5** show the results of the theta band frequency sensory stimulation impact on deep cerebellar nuclei neurons spike discharge *in vivo*. This project aimed to complete the picture of the theta sensory stimulation effect on cerebellar neurons activity *in vivo*. Indeed, sensory tactile stimuli organized in theta patterns have been previously observed to induce long-term plastic changes in cerebellar granule cells (Roggeri et al. 2008), Purkinje cells and molecular layer interneurons (Ramakrishnan et al. 2016) activity *in vivo*, but whether and how cerebellar nuclear neurons modify their discharge properties in response to theta patterned sensory stimulation had not been previously explored.

The second point is closely related to the cerebellar role in cognition. Recent findings reported the anatomical connection between the cerebellum (manly the dentate nucleus) and the prefrontal cortex in human (Palesi et al. 2015) and the *in vivo* electrophysiological evidences of a functional

reciprocal connection between cerebellum (manly the fastigial nucleus) and the medial prefrontal cortex in rodents (Watson et al. 2014; Watson et al. 2009). Starting from these findings, **chapter 6** is focused on the investigation of the connectivity between the cerebellum and the prefrontal cortex, a brain region known to be involved in higher-order functions. The presence of anatomical connections between these two structures led to the logical assumption that they are also functionally interconnected. Herein, we have characterized the medial prefrontal cortex neurons response patterns following the electrical stimulation of the contralateral fastigial and dentate nuclei, investigating whether and how the blockade of dopamine receptors expressed on mPFC neurons membranes affects their responses to the cerebellar stimulation. These preliminary data aimed to shed light on the cerebellar contribution to cognitive functions.

As a contribution to the role of the cerebellum in cognitive functions, **chapter 7** shows results of *in vivo* extracellular recordings from cerebellar Purkinje cells of L7-PP2B and littermate control mice. L7-PP2B mutants are mice with cerebellar Purkinje cell-specific knockout of calcium/calmodulin-activated protein-phosphatase-2B, which suffer from impaired intrinsic plasticity and postsynaptic long-term potentiation at parallel fibers-Purkinje cells synapses. These mice were subjected to a decision making task aimed to demonstrate, on the basis of genotypic, behavioral and electrophysiological differences, the hypothesis that cerebellar potentiation plays a key role in cognitive tasks.

In conclusion, **chapter 8** contains a general discussion in order to conclude and summarize the findings reported in the previous chapters.

4. Plastic changes in deep cerebellar nuclei resonate with low-frequency oscillations *in vivo*

Letizia Moscato[1], Licia De Propris[2], Simona Tritto[1], Lisa Mapelli[1], Egidio D'Angelo[1,2]

[1] Dept of Brain and Behavioral Sciences, University of Pavia, 27100 Pavia, Italy

[2] Brain Connectivity Center, C. Mondino National Neurological Institute, 27100 Pavia, Italy

In review at Journal of Neuroscience (October 2017)

The deep cerebellar nuclei (DCN) have been suggested to play a critical role in cerebellar learning and memory. However, the nature and properties of DCN plasticity *in vivo* remain unknown along with the relationship that plasticity might have with DCN oscillatory activity. Here, we have characterized DCN unit responses to sensory stimulation of the whisker pad in anaesthetized mice of either sex and analyzed the effects of theta-sensory stimulation (TSS), which is known to induce long-term plastic changes in the cerebellum granular and molecular layer. DCN single-unit recordings showed autorhythmic activity, and responded to sensory stimulation generating typical combinations of bursts and pauses, indicating activation of excitatory inputs entering the cerebellar cortex through mossy fibers and of cortical inhibitory outputs relayed by Purkinje cells. Interestingly, initial bursts and pauses were often followed by a low-frequency oscillation. TSS induced protracted changes in DCN unit activity, such that spike-related potentiation and suppression (SR-P and SR-S), either in units initiating the response with bursts or pauses, were correlated with stimulus-induced oscillations through resonant functions. The initial burst in burst-pause units showed an SR-P peak at 9 Hz, while the initial pause in pause-burst units showed an SR-S peak at 5 Hz. These results support the notion that plasticity at the synapses impinging on DCN

neurons can determine protracted changes in neuronal synaptic responsiveness following natural stimulation *in vivo* and that the sign and intensity of the changes are under control of low-frequency oscillations.

4.1 INTRODUCTION

Two aspects of cerebellar functioning, that have been emphasized in turn but proved hard to reconcile, are its pronounced oscillatory dynamics (Llinas 1988) and its role in sensory-motor learning (Albus 1971a; Marr and D. 1969). Key nodes in the cerebellar circuitry are the deep cerebellar nuclei (DCN), which convey rhythmic outputs to the motor system (Jacobson et al. 2008) and have been suggested to be the site of plasticity by lesion studies (Ohyama et al. 2003; Ohyama et al. 2006) and by changes in local field potentials induced by electrical stimulation of afferent fiber bundles (Racine et al. 1986). Multiple forms of plasticity have been reported in DCN synapses *in vitro* (Morishita and Sastry 1996; Ouardouz and Sastry 2000; Pugh and Raman 2009; Zhang and Linden 2006; Zhang et al. 2004)(reviewed in (D'Angelo 2014; D'Angelo et al. 2016b; Gao et al. 2012; Hansel et al. 2001b; Mapelli et al. 2015b) and have been proposed to play a critical role in associative cerebellar behaviors in animals (Medina and Mauk 1999) and in computational models (Antonietti et al. 2016a; Antonietti et al. 2016b; Casellato et al. 2015; D'Angelo et al. 2016a; Medina and Mauk 1999). Despite this evidence, the demonstration and nature of long-term plastic changes and their relationship with DCN oscillations *in vivo* is still lacking.

DCN neurons receive both excitatory inputs from collaterals of mossy fibers heading to the cerebellar cortex and inhibitory inputs descending from Purkinje cells. DCN neurons send output fibers to cerebral cortex (Watson et al. 2014) and various precerebellar nuclei (including the inferior olive), as well as to the cerebellar granular layer (Ankri et al. 2015; Gao et al. 2016), forming reverberating loops that have been predicted to sustain rebound excitation and oscillatory cycles (Hoebeek et al. 2010; Kistler and De Zeeuw 2003; Llinas and Muhlethaler 1988; Marshall and Lang 2004; Witter et al. 2013). DCN neurons are themselves autorhythmic

and respond to tactile stimulation generating typical discharge patterns, which reflect the combination of inhibitory and excitatory inputs (Canto et al. 2016; Rowland and Jaeger 2005; 2008). Interestingly, plasticity at excitatory and inhibitory DCN connections (long-term potentiation and depression, LTP and LTD) proved to be interrelated, so that excitatory plasticity depended on post-inhibitory rebound bursts (Pugh and Raman 2006) and inhibitory plasticity required coactivation of mossy fibers (Morishita and Sastry 1996; Ouardouz and Sastry 2000). It is therefore possible that oscillation in DCN neurons interfere with plasticity (Cheron et al. 2016; D'Angelo and De Zeeuw 2009), following induction schemes already identified in hippocampus and neocortex (Buzsaki 2006; Roy et al. 2014).

In this work, we have investigated whether theta sensory stimulation (TSS) *in vivo*, which proved able to induce plastic changes in the cerebellum granular and molecular layer (Ramakrishnan et al. 2016; Roggeri et al. 2008), could also induce plastic changes in DCN. Indeed, TSS induced a complex pattern of changes in DCN units, revealing a precise relationship between burst/pause patterns and the oscillations of DCN unit responses.

4.2 MATERIALS AND METHODS

Multiple single-unit recordings were performed from the fastigial nucleus of C57BL/6 mice of either sex (32.83±0.31 days old; n=33) under urethane anesthesia. Urethane exerts the anesthetic action through multiple weak effects, including a 10% reduction of NMDA, 18% reduction of AMPA and 23% enhancement of GABA-A receptor-mediated currents (Hara and Harris 2002). Urethane was preferred to ketamine or isoflurane because these latter drugs largely exert their action by blocking NMDA receptors (up to 80 and 60%, respectively; (Hara and Harris 2002)) and therefore may affect the induction of plasticity (Bengtsson and Jorntell 2007; Godaux et al. 1990; Marquez-Ruiz and Cheron 2012; Mawhinney et al. 2012; Muller et al. 1993).

All experimental protocols were conducted in accordance with international guidelines from the European Union Directive 2010/63/EU on the ethical use of animals and were approved by the approved by the ethical committee of Italian Ministry of Health (638/2017-PR).

Surgical Procedures

Mice were deeply anesthetized with intraperitoneal injections of urethane (Sigma). Induction (1.3g/kg urethane dissolved in 0.9% NaCl) was followed by booster injections (10% of the induction dose) in order to stabilize anesthesia, starting 30 minutes after induction and repeating 3-4 times every 30 minutes. The level of anesthesia was monitored by evaluating the leg withdrawal after pinching and spontaneous whisking. The animal was then placed on a custom-built stereotaxic table covered with a heating plate (HP-1M: RTD/157, Physitemp Instruments Inc, Clifton, NJ, USA). Body temperature was monitored with a rectal probe and maintained at 36°C through a feedback controller (TCAT-2LV controller, Physitemp Instruments Inc, Clifton, NJ, USA). The mouse head was fixed over the bregma to a metal bar connected to a pedestal anchored to the stereotaxic table. This arrangement allowed open access to the peri-oral area for air-puff stimulation. Surgery was performed to expose the cerebellar surface: local reflexes were reduced by subcutaneous application of lidocaine (0.2ml; Astrazeneca), then the skin and muscles were removed. Craniotomy of the occipital bone (-7.8mm AP, +0.50mm ML from bregma, in order to record from the fastigial nucleus) allowed to expose the cerebellar surface over the vermis. The *dura mater* was carefully removed and the surface was covered with saline (NaCl 0.9%; Sigma) to prevent drying.

Electrophysiological extracellular recordings

Quartz-coated platinum/tungsten fiber electrodes (1-5MΩ; Thomas Recording, Giessen, Germany) were used for neuronal recordings. Recording electrodes were positioned over the vermis, ipsilateral to the air puff stimulator, and lowered perpendicularly to the surface down to a depth of 2109.1±65.5 μm (n=33). The electrophysiological signals were digitized at 25 kHz, using a 300-5000 Hz band-pass filter, amplified and stored using

a RZ5D processor multi-channel workstation (Tucker-Davis Technologies, Alachua, FL, USA). DCN neurons were identified online by assessing recording depth, spontaneous activity, and stimulus-evoked responses. At the end of recordings, an electric lesion was made by injecting current through the recording electrode. The recording site was then confirmed by histological tissue processing (see below).

Sensory stimulation

Tactile sensory stimulation was performed using air-puffs (30ms pulses, 30-60 psi) delivered through a small tube ending with a nozzle (0.5 mm diameter) connected to a MPPI-2 pressure injector (Applied Scientific Instrumentation, Eugene, OR, USA) positioned 2-3 mm away from the snout area of the animal (Ramakrishnan et al. 2016; Roggeri et al. 2008). Following 5 minutes of spontaneous activity recording, low frequency stimuli (0.5 Hz) were delivered over the mouse upper lip, lower lip or whisker pad to activate the corresponding receptive fields and evoke the neuronal response (Bower and Woolston 1983; Morissette and Bower 1996; Ramakrishnan et al. 2016; Roggeri et al. 2008) (see Fig.1A). DCN single unit responses were monitored online by building peri-stimulus time histograms (PSTHs) triggered by the air-puffs. Once a responsive unit was detected, control stimuli were delivered for 20 minutes at 0.5 Hz. Then, a theta sensory stimulation (TSS) pattern (a burst of 100 air-puffs at 4 Hz) was delivered, followed by post-induction recordings for at least 40 minutes at 0.5 Hz. In 12 recordings TSS was not delivered, monitoring the stability of responses for at least 60 minutes.

Histology

The location of recording electrodes in the DCN was confirmed by electric lesions after the end of recordings. These were obtained by applying a 20 µA - 20 sec current pulse through the recording electrode connected to a stimulus isolator and a stimulator unit. Then, the mouse was perfused transcardially with Phosphate-Buffered Saline (PBS) followed by 4% formaldehyde. The fixated brain was removed and 20-μm-thick histological sections were obtained and stained with toluidine blue. The

histological confirmation of the recording sites was obtained by microscopic observation of the stained sections (see Fig. 1B).

Data analysis

Recordings were acquired using Openex software (Tucker-Davis Technologies) and analyzed offline using custom-written routines in MATLAB and Excel. Openscope (part of the Openex suite) was used to construct online peri-stimulus time histograms (PSTH) triggered by air-puffs, in order to identify responding neurons. Raw traces were analyzed and sorted offline using SpikeTrain (Neurasmus BV, Rotterdam, Netherlands) running under MATLAB (Mathworks, MA, USA). The stability of recordings was carefully assessed (< ±20% amplitude fluctuation over the duration of the recording) and only units with stable spike size were considered for further analysis. PSTHs and raster plots were used for the analysis of responses to stimulation, normally consisting of peaks and pauses emerging from background discharge. For convenience, 5 ms bin width was used to analyze peaks, while 15 ms bin width was used to analyze pauses. Peaks and pauses were identified as PSTH modifications exceeding twice the standard deviation of the basal frequency in the pre-stimulus period.

The effect of TSS was evaluated by measuring the corresponding changes in PSTH peaks and pauses. To this aim, we considered the post-TSS responses (computed over the first 15 min after TSS) that exceeded twice the standard deviation of the pre-TSS response (computed over the last 15 min before TSS). Positive changes were considered as a potentiation and negative changes were considered as a suppression of basal firing (a minority of units did not show any significant changes with respect to this criterion).

Statistical comparisons were carried out using paired or unpaired Student's *t*-test or Fisher's *F*-test. Data in the text are reported as mean ± SEM. Clustering analysis was performed using a MATLAB routine for *k*-means. Autocorrelation analysis on post-stimulus PSTHs was performed using the MATLAB routine *xcorr* (oscillation peaks normalization set to 1).

Fitting to the data was performed using routines written in OriginPro8 (OriginLab co., MA, USA). The Lorentzian function *y(x)* used to fit the frequency-dependence of plasticity changes was of the form:

$$y = y0 + \frac{2A}{\pi} \cdot \frac{w}{4(x - fc)^2 + w^2}$$

where *y0* and *A* are curve baseline and amplitude, *w* is curve width, *fc* is the resonance frequency.

4.3 RESULTS

Single-unit recordings were performed from the cerebellar fastigial nucleus in urethane anesthetized mice (Fig.1A). All units were spontaneously active and showed a basal frequency of 9.51±0.99 Hz (ranging from 4 to 27 Hz; n=33), in agreement with previous reports of spontaneous activity under urethane anesthesia (LeDoux et al. 1998; Sweeney et al. 1992). The recording site was confirmed by electric lesions made through the recording electrode and identified histologically (Fig.1B). Single-unit responses to low frequency tactile stimulation (0.5Hz) generated spike *bursts* and *pauses* modifying the basal discharge (Fig. 1C) that were likely to reflect the neuronal response to excitatory and inhibitory synaptic inputs impinging onto DCN neurons (Rowland and Jaeger 2005; 2008).

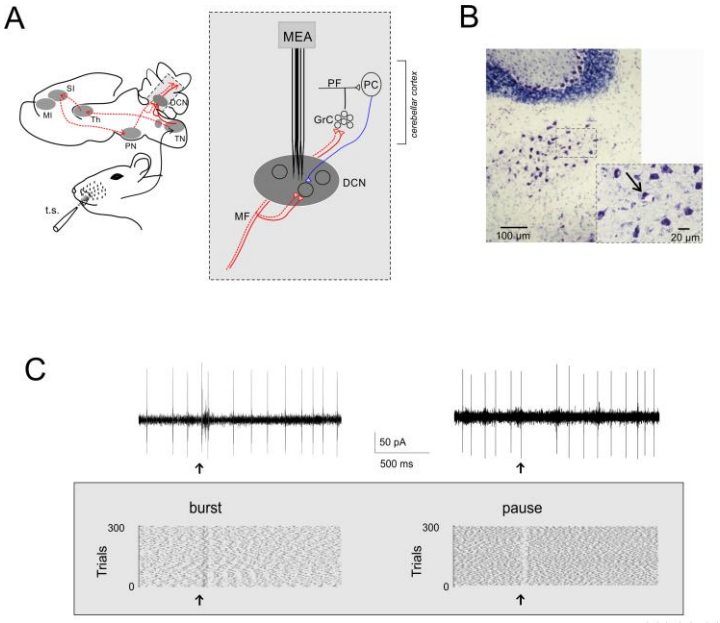

Figure 1. **Extracellular recordings from DCN units *in vivo*. A)** Schematic representation of the main pathways activated by air puff stimulation of the peri-oral region in mice: the trigemino-cerebellar (*solid red line*) and thalamo-cortical-pontine (*dashed red line*) pathways. The region in the grey box is expanded at the right, where the excitatory pathways brought by mossy fibers (MF) and the inhibitory fibers from Purkinje cells (PC) are represented. MI, primary motor cortex; SI, primary sensory cortex; Th, thalamus, PN, pontine nuclei; TN, trigeminal nucleus, DCN, deep cerebellar nuclei; MF, mossy fibers; GrC, granule cells; PF, parallel fibers; PC, Purkinje cell; t.s., tactile stimulation. **B)** Toluidine blue stained coronal cerebellar slice showing the electric lesion (*arrow*) made by the recording electrode in the fastigial nucleus. **C)** Two single-unit recordings showing a burst and a pause in response to tactile stimulation (*arrow*). The raster plots show the spike discharge during ~2s recordings and its change caused by tactile stimulation in 300 consecutive trials.

Bursts and pauses in DCN unit responses

Single-unit responses to low frequency tactile stimulation generated combinations of peaks and pauses in peri-stimulus-time-histograms

(PSTHs) and, in some cases, the response continued with an oscillation (see below). Over a total of 33 units, we identified 2 fundamental categories of patterns, with either the burst or the pause as the initial response (Fig. 2A).

When the *burst* initiated the response (n=17), some units (n=9) showed a single PSTH peak with latency of 15.20±2.62 ms (duration 14.70±3.41 ms), while other units (n=8) showed two PSTH peaks with latency of 9.87±1.99 and 33±3.7ms (duration of 8.12±1.31 and 15±3.27ms). These peak latencies corresponded to those reported for responses of granular layer neurons (Roggeri et al. 2008; Yue and Huguenard 2001), suggesting that the initial bursts most likely corresponded to synaptic excitation of DCN neurons through trigeminal and cortical mossy fibers (Fig. 2B).

When the *pause* initiated the response (n=16), it occurred with a latency of 21.75±4.81ms (duration of 30.38.5±5.20 ms). This delay was compatible with signal transmission along the mossy fiber - granule cell - Purkinje cell - DCN neuronal pathway (Ramakrishnan et al. 2016), suggesting that the initial pause most likely corresponded to DCN neuron inhibition by PCs.

Several units initiating the response with a burst (13 out of 17) showed a pause following peak(s), and several units initiating the response with a pause (7 out of 16) showed a burst following the pause (Fig.2A). The nature of these *burst-pause* and *pause-burst* patterns showed peculiar properties.

In *burst-pause* responses, the pause was significantly delayed (64.73±6.09 ms, n=13) compared to that measured when it initiated the response (p=0.0003). This longer delay suggests the intervention of additional mechanisms, like signal reentry through the recently discovered DCN-GrC connections (Gao et al. 2016) or through precerebellar nuclei (Kistler and De Zeeuw 2003).

In *pause-burst* responses, the bursts followed with a latency of 91.21±21.22 ms (duration 19.28±2.76 ms), that was significantly longer compared to that measured when it initiated the response (p=0.01). A

positive correlation was found between pause depth and the subsequent peak amplitude (R^2=0.86, *p*(F)=0.001, n=7) (Fig. 2C). A plausible explanation is that these bursts are non-synaptic and reflect a post-inhibitory rebound discharge in DCN neurons (Canto et al. 2016), which is the stronger the deeper the pause. These observations suggest the intervention of cellular mechanisms, like post-inhibitory rebound depolarization (Canto et al. 2016; Witter et al. 2013).

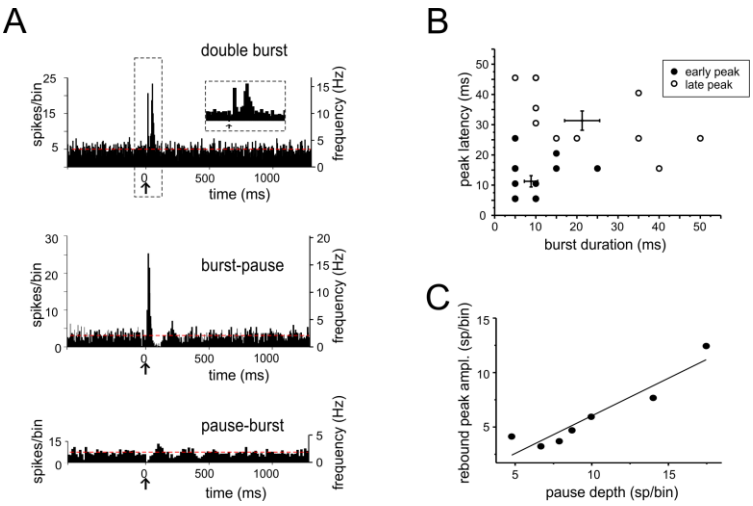

Figure 2. **Bursts and pauses in DCN unit responses to tactile stimulation. A)** Exemplar PSTHs obtained from DCN units showing different responses to tactile stimulation (*arrows*): double burst (5ms-bin), burst-pause (5ms-bin), and pause-burst (15ms-bin). Red dashed lines show the basal discharge frequency. **B)** In the pool of responses starting with a burst, two groups were discriminated using cluster analysis (k-means) on peak latency and burst duration. This results in the identification of early and late peaks, whose latencies are compatible with inputs from the trigeminal and cortical pathways conveying sensory stimuli to the cerebellum (cfr. Fig.1A). **C)** Characterization of pause-burst responses. A positive correlation was found between rebound-peak amplitude and pause depth (R^2=0.86, p(F)=0.001, n=7).

Spontaneous activity and stimulus-induced oscillations in DCN units

The PSTH elicited by tactile stimulation in several cases showed an *oscillation* following the initial peaks and pauses (Fig. 3A). This oscillatory pattern was apparent in autocorrelation analysis (Fig. 3B). The frequency / magnitude plot revealed a negative trend, with slower oscillations showing the larger magnitude and *vice versa* (Fig. 3C). K-means analysis identified two significantly different clusters of points, one at high frequency and the other at low frequency. Low-frequency oscillations were mostly in the theta band, with average oscillation frequency of 10.9±1.2 Hz (n=20).

The relationship between low-frequency stimulus-induced oscillations and spontaneous activity is shown in Figs 3D-E. The frequency of stimulus-induced oscillations tended to increase with spontaneous frequency (R^2=0.14, p(F)<0.06, n=20), while the magnitude of stimulus-induced oscillations decreased significantly with spontaneous frequency (R^2=0.35, p(F)<0.003, n=20). It should be noted that, out of 20 units, 8 were of the burst-pause and 12 of the pause-burst category. At a closer analysis, the burst-pause units showed a significantly higher magnitude (0.11±0.01 vs. 0.07±0.01; p=0.006, unpaired *t*-test) and lower spontaneous frequency (7.4±1.1 Hz vs. 10.7±1.2 Hz p=0.05, unpaired *t*-test) than the pause-burst units (Fig. 3C, D, E) suggesting the existence of two distinct functional classes of DCN neurons (see below).

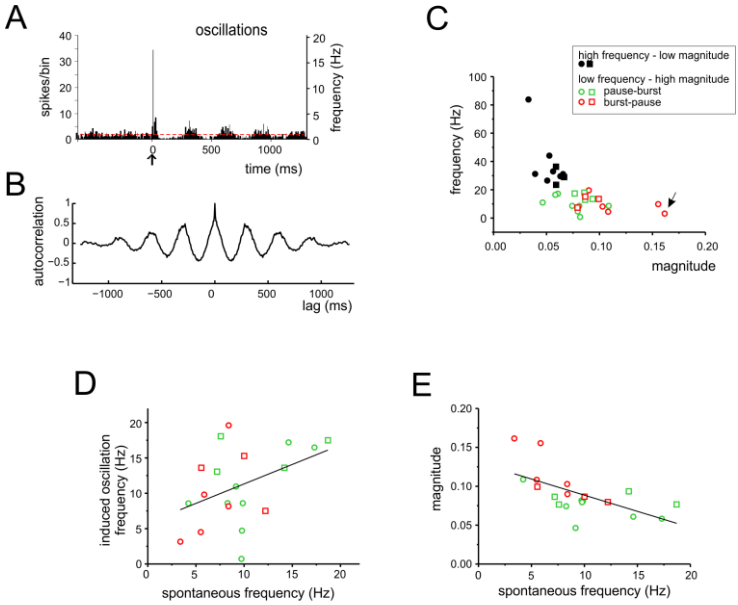

Figure 3. DCN unit oscillations following the initial response. A) PSTH obtained from a DCN unit showing low frequency oscillation following a burst-pause response. B) Autocorrelogram obtained from the unit shown in A (oscillation frequency 3.15 Hz; magnitude 0.16). C) The magnitude and frequency of oscillations deriving from the autocorrelation analysis shown in B were plotted for each unit. The k-means clustering revealed two separate groups of data, characterized by high frequency - low magnitude oscillations and low frequency - high magnitude oscillations. The arrow indicates the unit shown in panels A and B. D) Relationship between stimulus-induced oscillation frequency and spontaneous firing frequency for the low frequency - high magnitude oscillation units in C. The linear fitting shows a positive trend (R^2=0.14, p(F)=0.06). E) Relationship between magnitude of stimulus-induced oscillations and spontaneous firing frequency for the low frequency - high magnitude oscillation units in C. The linear fitting shows a positive trend (R^2=0.35, p(F)=0.003). In C, D, E, the data points are divided into burst-pause and pause-burst units, and circles represent the units that were further used for plasticity induction (see Figs. 4-5).

Multiple plastic changes induced by TSS in DCN unit responses

The cerebellar cortex in rodents is known to respond to TSS of the whisker pad with plastic changes in the granular and molecular layers (Diwakar et al. 2011; Prestori et al. 2013; Ramakrishnan et al. 2016; Roggeri et al. 2008). We therefore investigated whether the delivery of the same TSS pattern was able to affect DCN neuron responsiveness. We defined Spike-Related Potentiation (SR-P) and Spike-Related Suppression (SR-S) as the increase or decrease in spike response probability with respect to baseline (cf. Ramakrishnan et al., 2016), both in bursts and pauses. For simplicity we considered only the initial bursts and pauses, since their amplitude is not influenced by preceding electrical events. The values of changes were measured for each unit in the first 15 min following TSS with respect to the last 15 min before TSS.

TSS-induced changes in initial bursts. TSS was delivered in 10 recordings showing an initial excitatory burst (Fig.4A). A significant SR-P of the first PSTH peak was observed in 4 units (45.27±10.73%, n=4, paired Student's *t* test p=0.01; Fig.4A), while a significant SR-S was observed in another 5 units (-27.83±7.31%, paired Student's *t* test p=0.02). Only in 1 out of these 10 units, no significant changes were observed.

TSS-induced changes in initial pauses. TSS was delivered in 11 recordings showing an initial pause in the response (Fig.4B). A significant SR-P of the pause was observed in 4 units (48.43±14.77%, n=4, paired Student's *t* test p=0.004), while a significant SR-S of the pause depth was observed in another 5 units (-31.30±10.82%, n=5, paired Student's *t* test p=0.008; Fig.4B). In 2 units, no pause depth changes were found.

Stability controls. In 7 units showing an initial excitatory burst and in 5 units showing an initial pause, TSS was not delivered. In these units, the bursts and pauses remained stable for a duration similar to that of experiments in which the TSS was delivered (bursts: 4.7±11.7 % change, paired Student's *t* test, n=7, p=0.9; pauses: 5.6±10.0 % change, n=5, paired Student's *t* test, p=0.1). These controls ruled out possible spurious changes due to intrinsic response amplitude fluctuations with time.

Average time course. The average time course for burst and pause changes was constructed by grouping all the units in each given category. The SR-P and SR-S of peaks and pauses reported above were statistically significant for the first 15 minutes after TSS but returned back to baseline within 30 minutes (Fig. 4C).

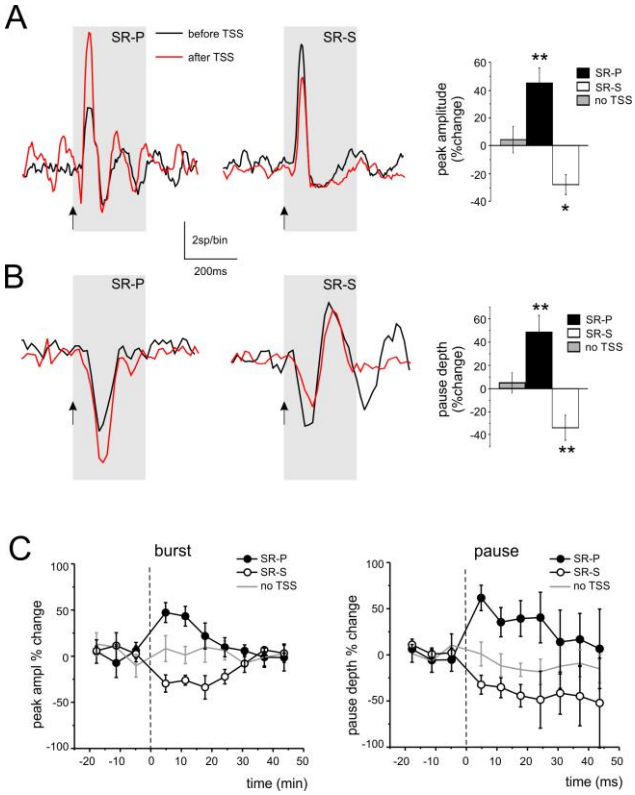

Figure 4. **Plastic changes induced by TSS in DCN unit responses**. **A)** Exemplar PSTHs illustrating the *peak* changes (SR-P or SR-S) induced by TSS in DCN units. The histogram shows the average percent changes in PSTH peak amplitude for all the units showing SR-P, SR-S, or stability controls (no TSS; * $p<0.05$, ** $p<0.01$). **B)** Exemplar PSTHs illustrating the *pause* changes (SR-P or SR-S) induced by TSS in DCN units. The histogram shows the average percent changes in PSTH peak amplitude for all the units showing SR-P, SR-S, or stability controls (no TSS; **

p<0.01). **C)** Average time-course of peak and pause amplitude percent changes normalized to the control period before TSS (*dashed line*) in the units showing SR-P, SR-S and in the stability group (TSS not delivered).

Correlation between plastic changes and oscillations

In Fig. 3, two functional classes of units have been identified based on their response pattern and low frequency oscillatory properties, summing up to a total of 8 burst-pause units and 12 pause-burst units. Here we have considered the relationship between plasticity changes and stimulus - induced oscillation frequency in the 5 burst-pause and 8 pause-burst units that received TSS. Peak changes in the *burst-pause* units followed a Lorentzian distribution peaking at 9.2 Hz with 56% SR-P and settling down to -18.9% SR-S at lower and higher frequencies (R^2=0.82; p(F)<0.02). Pause changes in the *pause-burst* units followed a Lorentzian distribution peaking at 5.2 Hz with -42% SR-S and settling to 31.2% SR-P at higher frequencies (R^2=0.72; p(F)<0.02). It should be noted that, in burst-pause and pause-burst units showing high frequency oscillations, average plastic changes settled around the asymptote of the Lorentzian fit (i.e. SR-S for burst-pause units and SR-P for pause-burst units). Thus, the SR-P/SR-S distributions resonated at low frequency with respect of the DCN unit oscillatory response but showed opposite changes in burst-pause and pause-burst units.

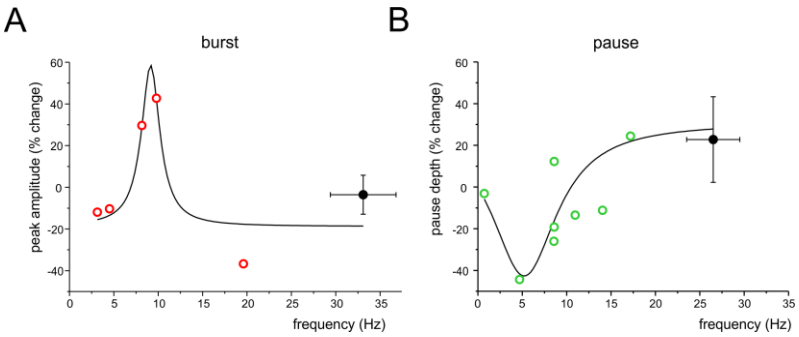

Figure 5. **Frequency-dependent distribution of response changes after TSS in low frequency oscillating units**. **A)** The plot shows the distribution of peak amplitude changes after TSS in burst-pause units with respect to stimulus induced oscillation frequency. The Lorentzian fitting (R^2=0.82; p(F)=0.02) shows a peak at 9.2 Hz. **B)** The plot shows the distribution of pause amplitude changes after TSS in pause-burst units with respect to stimulus induced oscillation frequency. The Lorentzian fitting (R^2=0.72; p(F)=0.02) shows a peak at 5.2 Hz. Both in A and B, open symbols identify the same low-frequency units reported in Fig. 3 and filled symbols are the average values (± SEM) of high frequency oscillation units.

4.4 DISCUSSION

DCN units were spontaneously active and responded to tactile sensory stimulation with different combinations of bursts, pauses and oscillations. Following theta-frequency stimulation, DCN units showed spike firing potentiation or suppression, SR-P or SR-S, both for bursts and pauses. To our knowledge, SR-P and SR-S are the first electrophysiological evidence that plastic changes can be induced by natural stimulation patterns in DCN neurons *in vivo*. Interestingly, the SR-P/SR-S distributions resonated at theta-frequency disclosing a complex relationship between DCN plasticity and cerebellar oscillatory dynamics.

The nature of DCN unit responses

All DCN units responded to tactile stimulation with short delays typical of the fast cerebellar reaction to sensory inputs. In some units (52%), a first burst occurred in about 10-14 ms and was followed (in half of the cases) by a second burst about 10 ms later. This pattern closely matches that observed in the granular layer (Morissette and Bower 1996; Roggeri et al. 2008), suggesting that DCN neurons can receive double mossy fiber activation through the trigeminal pathway and the somato-sensory cortex. The pauses occurring after the initial bursts were delayed by about 60 ms and could reflect signal reentry through the cerebellar cortex, either through extracerebellar loops (Kistler and De Zeeuw 2003) or through the recently discovered connections from DCN to the granular layer (Ankri et al. 2015; Gao et al. 2016). In the remaining units (48%), pauses were the first DCN

response with delays of about 21-22 ms, most likely reflecting signal transfer through the cerebellar cortex down to Purkinje cells and DCN. Actually, Purkinje cell excitation through mossy fibers and granule cells takes about 15 ms (Ramakrishnan et al. 2016) and an additional few milliseconds are then required to inhibit DCN cells. These pauses were often followed by a clear rebound burst probably due to intrinsic electroresponsiveness (Hoebeek et al. 2010; Witter et al. 2013).

Some units continued their response with an oscillatory cycle at low frequency (10.9±1.2 Hz), independent on whether the responses started with a burst or a pause. The frequency of oscillation induced by stimulation was not significantly correlated with spontaneous discharge in the same units (though a correlation was found for magnitude). Therefore, PSTH oscillations could not be fully explained by phase reset, since in that case the two frequencies should coincide (Solinas et al. 2007). Other factors that could influence the frequency of induced oscillations include intrinsic rebound properties of DCN neurons (Hoebeek et al. 2010; Witter et al. 2013) as well as signal reentry through intra- and extra-cerebellar circuits (Gao et al. 2016; Kistler and De Zeeuw 2003).

There were two groups of low-frequency oscillating units, one made of *burst-pause* and the other of *pause-burst* units, which turned out to differ for basal frequency and magnitude of stimulus-induced oscillations and, eventually, to show opposite frequency-dependent changes during plasticity. The potential relationship between these functional groups of DCN neuron, which may express different functional and wiring properties, and the DCN neuron subpopulations reported *in vitro* (Bagnall et al. 2009; Uusisaari and Knopfel 2012) remains to be determined.

Potential climbing fibers involvement in DCN neurons responses

Although our data are compatible with a prevailing activation of MFs, rather than climbing fibers (CFs), to account for DCN neurons responses as bursts and pauses, we cannot rule out a potential role of CFs. Indeed, CFs directly contact DCN neurons before entering the cerebellar cortex, where they excite PCs evoking complex spikes. CFs activation is theoretically able to directly excite DCN neurons or to indirectly inhibit

them (through PCs activation). Nevertheless, a number of considerations limit the potential role of CFs activation in the DCN responses described in this work.

Firstly, although whiskers stimulation is able to evoke complex and simple spikes activity in PCs of both awake and anesthetized rodents, the frequency of CFs-elicited complex spikes in anesthetized animals is lower compared to measurements in awake condition (Bosman et al. 2010; Ramakrishnan et al. 2016). Nevertheless, olivary neurons show low-threshold responses to the mechanical stimulation of the face in urethane anesthetized rodents (Cook and Wiesendanger 1976). Moreover, PCs (CFs-elicited) complex spikes following sensory tactile stimulation of the mouse whisker pad have been reported to occur with a delay of 40-50 ms from the stimulus (Ramakrishnan et al. 2016). Considering that both CF-PC and CF-DCN contacts are monosynaptic and CFs make synaptic contacts with DCN neurons before entering the cerebellar cortex, where they ultimately contact PCs, it is unlikely that the excitatory peaks observed in our data are generated by CFs activation. Overall, these considerations suggest that burst responses likely result from MFs activation rather than a conjunctive or independent CFs contribution.

Secondly, further considerations are needed concerning the two different types of inhibitory responses described in DCN neurons, pure initial pause and pause burst responses, both referable to PCs inhibitory projections onto nuclear neurons. It is reasonable to wonder which pathways come into play shaping the PCs output onto nuclear neurons resulting in these two different response patterns. It has been reported that the molecular layer interneurons (MLIs) and CFs are able to toggle PCs between up and down state, shaping the duration of the inhibitory responses observed in DCN neurons, though the physiological pattern of input that elicits their post-inhibitory rebound increase in firing has not been identified yet (Loewenstein et al. 2005; Oldfield et al. 2010). Recent findings have revealed a reverse correlation between DCN neurons rebound excitation following the inhibition and stimulus-evoked PCs firing pattern suggesting that rebound excitatory responses in nuclear neurons are triggered by the pause pattern of PCs firing rate and designating the PCs pause duration as a key factor for generating the rebound excitation (Dykstra et al. 2016).

Moreover, recent *in vivo* findings show that tactile peripheral activation of CFs receptive fields is able to evoke post-inhibitory rebound responses in DCN neurons via CF-PC pathway whereas the PCs activity MFs driven is able to generate a prominent inhibition but it fails to induce rebound, at least after cat forebrain stimulation (Bengtsson et al. 2011). Thus, profound rebound responses seem to occur only when strong afferent inputs drive a sufficiently synchronized CFs activation to engage a large portion of the PCs innervating the same DCN neuron (Bengtsson et al. 2011). As a conclusion, we cannot rule out a possible involvement of CFs input concerning the generation of rebound burst after pauses in DCN neurons.

Oscillation-dependent changes of DCN unit responses during plasticity

In *burst-pause* units, burst SR-P was maximal at 9.2 Hz (109 ms burst/pause cycle), while SR-S occurred at <5Hz and >20 Hz. In *pause-burst* units, pause SR-S was maximal at 5.2 Hz (192 ms pause/burst cycle), while SR-P occurred at >20 Hz. These SR-P and SR-S properties suggest the intervention of frequency-dependent forms of synaptic plasticity at DCN synapses, that may be governed in an opposite manner depending on different neuronal subpopulations.

The changes in initial burst responses are related to plasticity at the mossy fiber - DCN synapse. *In vitro*, at this connection, the main notion is that LTP is generated when a burst precedes a pause by 100-400 ms and is then followed by a rebound burst, while LTD occurs otherwise (Pugh and Raman 2006). Therefore, these forms of LTP and LTD may provide the basis to explain frequency-dependent SR-P and SR-S of initial bursts in burst-pause units. A form of LTD induced at high-frequency may also contribute to SR-S at >20 Hz (Zhang and Linden 2006).

The changes in initial pause responses are related to plasticity at the Purkinje cell - DCN synapse. *In vitro*, at this connection, the main notion is that both LTP and LTD require mossy fiber activation to be induced (Morishita and Sastry 1996; Ouardouz and Sastry 2000). Thus, these forms of LTP and LTD may provide the basis to explain SR-P and SR-S of pauses in pause-burst units. It should be noted that plasticity of the pause could also be influenced by changes occurring in the cerebellar cortex upstream

DCN. In particular, the robust potentiation of Purkinje cell responses observed using this same TSS induction protocol (Ramakrishnan et al. 2016) may contribute to SR-P of the pause at >20 Hz.

A puzzling issue is about the time course of SR-P and SR-S, which decayed over 30 min. Both in rodents and humans, cerebellar learning has been predicted to occur in two steps, a faster one in the cerebellar cortex (granular and molecular layer) and a slower one in DCN (Attwell et al. 2001; Medina and Mauk 2000; Monaco et al. 2014; Smith et al. 2006). Mathematical modeling further predicts that fast plasticity at the parallel fiber Purkinje cell synapse would be able to tune slow and more stable plasticity in DCN (Casellato et al. 2014; Garrido et al. 2013; Medina et al. 2001). So why *in vivo* recordings have shown more persistent changes in the granular layer (Roggeri et al. 2008) and molecular cell layer (Ramakrishnan et al. 2016) that in DCN? There are three key issues to consider. First, more intense or repeated stimulation may be needed to promote plasticity consolidation in DCN. Secondly, here DCN was not entrained in sensori-motor feedback that enhances and gates cerebellar oscillations (Marshall and Lang 2004). Thirdly, there was no attentional or motivational state, as the animal was anaesthetized. Indeed, neuromodulation by noradrenaline, acetylcholine or serotonine is thought to be critical to drive oscillations and plasticity and promote learning (Schweighofer et al. 2004; Sugihara et al. 1995).

4.5 *Conclusions*

The tight relationship between DCN plasticity and oscillatory dynamics engaged by natural stimuli reconciles two key cerebellar functional theories. Oscillatory activity in DCN may not just be needed to gate motor activity (Llinas 1988; Marshall and Lang 2004) but also to control plasticity and the acquisition of sensori-motor engrams (Cheron et al. 2016; D'Angelo and De Zeeuw 2009). In this sense, it is particularly valuable the observation that the peak of resonant plasticity curves was in the theta-band, which is known to favor the induction of plasticity in hippocampal and cortical synapses (Buzsaki 2006; Roy et al. 2014). It is

tempting to speculate that the frequency of oscillations, that controlled SR-P/SR-S distributions in burst-pause and pause-burst units, may provide a key signal capable of binding DCN plasticity to specific neuronal ensembles and brain states (Buzsaki 2006; Buzsaki 2005; Timofeev 2011). The frequency dependence of burst and pause changes *in vivo* prompts for a further characterization of LTP and LTD mechanisms *in vitro,* also considering that the opposite frequency-dependence of plasticity in burst-pause and pause-burst units supports the existence of functionally distinct DCN neuronal populations. New experiments *in vivo* and computational modeling (Casellato et al. 2014; Luque et al. 2014; Medina and Mauk 2000) may then help addressing the impact of these opposite frequency-dependent forms of plasticity during cerebellar adaptation and learning.

5. Theta-patterned tactile stimulation modifies deep cerebellar nuclei neurons responsiveness *in vivo*

Letizia Moscato[1], Lisa Mapelli[1], Licia De Propris[2], Simona Tritto[1] and Egidio D'Angelo[1, 2]

[1] University of Pavia, Dept. of Brain and Behavioral Sciences, Italy

[2] Brain Connectivity Center, C. Mondino National Neurological Institute, Italy

Front. Cell. Neurosci. Conference Abstract: The Cerebellum inside out: cells, circuits and functions. doi: 10.3389/conf.fncel.2017.37.000022.

5.1 *Introduction*

Several forms of synaptic plasticity have been described in the cerebellar network in vitro, but how plasticity may be induced in vivo remains poorly explored. Sensory tactile stimuli organized in theta patterns have been reported to induce long-term changes in cerebellar granule cells (Roggeri et al. 2008), Purkinje cells and molecular layer interneurons (Ramakrishnan et al. 2016) *in vivo*. Deep cerebellar nuclei (DCN) neurons are known to respond to low frequency sensory stimulation through typical discharge patterns reflecting the inhibitory and excitatory inputs converging onto these nuclei, provided by Purkinje cells and mossy fibers respectively (Rowland and Jaeger 2008). Nevertheless, whether and how DCN are able to modify their discharges following theta-patterned sensory stimulation remains unexplored. Herein, we addressed this issue performing single-unit recordings in vivo, from the medial nucleus of anesthetized mice. Our results provide the first evidence that DCN neurons are indeed able to modify their discharge properties following sensory stimulation in vivo, completing the picture of the theta sensory stimulation (TSS) impact on cerebellar neurons discharge in vivo.

5.2 *Materials and Method*

Multiple single-unit recordings were performed from the medial nucleus of C57BL/6 mice (31,4±0.5 days old; n=20) under urethane anesthesia. Recording electrodes were located over the vermis (-7.8 AP, +0,50 ML from bregma), ipsilateral to the stimulus source and lowered perpendicularly to the surface at a depth of 2002±68 μm (n=20). DCN neurons were identified by recording depth, spontaneous activity, stimulus-evoked responses, electrical lesion of the recording site and histological sections. Tactile sensory stimulation was performed using air-puffs (100 pulses- 30 ms- 30-60 psi) delivered to the mouse lips or whisker pad to evoke the neuronal responses. DCN neurons responses were revealed in real-time by making peri-stimulus time histogram (PSTH) during the on-going experiment. Following 5 minutes of spontaneous activity recording, air-puffs were delivered at 0.5 Hz to reveal the stimulus-evoked responses. Once the responsive neuron was detected, control stimuli at 0.5 Hz were delivered for 20 min. Then, a theta sensory stimulation (TSS: 100 air-puffs at 4 Hz) was delivered, followed by post-induction control at 0.5 Hz for at least 40 minutes. Recordings were analyzed offline using custom-written software in MATLAB and Excel. PSTHs constructed with 5 or 15 ms bin widths and raster plots of 300 trials were used for the analysis. Spike-related changes of the neuronal responses were evaluated from the corresponding PSTHs. Spike-related changes of the responses after TSS over than ± 10% were considered for potentiation or depression. Statistical comparisons were carried out using the unpaired Student's t-test unless otherwise stated or one-way ANOVA in Origin software. Data in the text are reported as mean ± SEM.

5.3 *Results*

Tactile stimulation evoked 3 typical patterns of peaks and pauses in the peri-stimulus-time-histograms (PSTHs): (1) Pure inhibition (pause occurring at 20.23±4.50 ms; duration 28.82±11.42 ms; n=5); (2) excitation followed by inhibition (short-latency peak at 14.10±4.53 ms; duration 13.65±4.54 ms; n=7; Figure 1A); (3) excitation following inhibition (long-

latency rebound peak at 88.34±24.26 ms, duration 17.28±3.42 ms; n=4). We have also observed pure excitation (only short-latency peak; n=2), in these cases the onset of the peak responses (13.10±2.15ms) was similar to that of the above mentioned cells with short-latency excitation followed by inhibition. Strikingly, when the inhibition followed the short-latency excitation, the onset of the pause was delayed, compared to the onset of the pause observed in pure inhibition responses (62.59±7.14 ms, duration 37.33±8.56ms, $p<0.00002$). In some cells, showing short-latency excitation responses, we observed a recurrent long-latency rebound excitation that occurred every 205.6±48.5 ms for 1350.4±265.3 ms (n=2), or a second peak following the first one (second peak delay to the first peak: 16.4±4.2 ms; duration= 16.4±3.6ms; n=2). The TSS protocol induced significant amplitude changes in DCN neurons responses, though lasting for no longer than 30 minutes: increase of peak or pause amplitudes in 10 neurons (peak: 41.2±17.6%, n=5, $p<0.01$; pause: 28.4±10.1%, n=5, $p<0.003$; Figure 2A); decrease of peak or pause amplitudes in 8 neurons (peak: -18.5±5.2%, n=4, $p<0.02$; pause: -20.3±4.6%, n=4, $p<0.005$; Figure 2B). No significant amplitude changes were observed in 2 neurons. Interestingly, we did find a positive correlation between the variation of peak and pause amplitudes after TSS, in cells showing short-latency excitation followed by inhibition, with a tendency of the pauses amplitude to increase or decrease according with the corresponding variation of the peaks amplitude (and/or viceversa) ($R^2=0.60$, $p<0.02$, n=6).

5.4 *Discussion and Conclusions*

In in vivo urethane anesthetized mice, facial tactile stimulation evokes typical patterns of peaks and/or pauses responses in the PSTHs, which likely reflect the different combinations of excitatory and inhibitory synaptic inputs they may receive. The average latency of the inhibitory responses was well in line with the signal transmitted through granule cell-Purkinje cell pathway to DCN. The onset of the short-latency excitation well-matched with the delay of the signals known to be transmitted to DCN through the trigeminal pathway. The long-latency rebound excitation following the inhibition was likely due to disinhibition of DCN discharge

caused by a pause in Purkinje cells activity, which is known to determine a rebound increase in DCN neurons firing (Dykstra et al. 2016). Sensory stimuli organized in theta-patterns (TSS) proved able to induce spike-related amplitude changes in DCN responses, showing transient but significant increases or decreases of their discharge. In particular, when both short-latency excitation (mossy fibers driven) and inhibition (Purkinje cells driven) coexisted in the same neuron, a positive correlation was revealed in these two changes of neuronal response. These results suggest an interplay between excitatory and inhibitory synaptic inputs onto DCN neurons that is likely to affect the direction of the TSS-induced changes. Taken together these results suggest that theta-pattern stimulation engages multiple discharge modifications distributed along Purkinje cell-DCN and mossy fiber-DCN pathways. Excitatory and inhibitory plasticity impinging on nuclear neurons could act synergistically to modify processing and integration of sensory information, playing a crucial role in shaping the cerebellar output.

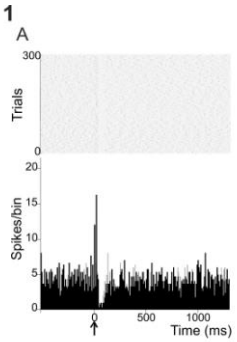

FIGURE 1 | Raster plot and PSTH of a representative DCN response to sensory tactile stimulation. (A) Samples of cell responding with short-latency excitation followed by inhibition.

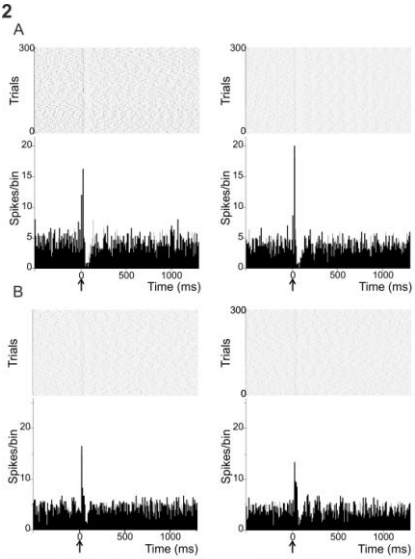

FIGURE 2 | Raster plots and PSTHs of representative DCN responses to TSS. (2A,2B) Samples of peaks amplitudes before and after TSS. (A) DCN neurons showed an increase of peak amplitude after TSS. (B) TSS induced a decrease of peak amplitude.

6. Cerebello-prefrontal cortex connection investigated by *in vivo* single-unit recordings

Letizia Moscato[1], *Lisa Mapelli*[1], *Egidio D'Angelo*[1, 2]

[1] University of Pavia, Dept. of Brain and Behavioral Sciences, Italy

[2] Brain Connectivity Center, C. Mondino National Neurological Institute, Italy

In preparation

The anatomical connection between the cerebellum and cerebral cortical areas subserving higher order functions, such as the medial prefrontal cortex (mPFC), suggests a potential cerebellar contribution to cognition. Abnormal cerebellar-prefrontal cortex interactions result in a subthreshold dopamine release in the mPFC which is associated with several cognitive dysfunctions, suggesting that the cerebellum plays a key role in determining the correct dopamine levels that guarantee mPFC appropriate functioning.

Herein, we characterized neurons responses in the prelimbic cortex (PrL), that is part of the mPFC, following electrical stimulation of the contralateral fastigial or dentate nuclei. Furthermore, using selective dopamine receptors antagonists, we pharmacologically explored whether and how the dopamine efflux, supposedly induced in the PrL by cerebellar stimulation, modulated the evoked PrL responses. PrL neurons responded to cerebellar nuclei stimulation with two typical discharge patterns, both characterized by an initial pause in PrL activity, followed only in some cases by a burst. The co-application of selective dopamine D1-like and D2-like receptor antagonists (SCH23390 and sulpiride, respectively) showed a modulatory effect on both PrL neurons spontaneous firing rate, and on responses amplitude and duration. Notably, PrL pause responses were not abolished, although their duration was significantly reduced. The administration of D1-like and D2-like receptor antagonists promoted a significant pause amplitude increase in concert with an increase in firing

frequency, most likely reflecting the same phenomenon. Overall, these findings demonstrate physiological interactions between the cerebellum and the PrL of the mPFC, providing insights of a complex functional interplay between these two regions.

6.1 INTRODUCTION

Although the cerebellum is predominantly considered a sensorimotor structure, several findings stand for a pivotal cerebellar role in non-motor functions as well. Anatomical tracing studies in humans showed a prominent interconnection between the cerebellum and neocortical areas involved in cognition, including the prefrontal cortex *(Palesi et al. 2015)*, and *in vivo* electrophysiological studies in rodents supported the same finding, reporting a bidirectional connection between these brain regions *(Watson et al. 2014; Watson et al. 2009)*.

In recent years, understanding the nature of the connection between the cerebellum and the prefrontal cortex became the goal of an increasing number of studies. Abnormal prefrontal-cerebellar interactions co-occur in several cognitive disorders, ranging from schizophrenia to autism spectrum disorders *(Andreasen et al. 1996; Andreasen and Pierson 2008; Fatemi et al. 2012; Whitney et al. 2008)*, and the neuronal mechanisms underlying these pathologies have not been unraveled yet, engaging new investigations. Structural and functional abnormalities, such as cerebellar hypoplasia, reduced number of Purkinje cells, increased volume of frontal lobe cortex, positively correlate with autistic symptoms *(Palmen et al. 2004; Vargas et al. 2005; Whitney et al. 2008)* whilst schizophrenic patients exhibit abnormalities in the cerebellar vermis *(Henze et al. 2011; Lawyer et al. 2009; Okugawa et al. 2007)* and a reduction of the cerebellar peduncle white matter, which is known to contain fibers that connect the cerebellum with cerebral cortical areas *(Kyriakopoulos et al. 2008)*.

It is noteworthy that decreased dopamine release in the mPFC has been associated with autism and schizophrenia *(Bennett 1998; Ernst et al. 1997)* suggesting that higher cognitive functions may depend on a finely

regulated dopaminergic transmission to the mPFC. Electrophysiological and amperometric studies have shed light, respectively, on the existence of a cerebello-prefrontal cortex bidirectional connection *(Watson et al. 2014; Watson et al. 2009)* and cerebellar modulation of mPFC dopamine release in anesthetized rodents *(Mittleman et al. 2008; Rogers et al. 2011)*. It has been reported that the electrical stimulation of the fastigial nucleus evokes typical response patterns in the prelimbic subdivision (PrL) of the mPFC *(Watson et al. 2014)*. This connection is reciprocal, thus the electrical stimulation of the PrL evokes field potential responses in Purkinje cells (PCs) of the cerebellar vermis, although smaller amplitude responses were present in the paravermal and lateral cerebellar cortex *(Watson et al. 2009)*. Moreover, it has been shown that the stimulation of the dentate nucleus (DN) of the cerebellum evokes dopamine release in the mPFC of urethane-anesthetized mice via dopaminergic projection from the ventral tegmental area (VTA) or glutamatergic projections from the mediodorsal and ventrolateral nuclei of the thalamus *(Rogers et al. 2011)*. The VTA contains also GABAergic neurons which project to the PFC and they may provide their contribution via GABAergic modulation *(Hnasko et al. 2012; Omelchenko and Sesack 2009)*. Furthermore, the cerebellum may also affect the prefrontal firing rate and dopamine release via basal ganglia. In fact, the stimulation of the DN influences neuronal firing rates *(Li and Parker 1969; Ratcheson and Li 1969)* and dopamine levels in the substantia nigra and caudate nucleus (Nieoullon et al. 1978) which in turn project to the PFC *(Maurice et al. 1999; Middleton and Strick 1994)*.

However, the mechanisms through which the cerebellum affects the dopaminergic transmission to the PFC are largely unknown. Dopamine is a neuromodulator and it is not an excitatory or inhibitory neurotransmitter (Seamans and Yang 2004). It has been reported to exert a mixture of contrasting effects on pyramidal cells and local interneurons engaging several classes and subtypes of dopamine receptors which are also mixed and not uniformly distributed among prefrontal neurons membranes *(Floresco and Magyar 2006; Floresco et al. 2006)*. In this perspective, whether the dopamine modulation is attributable to its direct actions on pyramidal neurons or indirect modulation via interneurons becomes also difficult to explore. It has been shown that dopamine exerts its

neuromodulatory action by decreasing spontaneous and evoked activity in mPFC neurons *(Gulledge and Jaffe 1998)*, although other findings report a dopamine-mediated increase in neuronal excitability *(Buchta et al. 2017; Otani et al. 2015; Trantham-Davidson et al. 2008).* Dopaminergic fibers target several brain areas and exert heterogeneous effects within the same local circuit as well as across networks. Several studies report a dopamine-mediated inhibitory modulation of hippocampal pyramidal cells excitability *(Cantrell et al. 1997; Pockett 1985; Stanzione et al. 1984)*, whereas other findings provide evidences of an excitatory effect on the same target cells *(Malenka and Nicoll 1986; Pedarzani and Storm 1995)*, puzzling the picture of the dopamine modulatory role and making difficult to reconcile reports of dopamine impact on specific cells types within a given region.

Herein, we characterized mPFC PrL neurons responses following the electrical stimulation of the contralateral cerebellar fastigial and dentate nuclei. Furthermore, using selective dopamine receptors antagonists, we pharmacologically explored whether and how PrL neurons spontaneous and evoked activities are influenced by the dopaminergic system. PrL neurons responded to cerebellar stimulation with two typical discharge patterns, both characterized by an initial pause in spontaneous activity, that could be followed in some cases by a burst. The co-application of selective dopamine D1-like and D2-like receptor antagonists (SCH23390 and sulpiride, respectively) did not abolish PrL pause responses but it had a modulatory effect on both PrL neurons spontaneous firing rate, and responses amplitude and duration. The administration of the D1-like and D2-like receptor antagonists promoted a significant pause amplitude increase in concert with an increase in firing frequency. These amplitude changes were likely driven by the increased firing frequency itself, promoted by dopamine receptors antagonists.

Overall these findings demonstrate physiological interactions between the cerebellum and the PrL of the mPFC, providing insights of a functional interplay between these two regions. In particular, these findings become relevant for two main perspectives. First, they provide new clues in the investigation of cerebello-prefrontal cortex connection, which is poorly understood even in the nature of this connection. While the cerebellum-mediated dopaminergic release in the mPFC has gained some attention in

the last decade, very little is known about the nature and rules of this connection. Here, we found that the cerebellar drive over the mPFC goes beyond the dopaminergic control, since the responses were not abolished by dopamine receptors blockade, although their duration decreased. Secondly, concerning the impairments in various cognitive disorders displaying abnormalities in the cerebellum-mediated dopaminergic transmission to the mPFC, the present study provides a new framework for understanding neuronal correlates underlying dopamine-related cognitive deficits involving the mPFC.

6.2 MATERIALS AND METHODS

Multiple single-unit recordings were performed from the mPFC of C57BL/6 mice of either sex (30.02±0.21 days old; n=71) under urethane anesthesia. Urethane exerts its anesthetic action through multiple weak effects, including a 10% reduction of NMDA, 18% reduction of AMPA and 23% enhancement of GABA-A receptor-mediated currents *(Hara and Harris 2002)* and therefore it unlikely affects stimulus evoked responses and dopamine mediated effects on mPFC neurons.

Surgical Procedures

Mice were deeply anesthetized with intraperitoneal injections of urethane (Sigma). Induction (1.3g/kg urethane dissolved in 0.9% NaCl) was followed by 3-4 booster injections (10% of the induction dose), administrated every 30 minutes, in order to stabilize deep anesthesia. The level of anesthesia was monitored by evaluating the leg withdrawal after pinching and spontaneous whisking. The animal was then placed on a custom-built stereotaxic table covered with a heating plate (HP-1M: RTD/157, Physitemp Instruments Inc, Clifton, NJ, USA). Body temperature was monitored with a rectal probe and maintained at 36°C through a feedback controller (TCAT-2LV controller, Physitemp Instruments Inc, Clifton, NJ, USA). The mouse head was fixed over the bregma to a metal bar connected to a pedestal anchored to the stereotaxic table. The exposure of the cerebellar surface was performed following

surgical procedures. Cutaneous reflexes were reduced by subcutaneous application of lidocaine (0.2ml; Astrazeneca), the skin and muscles were removed and a subsequent craniotomy was performed over the cerebellum and mPFC to expose the surface to electrodes placement (**FN**: -7.8 AP, +0.50 ML, +2.4 DV; **DN**: -7.8 AP, +2.5 ML, +2.6 DV; **PrL**: +2.8 AP, 0.25 ML, +0.6 DV). The *dura mater* was carefully removed and the surface was covered with saline solution (NaCl 0.9%; Sigma) to prevent drying.

Electrophysiological extracellular recordings

Quartz-coated platinum/tungsten fiber electrodes (1-5MΩ; Thomas Recording, Giessen, Germany) were used for neuronal recordings. Recording electrodes were positioned over the mPFC, contralateral to the stimulus source, and lowered perpendicularly to the surface down to a depth of 682.27±34.50 μm (n=71). The electrophysiological signals were digitized at 25 kHz, using a 300-5000 Hz band-pass filter, amplified and stored using a RZ5D processor multi-channel workstation (Tucker-Davis Technologies, Alachua, FL, USA). PrL neurons were identified by histological tissue processing of the electric lesions made at the end of each experiment through the recording electrodes. The location of the stimulating electrode (placed onto the FN or DN) was verified by histological tissue processing of the electric lesion.

Electrical stimulation

Electrical stimulation (21 pulses, 100Hz, 100 μA, repeated every 5 s) was performed using a bipolar tungsten electrode (0.5 MΩ; World Precision Instruments Inc, Sarasota, FL, USA) connected to a stimulator unit through a stimulus isolator. These stimulus parameters have already proved able to drive cerebellar nuclei output. Indeed, it has been reported that trains of stimuli (100 pulses, 100Hz, 100 μA) delivered every 5 seconds to the FN are required to drive the cerebellar output, evoking detectable responses in mPFC neurons (Watson et al. 2014). Similar stimulation parameters (10 stimuli, 50Hz, 100pA) pilot also FN output to the vestibular nuclei (Bagnall et al. 2009). Furthermore, high-frequency cerebellar stimulation (100 pulses, 50 Hz, 200 μA) is reported to evoke prominent dopamine efflux in the mPFC (Mittleman et al. 2008). By

reconciling these reports, we have defined a similar stimulation protocol which has proved to be effective in evoking cortical neurons responses and likely dopamine efflux. The stimulating electrode was lowered to the surface down to a depth of 2400 or 2600 µm, in order to stimulate FN or DN, respectively.

Over 71 PrL cells recorded, we examined the effect of FN stimulation in 10 cells, in order to characterize PrL response patterns following FN stimulation.

In 38 out of 71 cells, we characterized PrL response patterns following DN stimulation.

In 12 out of 71 cells the antagonists of dopamine receptors were superfused, after 10 min control of PrL neurons responses to DN stimulation. D1-like and D2-like dopamine receptor antagonists were co-applied and PrL neurons were recorded for further 30 min, during which the same pattern of electrical stimuli was delivered to the DN.

11 out of 71 cells were recorded in control condition for 40 min (antagonists were not applied and 21 pulses at 100Hz, 100 µA, repeated every 5 s, were delivered to DN), to rule out possible spurious changes due to intrinsic response amplitude fluctuations overtime which may create bias against the effects of the antagonists.

Pharmacology

All drugs were superfused in a subset of experiments onto the PrL surface [44 mM SCH23390 hydrochloride (selective D1-like antagonist) and 36mM (S)-Sulpiride (selective D2-like dopamine antagonist; abcam]. The drugs were co-applied immediately after the control recording period and then maintained throughout.

Histology

The location of recording electrodes in the PrL was confirmed by histological tissue processing of the electric lesions made after the end of each experiment. The electric lesion was performed applying 20 µA current

for 20s, using the same recording electrodes connected to a stimulator unit through a stimulus isolator. The location of the stimulating electrode (placed into the FN or DN) was verified by histological tissue processing of the electrical injury due to the electrical stimulation (100 μA) during the experimental condition. Histological tissue processing was performed as follow. After the mouse was perfused transcardially with Phosphate-Buffered Saline (PBS) followed by 4% formaldehyde, the fixated brain was removed and 20-μm-thick histological sections were stained with toluidine blue. The histological confirmation of the recording/stimulation sites was obtained by microscopic observation of the stained sections.

Data analysis

Recordings were acquired using Openex software (Tucker-Davis Technologies) and analyzed offline using custom-written routines in MATLAB and Excel. Raw traces were analyzed and sorted offline using SpikeTrain (Neurasmus BV, Rotterdam, Netherlands) running under MATLAB (Mathworks, MA, USA). For convenience, peri-stimulus time histograms (PSTHs) constructed with 100 ms bin width were used for the analysis of responses to stimulation, normally consisting of pauses, sometimes followed by peaks, emerging from background discharge, whilst 20 ms bin width was used to measure latency and duration of the responses. Pauses and peaks were identified as PSTH modifications exceeding once the standard deviation of the basal frequency in the pre-stimulus period. 30 out of 71 units did not show any significant change with respect to this criterion.

The effects of the antagonists were evaluated by measuring the corresponding changes in PSTHs pauses amplitude compared to control response. To this aim, we considered the post-antagonists administration response (computed over the 10, 20 and 30 min after antagonists administration) that exceeded once the standard deviation of the control response (computed over 10 min before agonists administration). Positive changes were considered as antagonists-mediated increase and negative changes were considered as a decrease of the neuronal responsiveness to the stimulation.

To test whether dopamine receptor antagonists influence spontaneous firing rate and coefficient of variation of the inter-spike interval (CV2, which provides information about the spiking regularity), firing rate and CV2 were measured after antagonists superfusion and compared to control measurements.

Fitting to the data was performed using routines written in OriginPro8 (OriginLac co., MA, USA).

Statistical comparisons were carried out using paired or unpaired Student's *t*-test. Data in the text are reported as mean ± SEM.

6.3 RESULTS

Single-unit recordings were performed from the PrL of the mPFC in urethane anesthetized mice. All units were spontaneously active and showed a basal frequency of 2.29±0.25 Hz (n=71; Fig. 1A,B), in agreement with previous reports of PrL neurons spontaneous activity in urethane anesthetized rodents *(Watson et al. 2014)*. The recording/stimulating sites were marked by electrical lesion and confirmed histologically (Fig. 2A,B).

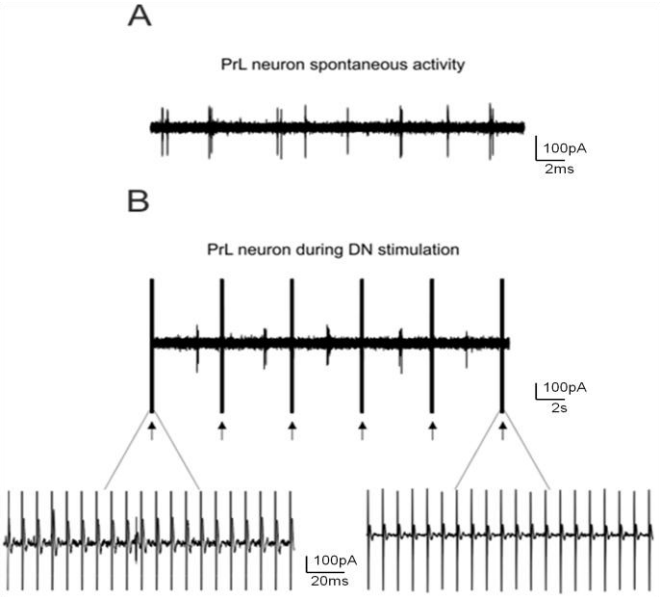

Figure 1. Extracellular recordings from PrL neurons *in vivo*. A) Example of PrL neuron spontaneous activity. **B)** Example of PrL neuron activity during the electrical stimulation of the DN nucleus.

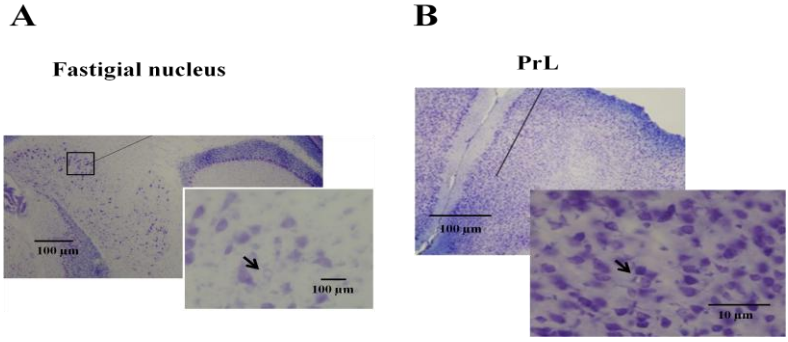

Figure 2. Histological confirmation of the recording/stimulating sites. A) Toluidine blue stained coronal cerebellar slice showing the electrical lesion (arrow) made by the stimulating electrode in the fastigial nucleus. **B)** Sagittal section showing electrical lesion made by the recording electrode in the PrL.

FN stimulation impact on PrL neurons

We characterized PrL evoked responses following the FN stimulation in 10 out of 71 PrL cells. Over 10 cells recorded, PrL neurons responded to the FN stimulation with two typical response patterns: 30% (n=3) showed pure inhibition (consisting in a spike firing suppression consequent to the stimulation and represented by a PSTH pause; Fig.3A), and 20% (n=2) biphasic response consisting in a long-latency rebound excitation following the initial inhibition (consisting in a post-inhibitory firing increase, represented by a PSTH peak following the initial pause; Fig.3B). 50% (n=5) of the cells did not respond to the stimulation, with respect to our criterion (for details see material and method).

Pure pause responses occurred with a latency of 12±4.8 ms (duration: 220±20 ms; n=3). Biphasic responses showed a pause latency of 13.33±3.33 ms (duration: 140±60 ms; n=2) and peak latency of 250±10 ms (duration 110±90 ms; n=2).

Spontaneous firing rate and CV2 (measured when electrical stimuli were not yet delivered) did not differ from the spontaneous firing rate and CV2 measured after starting with FN stimulation, in which repetitive electrical stimuli were delivered to FN every 5s (p=0.3 and p=0.1, n=5; respectively; paired Student's t-test) suggesting that the stimulation protocol did not modify PrL spontaneous activity.

These results are in agreement with previous *in vivo* findings of PrL neurons responses to FN stimulation *(Watson et al. 2014)*.

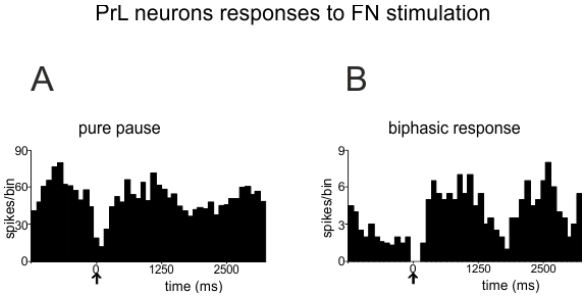

Figure 3. PrL response patterns to FN stimulation. Exemplar PSTHs obtained from PrL neurons showing two different response patterns to the electrical stimulation of FN. The black arrow indicates the stimulus onset. **A)** Pure inhibition. **B)** Biphasic response.

DN stimulation impact on PrL neurons

In 38 out of 71 cells, we characterized PrL evoked responses following the DN stimulation. Over 38 cells recorded, PrL neurons showed two constant response patterns, consisting in pure inhibition (24%) and biphasic response (16%). Pure pause responses occurred with a latency of 11.11±4.84 ms (duration: 214.28±14.93 ms, n=9; Fig.4A). Biphasic responses showed a pause latency of 10±4.47 ms (duration: 153.33±24.03 ms, n=6) and peak latency of 193.33±17.63 ms (duration 150±29.55 ms; n=6; Fig.4B). 60% (n=23) of the cells did not respond to the stimulation, with respect to our criterion.

Moreover, pure pause responses showed a positive correlation between pause depth and basal frequency, with a tendency of the pause to increase or decrease, according to the corresponding variation of the basal frequency (and/or vice versa), whilst biphasic responses display a positive correlation between peak and pause amplitude changes, suggesting a possible interplay between cellular mechanisms underlying these two different component of the response (Fig. 5A,B). Interestingly, pause amplitudes in cells showing biphasic responses did not correlate to basal frequency, as the pure pause responses did. Taken together, these data

suggested that the two different response patterns might be characteristic of two different neuronal types. Indeed, the presence of the post-inhibitory rebound excitation suggests the intervention of different cellular mechanisms. It is therefore reasonable to cluster these responses into two separate categories.

Spontaneous firing rate and CV2 (measured when electrical stimuli were not delivered) did not differ from the spontaneous firing rate and CV2 measured after starting with DN stimulation, in which repetitive electrical stimuli were delivered every 5 s (p=0.1 and p=0.6, respectively; paired Student's t-test) suggesting that the stimulation protocol did not modify PrL spontaneous activity. This was true for both types of responses.

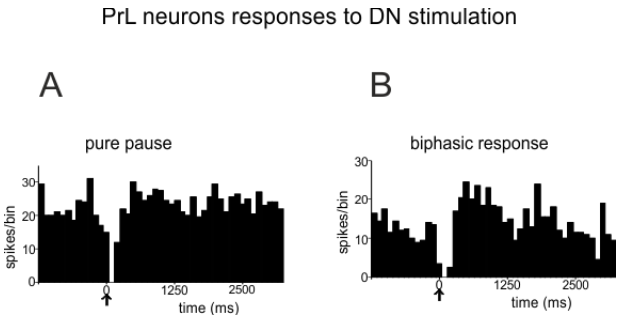

Figure 4. PrL response patterns to DN stimulation. Exemplar PSTHs obtained from PrL neurons showing two different response patterns to DN electrical stimulation. The black arrow indicates the stimulus onset. **A)** Pure inhibition. **B)** Biphasic response.

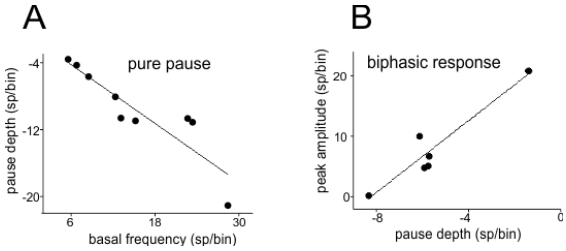

Figure 5. Characterization of PrL responses. A) Positive correlation found between pause depth and basal frequency in cells responding with pure pause (R^2=0.78, p(F)=0.001, n=9). **B)** Positive correlation found between pause depth and rebound peak amplitude in cells showing biphasic responses (R^2=0.87, p(F)=0.003, n=6). No correlation was found between pause depth and basal frequency (R^2=0.09, p(F)=0.2, n=6) and between rebound peak amplitude and basal frequency (R^2=0.1, p(F)=0.5).

FN vs. DN stimulation effects on PrL neurons

The FN stimulation evoked pure pause responses with a latency of 12±4.8 ms (duration: 200±20 ms; n=3) whilst pure pause responses following DN stimulation occurred with a latency of 11.11±4.84 ms (duration: 214.28±14.93 ms, n=9). Neither latency nor duration of the responses significantly differed between PrL pause responses to FN or DN stimulation (p=0.9 and p=0.2; unpaired Student's *t*-test). The mean depth of pure inhibitory responses to FN stimulation (-16.17±8.54 spike/bin; n=3) did not significantly differ from pause depth measured in pure inhibitory responses evoked by DN stimulation (-9.56±1.75 spike/bin, n=9; p=0.2; unpaired Student's *t*-test).

In cells showing biphasic response, the onset and duration of the initial pause evoked by FN stimulation (onset: 13.33±3.33 ms, duration: 140±60 ms; n=2) was not significantly different from the onset of pause following DN stimulation (onset: 10±4.47 ms, duration: 153.33±24.03 ms, n=6) (p=0.9 and p=0.2, respectively; unpaired Student's *t*-test). Neither latency of the peaks after pauses (250±10 ms after FN stimulation (n=2) vs. 193.33±17.63 ms after DN stimulation (n=6)) nor their duration (110±90

ms after FN stimulation vs.150±29.55 ms after DN stimulation) differed after FN or DN stimulation (p=0.6 and p=0.8; unpaired Student's *t*-test). The mean amplitude of peaks after pauses responses to the FN stimulation (3.43±0.2 spike/bin; n=2) did not significantly differ from those evoked by DN stimulation (8.02±2.86 spike/bin, n=9; p=0.4; unpaired Student's *t*-test). Surprisingly, although PrL neurons responses to FN vs DN stimulation showed no differences, the spontaneous firing rate of the groups of neurons responding to FN or DN was statistically different (p=0.0004; unpaired Student's *t*-test). This result might suggest that different subpopulation of PrL neurons are contacted by FN and DN functional connections. Nevertheless, it has to be noted that the different size of the compared samples, and in particular the low number of observations of FN stimulation responses, will require additional experiments in order to further explore this issue.

Effect of D1-like and D2-like receptor antagonists on evoked PrL inhibitory responses.

The effect of dopamine antagonists on evoked PrL inhibitory responses was studied by measuring the corresponding amplitude changes in PrL responses. In addition, evoked firing frequency and CV2, after the co-administration of the antagonists, were measured and compared to control measurements.

12 out of 71 cells were recorded for 10 min in control condition, applying the same stimulation used above on DN. Then, D1-like and D2-like dopamine receptor antagonists were co-applied and maintained for until the end of the experiment, and PrL neurons were recorded for further 30 min, during which the same stimulation as in control was delivered to the DN. Again, DN stimulation evoked two constant response patterns, consisting, in most of the cases, in an initial pause only, although a smaller population of PrL neurons exhibited a biphasic behavior in which the initial inhibition was followed by a subsequent excitation. Therefore, we clustered PrL neurons into two groups based on their response patterns, and we separately analyzed the effect of dopamine antagonist on each cluster. Over

12 cells recorded, 75% (n=9) showed initial pause only, 17% (n=2) showed biphasic responses, 8% (n=1) cell did not respond with respect to our criterion.

11 out of 71 cells have been recorded in control condition (i.e. stability recordings, in which antagonists were not applied while the same stimulation pattern as above was delivered to DN) for a duration similar to the experiments reported above, in which dopamine receptors antagonists were co-applied (40 min). Over 11 cells recorded for stability recordings, 73% (n=8) responded with an initial pause only, 18% (n=2) exhibited biphasic response, 9% (n=1) did not respond.

As specified above, our data suggest that two different classes of neurons might be involved in producing the two response patterns observed (pure pause or biphasic). Given the little amount of observations of the biphasic response in these experiments, only the analysis concerning the pure pause responses will be reported.

First of all, dopamine receptors antagonists superfusion determined a significant increase in spontaneous PrL neurons firing, evident after 10 min from the drugs application on the brain surface (after 20 min of antagonists administration: +94.90±0.61%, n=9, p=0.02).

Interestingly, the administration of the selective dopamine receptors antagonists did not abolish inhibitory evoked responses in PrL (this is true for both response patterns, Fig.6A,B). Time courses of the normalized pause depth changes (in which only cells displaying pure pause responses were included) showed a significant depth increase, compared to control measurements (Fig.7A). The increase became significant 10 min after the antagonists administration and it remained significant within the next 20 minutes (Fig.7B,C). Nevertheless, this effect on pause response depths closely followed the spontaneous firing rate increase (Fig.8A,B). A difference was detected in pause duration before and 20 min after dopamine receptors antagonist perfusion (-10.87±10.62%; p=0.03 paired Student's *t*-test).

As already specified above, cells showing a biphasic behavior have been excluded from the time courses data-set. Indeed, the presence of the post-inhibitory rebound excitation suggests the intervention of different cellular mechanisms, that are likely to be associated with a different distribution of dopamine receptors. Moreover, the cellular mechanisms underlying inhibitory and post-inhibitory rebound increase might therefore influence each other, as suggested by the positive correlation found in control experiments, making reasonable to cluster them in a separated category. Furthermore, time courses of the normalized pause depth changes have not been provided for the biphasic response category because of the small number of observations. Nevertheless, it could be worth reporting here that these preliminary data suggest an opposite trend after drugs co-application, in which a decrease in pause depth is accompanied by a decrease of the spontaneous firing frequency (data not shown).

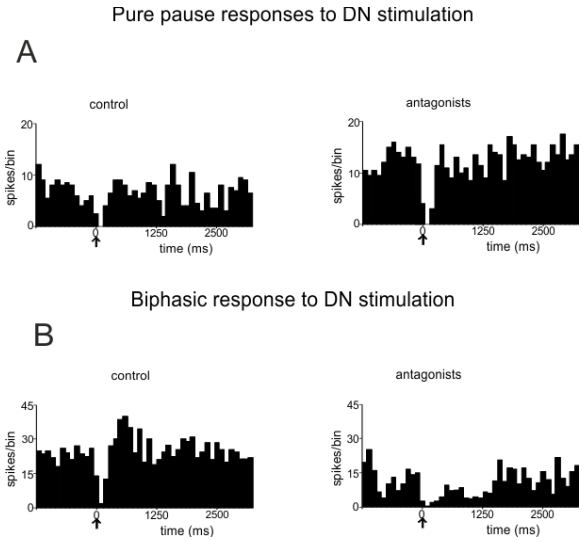

Figure 6. Comparative exemplar PSTHs of PrL response patterns before and 20 minutes after antagonists administration, showing that evoked inhibitory responses are not abolished by the antagonists application. **A)** Pure pause responses. **B)** Biphasic responses.

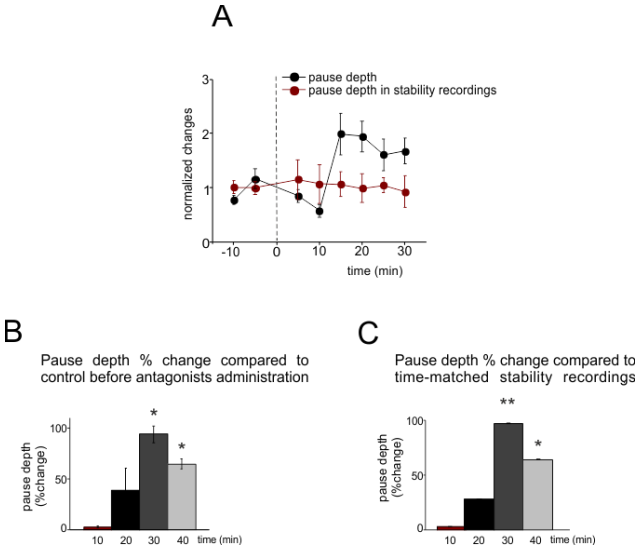

Figure 7. Spike-related amplitude changes after D1-like and D2-like dopamine receptors antagonists co-administration. A) Normalized time-course of pause depth average changes normalized to the control period before antagonists administration (*dashed line*), in neurons displaying pure inhibitory responses. **B)** The histograms show the average pause depth percent changes with time (10, 20 and 30 minutes after antagonists administration), normalized to their control period before the antagonists administration, in PrL neurons responding with pure inhibition. **C)** The histograms show the average pause depth percent changes with time (10, 20 and 30 minutes after antagonists administration), normalized to the corresponding average pause depth of the stability recordings in which the antagonists were not administrated, in PrL neurons responding with pure inhibition. * $p<0.05$, ** $p<0.01$, *** $p<0.001$

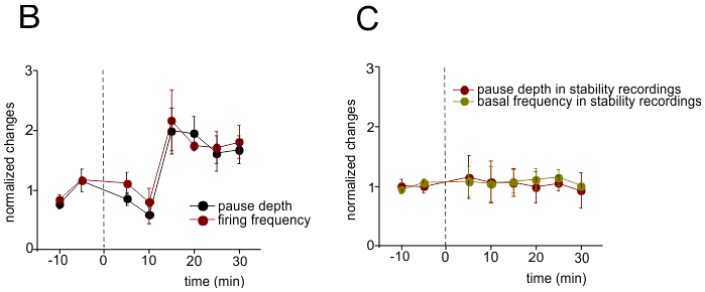

Figure 8. Firing frequency changes following antagonists administration. A) Time course of normalized pause depth changes after antagonists superfusion, normalized to 10 minutes of control period before antagonist administration (*dashed line*), compared to the corrisponding normalized changes in basal frequency after antagonists superfusion. **B)** Time course of normalized pause depth in stability recordings (antagonists were not applied), normalized to the first 10 minutes of stability control, compared to the corrisponding normalized basal frequency in stability recordings.

6.4 DISCUSSION

PrL neurons were spontaneously active and they responded to electrical stimulation of cerebellar nuclei with two different response patterns. In most cases, the cerebellar stimulation evoked pure pause responses (71% of all the neurons responding to FN or DN stimulation), less frequently followed by a rebound peak (29% of all the neurons responding to FN or DN stimulation).

Nature of the PrL evoked responses

Cerebellar stimulation evoked PrL pauses responses with a latency of about 13 ms. Our findings closely matched with previous electrophysiological studies in which the stimulation of the FN resulted in similar short latency pause responses in PrL neurons firing in rats *(Watson et al. 2014)*. Moreover, the stimulation of the DN was previously proved able to evoke short latency field potential responses in the prefrontal cortex of monkey *(Sasaki et al. 1979)*.

In some cases, cerebellar stimulation evoked biphasic responses in which the initial pause was followed by a delayed increase in firing. These two different response patterns were likely to depend on different neuronal types, since their different properties in terms of correlation with spontaneous activity and the absence or presence of a rebound-like peak following the pause in the PSTHs. It seemed reasonable therefore to consider the neurons responding with pure pause or biphasic response as different clusters of cells. Interestingly, this difference seemed to be maintained in the experiments in which dopamine receptors were blocked (although these are only preliminary observations). Indeed, PFC neurons exhibit a mixed expression of dopamine receptor subtypes which might explain, at least in part, the heterogeneity of the responses. It has been reported that the cerebellar stimulation is able to evoke dopamine release in mPFC neurons and that dopamine exerts its modulatory effect via activation of D1-like and D2-like dopamine receptors. These receptors are not uniformly distributed among PrL neurons, likely generating heterogeneous combinations of response patterns. *In vitro* studies reported that dopamine has a temporally biphasic effects on GABAergic inputs to pyramidal neurons of PFC, causing an initial reduction of evoked inhibitory post-synaptic currents (eIPSCs) mediated by D2-like receptors, followed by a delayed increase in eIPSCs amplitude promoted by D1-like receptors. To complicate the picture, several neurons exhibited different response combinations, consisting in sole initial decrease, only delayed increase or they remained unchanged *(Seamans et al. 2001)*. *In vivo* studies reported that dopamine reduced the excitability of PFC pyramidal cells by decreasing the number of evoked spikes and they input resistance via D2-like receptors activation *(Gulledge and Jaffe 1998; Parfitt et al. 1990; Seamans et al. 2001; Sesack and Bunney 1989)*. In contrast, other *in vivo* reports suggested the opposite, providing evidences that the dopaminergic mediated decrease in firing is associated with D1-like receptors activation *(Sawaguchi and Goldman-Rakic 1991; Williams and Goldman-Rakic 1995; Zahrt et al. 1997)*. In this scenario, it is not easy to reconcile reports that might help us understanding the nature of the observed responses. However, it is generally agreed that dopamine influences the neuronal responsiveness manly affecting intrinsic excitability and input resistance,

which in turn results in facilitation or suppression of spontaneous and evoked spiking.

Dopaminergic component of PrL responses to cerebellar stimulation and potential pathways involved

Cerebellar stimulation has been shown to influence mPFC firing and dopamine release via projection from several brain areas such as VTA, thalamus or basal ganglia. Tracing studies reported that VTA receives bilateral projections from lateral and interposed cerebellar nuclei with a contralateral predominance, but not from the fastigial nucleus *(Ikai et al. 1992)*. Moreover, VTA contains GABAergic neurons which have been reported to project to the PFC *(Hnasko et al. 2012; Omelchenko and Sesack 2009)* and they may be responsible for the observed inhibitory responses, at least for those consequent to DN stimulation. Thus, the DN stimulation might engage VTA GABAergic projection to mPFC. Furthermore, the electrical stimulation of the VTA, as well as local application of dopamine, were reported to inhibit spontaneous activity in most PFC neurons *(Pirot et al. 1992)*, corroborating our findings, which provide evidence of the excitatory effect on PrL neurons activity by antagonizing dopamine receptors. Interestingly, the inhibitory effect observed in our data following cerebellar stimulation could be explained, at least in part, by the dopaminergic system activation, suggesting that inhibitory afferences to the PrL are involved. A possible candidate might be the GABAergic projections starting from the VTA, as cited above. Moreover, our data support the idea that cerebellar drive over the mPFC is modulated by the dopaminergic system (since response duration is modified in absence of responsiveness to dopamine), but it is not completely explained by that (since the response to cerebellar activation is present even after blocking dopaminergic receptors).

Concerning the inhibitory responses following the FN stimulation, they might be evoked via thalamic pathway. Indeed, FN projections might reach the PFC through glutammatergic thalamic nuclei projection which indirectly promote pyramidal neurons inhibitory responses via local inhibitory interneurons activation. This speculation sinks its roots into the hypothesis that DCN neurons reach the PFC through different pathways

according to their function. The lobule VII of the vermis, in which fastigial nuclei lie, deep in the cerebellar white matter, is a cerebellar region notoriously involved in the control of eye movements. From this perspective, the logical assumption might be that the connection between FN and higher order regions, such as the PrL, subserves the control and adaptation of eye movements in goal-directed behaviour instead of cognitive information processing *per se*, thus being mediated by a sensory relay station, such as the thalamus. This latter is indeed known to relay cerebellar motor-sensory information related to ocular adaptation and movements, whilst DN, as suggested by its connection with VTA, might subserve cognitive functions. Although fascinating, these hypothesis are mere speculations at the moment, since our data did not support any significant difference in the responses observed in PrL neurons after stimulation of FN vs. DN regions. Nevertheless, our data suggest that two different types of PrL neurons might be involved in responding to cerebellar FN or DN.

6.5 Conclusions

These findings demonstrated effective interactions between the cerebellum and the PrL of the mPFC, providing insights of a functional interplay between these two regions. Although preliminary, our results suggested the existence of at least two distinct classes of cells, among the PrL neurons that receive functional connections from the cerebellum. Moreover, our data support a predominant role of the dopaminergic modulation of PrL neurons activity, suggesting the possibility that the two different classes of neurons reported above might respond differently to the dopaminergic input. Interestingly, the pause in PrL neurons firing following cerebellar stimulation was not mediated by the dopaminergic system, suggesting that cerebellar drive over the PrL might go beyond the modulatory role investigated so far. Indeed, the high majority of the investigations of the cerebellar influence on the prefrontal cortex is related to the cerebellum-induced dopaminergic release, as a key determinant in various cognitive disorders. The present study provides a new framework for understanding neuronal correlates underlying cognitive deficits

characterized by impaired cerebello-prefrontal connections, being aware that the altered dopaminergic control over the mPFC might be only a part of the story.

7. Cerebellar potentiation and learning a whisker-based object localization task with a time response window

Rahmati N[1], Owens CB[1], Bosman LW[1], Spanke JK[1,2], Lindeman S[1], Gong W[1], Potters JW[1], Romano V[1], Voges K[1], Moscato L[1], Koekkoek SK[1], Negrello M[1], De Zeeuw CI,2[1,2]

[1]Department of Neuroscience, Erasmus MC, 3000 CA, Rotterdam, The Netherlands, and [2]Netherlands Institute for Neuroscience, Royal Academy of Arts and Sciences, 1105 BA, Amsterdam, The Netherlands.

Journal of Neurosci. 2014 Jan 29; 34(5):1949-62. doi: 10.1523/JNEUROSCI.2966-13.2014.

Whisker-based object localization requires activation and plasticity of somatosensory and motor cortex. These parts of the cerebral cortex receive strong projections from the cerebellum via the thalamus, but it is unclear whether and to what extent cerebellar processing may contribute to such a sensorimotor task. Here, we subjected knock-out mice, which suffer from impaired intrinsic plasticity in their Purkinje cells and long-term potentiation at their parallel fiber-to-Purkinje cell synapses (L7-PP2B), to an object localization task with a time response window (RW). Water-deprived animals had to learn to localize an object with their whiskers, and based upon this location they were trained to lick within a particular period ("go" trial) or refrain from licking ("no-go" trial). L7-PP2B mice were not ataxic and showed proper basic motor performance during whisking and licking, but were severely impaired in learning this task compared with wild-type littermates. Significantly fewer L7-PP2B mice were able to learn the task at long RWs. Those L7-PP2B mice that eventually learned the task made unstable progress, were significantly slower in learning, and showed deficiencies in temporal tuning. These differences became greater as the RW became narrower. Trained wild-type mice, but not L7-PP2B mice, showed a net increase in simple spikes and complex spikes of their Purkinje cells during the task. We conclude that cerebellar processing, and potentiation in particular, can contribute to learning a whisker-based object

localization task when timing is relevant. This study points toward a relevant role of cerebellum–cerebrum interaction in a sophisticated cognitive task requiring strict temporal processing.

7.1 Introduction

Active touch by mystacial vibrissae forms a major source of sensory information for rodents (Carvell and Simons 1990; Hartmann 2009). Head-fixed mice can be trained to exploit such active exploration to associate the position of a stimulation bar in their whisker field with the availability of a water reward (O'Connor et al. 2010a; O'Connor et al. 2010b). Whisker-based object localization has been shown to involve correlated neuronal activity in the barrel cortex (S1) and the whisker motor cortex (M1) (Xu et al. 2012). However, it is unclear whether other brain regions also contribute to such tasks. Given the numerous brain regions involved in whisker control, and their intricate connections (Bosman et al. 2011; Kleinfeld and Deschênes 2011), one may expect other areas to also play a role in whisker-based object localization. Here we focus on the cerebellum, a region important for sensorimotor integration, central to the whisker system, and required for procedural learning and accurate timing of fine movements (Bosman et al. 2010; De Zeeuw et al. 2011; Grodd et al. 2001).

Purkinje cells are the sole output neurons of the cerebellar cortex. Their activity depends on both synaptic and intrinsic plasticity (Gao et al. 2012; Hansel et al. 2001a; Ito 2001). In the absence of calmodulin-activated protein phosphatase 2B (PP2B), both the enhancement of intrinsic excitability of Purkinje cells and long-term potentiation at the parallel fiber-to-Purkinje cell synapses are impaired, resulting in increased simple spike-firing regularity (Schonewille et al. 2010). Purkinje cell-specific PP2B knock-out (L7-PP2B) mice show deficits in motor learning and consolidation, as demonstrated during adaptation of the vestibulo-ocular reflex and eyeblink conditioning (Schonewille et al. 2010). To date, of all currently available cell-specific cerebellar mouse mutants that are not ataxic, the L7-PP2B mutant shows the most prominent deficits in

procedural learning (De Zeeuw et al. 2011; Gao et al. 2012). Yet, when subjected to standard nonmotor tasks, like the Morris water maze, fear conditioning, or social interaction task in which no fine temporal control is required, the L7-PP2B mutants do not show abnormal performance (Galliano et al. 2013).

The primary objective of this study was to investigate whether, and if so to what extent, the potentiation of intrinsic activity and synaptic strength of Purkinje cells in the cerebellum is required for a localization task in which the response has to be given within an allotted response period following the insertion of a bar into the whisker field. To this end, we tested L7-PP2B mice using a modified version of the object localization task introduced by O'Connor et al. (2010a) while subsequently tightening temporal constraints of the response. We demonstrate that L7-PP2B mutants are severely impaired in learning this whisker-based object localization task. The cerebellar contribution to this learning task was further corroborated by electrophysiological recordings showing a net upregulation of Purkinje cell activity during trials in wild-type (WT) mice, but not in L7-PP2B mice. Thus, we show for the first time that this learning task can depend in part on plasticity and/or processing in the cerebellum when response timing is relevant.

7.2 Materials and Methods

The generation of mice lacking functional PP2B in their Purkinje cells has been described previously (Schonewille et al. 2010). Briefly, we used crossings of mice in which the gene for the regulatory subunit (CNB1) of PP2B was flanked by loxP sites (Zeng et al. 2001), with transgenic mice expressing Cre under control of the L7 promoter (Barski et al. 2000). L7-Cre$^{+/-}$-*cnb1*$^{f/f}$ mice (i.e., L7-PP2B mice) were compared with littermate controls (i.e., WT mice), consisting of L7-Cre$^{-/-}$-*cnb1*$^{f/f}$ and L7-Cre$^{-/-}$-*cnb1*$^{+/+}$ mice. All experimental procedures were approved by the institutional animal welfare committee, as required by Dutch law.

LICKING BEHAVIOR.

Since licking behavior was used as the behavioral readout of the localization task (see below), we first assessed the overall performance during baseline licking in 10 female L7-PP2B mice and 9 female WT littermates that were 20–25 weeks old. Baseline licking was measured in the home cages of naive mice by measuring threshold crossings in the junction potential between an aluminum floor plate and the spout of a normal drinking bottle with the use of an AD converter operating at a sample rate of 6 kHz (RZ2, Tucker-Davis Technologies; **Fig. 1***A*). Our experimental design was based on that of the study by (Hayar et al. 2006). Since mice normally lick very sparsely, they were deprived of water for 20 h before the period of experimental testing, which lasted ~1 h. We restricted our analysis of baseline performance to bouts of rhythmic licking, which were defined by the occurrence of at least two licks with a maximal interlick interval of 175 ms (**Fig. 1***A*). Licking during the training paradigm was detected by laser beam crossings at the lickport. To avoid double detections, we used a dead time of 20 ms.

Auto-correlograms with a bin width of 5 ms were made of the lick times in the home cage, as well as during the association task and the object localization task (see below). Side peaks were normalized to the center peak and detected as local maxima. The amplitude of these first side peaks was considered to be the strength of the rhythmicity. Rhythmic licking predominantly occurred at frequencies between 6 and 12 Hz. Further quantitative analysis was performed in this frequency band. Licking was considered to be rhythmic if the first side peak exceeded the average ± 3 SDs of the period between 1000 and 800 ms before each lick.

WHISKING BEHAVIOR.

Since whisking behavior was used as the critical sensory detection mechanism for the localization task (see below), we also assessed the overall performance during free whisking in 11 adult female L7-PP2B and 10 adult female WT littermates (**Fig. 1***E–I*). We decided to keep all whiskers intact. Spontaneous whisker movements in head-restrained mice were recorded with a high-speed video camera (full frame rate 1000 Hz;

A504k camera, Basler), using a red LED panel (λ = 640 nm) as backlight. In addition, videos were made during selected sessions of the training paradigm (see below; **Figs. 2**, **3**, **4**). The latter videos were recorded with a full frame rate of 160 Hz (piA640–210gm camera, Basler) and infrared lighting to avoid luminance of the training environment (λ > 900 nm).

To establish the periods during which the mice actively moved their whiskers, we estimated whisker motion using the BlockMatcher function in Matlab (MathWorks). First, we selected a rectangular region of interest containing the proximal part of the whiskers. This region was sliced into a grid with rectangular blocks. Across contiguous frames, each block was transformed by a rotation and translation, such that the distance between the blocks in consecutive frames was minimized. The whisker motion was calculated as the Pythagorean addition of the translation and the rotation of all blocks (**Fig. 1***F*). To validate the automated algorithms for both whisker motion periods, and for whisker angle and position tracking, we also tracked individual whiskers manually in 25 video fragments. This was done by marking in each frame the position of the follicle and the intersection of the whisker with a line parallel to the body axis at ~1 cm lateral to the whisker pad. It turned out that the motion detection could reliably detect periods during which whisker movements occurred. The extent of whisker movements was further illustrated using SD projection plots of video fragments (ImageJ, National Institutes of Health). During the training paradigms, each video fragment reflected the activity during a single response window (RW; see below). Here we used pseudo-colored SD projection plots to illustrate the whisker movements over time.

The outcome of the motion estimation algorithm was used to truncate the video files in time to process only those periods of the video files that show whisker motion (see below). To this end, the variability in the motion estimation result was evaluated with a sliding window approach that calculated the local SD of the signal. In a second step, this local SD signal was thresholded to identify periods of motion. During the periods in which the whisker moved, we tracked them automatically using the BIOTACT Whisker Tracking Tool (BWTT) with the sdGeneric, stShapeSpaceKalman, ppBigExtractionAndFiltering, and

wdIgorMeanAngle plugins (http://bwtt.sourceforge.net; for details, see (Perkon et al. 2011). Briefly, we first determined the position of the snout in each frame semiautomatically by fitting a template to the snout. After masking the snout and subtracting the unmoved background from each frame, the whiskers themselves were traced in a radial approach. The algorithm detected edges in the frame in consecutive concentric snout-shaped masks around the actual snout mask. Ultimately, we detected the start and end nodes of the fitted line segments, and calculated the angles of the whiskers from these values.

The final BWTT result provided us with the angles of all detected whiskers per video frame. To relate the angles across frames to the tracks, we wrote an algorithm that predicts track values in consecutive frames based on the position and velocity in the angular value as well as the *y*-position of the last video frames. The predicted track values for the next frame were compared with the detected values in the next frame and were assigned according to a minimum deviation approach between them (within reasonable bounds; **Fig. 1***G*).

The frequencies and amplitudes of individual whisking bouts were derived from the automatically tracked whisker movements. We defined a whisking bout as a period of at least three consecutive sweeps with a minimal amplitude of 10°. The frequency was derived from three consecutive sweeps, and the amplitude was defined as the difference between the rostral-most and caudal-most positions during these three sweeps. The tracked whisker was taken from the caudal half of all whisker tracks, preferably the caudal-most full track. The traces in **Figures 3***D* and **4***D* were made from videos with a lower frame rate (160 Hz) and infrared illumination. To account for changes in the number of visible whiskers across frames (e.g., because of overlapping or merging with the snout mask during a retraction), we discarded the whiskers with positions >75% and <25% of the position distribution, which tend to disappear from the frame, thereby keeping the ones close to the center of the whisker field. In each frame, the whisker position distributions were calculated from the cumulative distribution of whisker positions derived from 10 frames before and after the frame of interest.

HABITUATION AND ASSOCIATION STAGE.

We prepared 14 female L7-PP2B mice and 16 female WT littermate controls, all of which were 20–25 weeks of age and carried a body weight of 22–25 g, for behavioral testing. These mice received a magnetic pedestal that was attached to the skull above bregma using Optibond adhesive (Kerr Corporation) under isoflurane anesthesia (2–4% v/v in O_2). Postsurgical pain was treated with 5 mg/kg carprofen (Rimadyl, Pfizer) and 5 mg of lidocaine (Braun). After 2 d of recovery, mice were put on water restriction (1 ml/d), while food was available *ad libitum*. On the fourth, fifth, and sixth days of water restriction, mice were put in a head-fixed position using the magnetic pedestal and habituated to the experimental setup for one 15 min session per day. During these sessions, water drops (~20 μl/lick) were triggered upon breaking the laser beam of the lick port. The mice did not receive extra water after the habituation sessions.

Upon completion of the habituation phase, the mice progressed to the association task to ensure that the L7-PP2B mutants and WT mice had similar levels of motor and sensory performance at the onset of localization training. In this respect, our protocol deviated from that in the study by O'Connor et al. (2010a), which was designed to describe correlates with cerebral cortical activity rather than to compare cerebellar phenotypes. During the association task, the mice learned to associate the rising of a bar (~1 mm diameter) into their right whisker field with the availability of water at the lickport ("go trials"). The association trials started with a horizontal movement of the stimulation bar below the reach of their whiskers (lasting for 2 s), followed by a vertical movement (lasting for 850 ms) that placed the bar inside the whisker field (~5 mm posterior and 10 mm lateral to the tip of the nose; **Fig. 2***A*). Mice were able to touch the stimulation bar at some point during vertical rise of the stimulation bar. The exact moment of touch depended on the length and position of the whiskers at that time. To indicate the point in time in which the whisker could touch the bar during vertical rise before onset of the RW, we indicated the period of upward movement with green shading in **Figures 2**, **3**, and **4**. Once the bar reached its highest position, the RW opened. A water droplet was triggered at the onset of the first lick in this window (**Figs. 2**, **3**, **4**, RW

indicated with gray shading). The droplet remained at the lickport for the duration of the RW until all remaining water was sucked out of the lickport and the bar moved downward, returning to its starting position via the same route and at the same speed. When the animal did not respond to the stimulation during the RW during a trial, the next trial was postponed by an extra 3 s, delaying the possibility of reinforcement at the next trial. Licking outside the RW did not have any positive or negative consequences, except for the absence of water outside the RW. Each mouse was trained for one session consisting of 100 trials per day. The association task was completed as soon as a mouse licked at least once within the RW in at least 80% of the trials for at least two consecutive sessions. To minimize visual cues, the entire task took place in complete darkness, except for some sessions in which we made a video of the whisker movements using infrared illumination; these videos were recorded with a full frame rate of 160 Hz using infrared lighting at $\lambda > 900$ nm.

LOCALIZATION LEARNING.

Following completion of the association task, mice continued with the object localization task, consisting of go trials and trials in which the mice were taught to refrain from licking ("no-go trials") on the following day. During a go trial, the stimulation bar moved horizontally in the caudal direction from the neutral position below the right whisker field to ~5 mm posterior to the nose and then vertically into the whisker field, as described above. During a no-go trial, the stimulation bar moved horizontally from the neutral position into the rostral direction below the whisker field to ~5 mm anterior to the nose, and then vertically into the whisker field. The no-go position was outside the whisker field at rest, but could be reached during active whisking. The actual distance between the go and the no-go position depended on the size of the head and varied between 8 and 11 mm. A trial always began from and ended with the stimulation bar at rest in the neutral position, which was in the middle between the go and the no-go position, to ensure that the timing of any possible auditory cues during go and no-go trials was identical. During rest at the neutral position and during the horizontal movements, the stimulation bar was well below the reach of the whiskers. For both types of trials, the RW started as soon as the vertical movement of the bar was completed, but only during the go trials were the

mice were rewarded with a drop of water when they licked the lickport within the RW. The total duration of a trial was ~6.2–7.7 s, depending on the duration of the RW, followed by an intertrial interval of 7 s in correct trials. An incorrect response (not licking) during a go trial resulted in an extra intertrial interval of 3 s, whereas an erroneous response (licking) during a no-go trial resulted in an extra intertrial interval of 8 s (**Fig. 3***A*). Each (daily) session consisted of 100 pseudo-randomized trials (50% go trials and 50% no-go trials) or until the mouse discontinued licking, which was defined as not showing any responses for 10 consecutive trials. For each session, we calculated the percentage of correct trials, taking both the go and the no-go sessions into account. Once the mice performed at ≥80% correct during two consecutive sessions of the localization task with an RW of 2000 ms, the RW was decreased to 500 ms (via an intermediate step using an RW of 1000 ms; **Figs. 3, 4, 5**). Mice that did not learn the 2000 ms localization task within 35 sessions were considered nonperformers, and they were not tested any further. For control, we cut all whiskers in 10 mice (under isoflurane anesthesia) following completion of the 500 ms localization task, and we tested their performance again on the next day.

CONSTRUCTING LEARNING TRAJECTORIES.

For each session, we plotted the average hit rate and average false alarm rate per group of all mice (**Fig. 6**). To this end, we calculated the hit rate [i.e., the fraction of correct responses (licks) during the go trials relative to all go trials] and the false alarm rate [i.e., the fraction of incorrect responses (licks) during the no-go trials relative to all no-go trials] for each mouse and for each session. Linear regression lines were fitted to the group averages, and the deviation from the linear regression was calculated as the least-squares difference (SigmaPlot, Systat Software). The sensitivity index (d') was calculated using the z-transformations of the hit rate and the false alarm rates [$d' = z(\text{hit rate}) - z(\text{false alarm rate})$], assuming a Gaussian distribution. The 80% correct level corresponded to a d' score of ~1.7 (Huber et al. 2012).

ELECTROPHYSIOLOGY.

Electrophysiological recordings were performed in awake mice as described previously (Bosman et al. 2010). Briefly, mice first received a craniotomy of the occipital bone under isoflurane anesthesia (4% v/v in O_2). Postsurgical pain was treated with carprofen (5 mg/kg, s.c.; Rimadyl, Pfizer) and lidocaine (~1 μg applied to the wound). After surgery, mice were allowed to recover for at least 3 d before retraining and electrophysiological recordings. Single-unit recordings were made using quartz-coated platinum/tungsten electrodes (2–5 MΩ, outer diameter = 80 μm; Thomas Recording). The electrodes were placed in an 8 × 4 matrix (Thomas Recording), with an interelectrode distance of 305 μm over crus 1 and crus 2 ipsilateral to the whisker stimulation bar. All recordings were made at a minimal depth of 500 μm. The electrophysiological signal was digitized at 25 kHz, using a 30–6000 Hz bandpass filter, 22× preamplified and stored using a RZ2 multichannel workstation (Tucker-Davis Technologies). Spikes were detected off-line using SpikeTrain (Neurasmus) or a custom program written in Labview (National Instruments). We identified Purkinje cell activity by the presence of both complex spikes and simple spikes. Complex spikes were recognized based on the presence of spikelets following the initial spike. For each recording, we constructed a histogram of simple spike time stamps triggered by complex spike time stamps. We accepted a recording as a single unit if the 7 ms following a characteristic complex spike were devoid of simple spikes. Further analysis was exclusively done on single-unit Purkinje cell recordings that had a clear signal-to-noise ratio. The recording was split into “intertrial” and “trial” periods, and was further analyzed only if we had at least 50 s of each period. The trial period consisted of the time during the vertical rise of the bar, the RW, and the complete time of the vertical descent of the bar following the RW. The intertrial interval was defined as the period between the end of the (second) horizontal movement of one trial and the start of the (first) horizontal movement of the next trial. The local variation in simple spike firing (CV2) was calculated as $CV2 = 2\,|ISI_{n+1} - ISI_n|/(ISI_{n+1}+ISI_n)$, where ISI is the interspike interval (Shin et al. 2007).

DATA ANALYSIS.

Summed learning curves were made for both the association stage and the object localization task. First, we calculated for each mouse and each session the percentage of correct responses, and divided that percentage by the number of mice in that group. For example, if the group size was 14 mice, each individual mouse had a normalized success rate between 0% and 100%/14 = 7.14%. Next, we sorted the mice per group based on the number of sessions they required to reach criterion. The lowest line represents the normalized learning curve for the mouse that needed the most sessions. The second line from below is the sum of the normalized success rate of the first mouse plus that of the second mouse and so on. Each additional line is the sum of the normalized success rates of that mouse and of the mice represented by the lines below that line. As a consequence, the top line represents the group average. Unless stated otherwise, data are represented as the mean ± SEM, and statistical testing was performed using Student's *t* test. For unrelated tests, we used a 5% level of significance. For repeated tests, the level of significance was corrected using Bonferroni's correction ($\alpha_{corr} = \alpha/n$ with $\alpha = 0.05$ and n = number of tests). Where Bonferroni's correction was applied, α_{corr} is mentioned in the text.

7.3 Results

Licking in freely moving mice is comparable across genotypes

Since we are using licks as the readout parameter of learning capabilities during the object localization task, putative deficits in motor aspects of licking could in principle create a bias in the learning performance. Therefore, we first studied the licking behavior of WT and L7-PP2B mice in their home cages.

Both WT ($n = 9$) and L7-PP2B mice ($n = 10$) licked during multiple periods. Such licking periods often consisted of a few bouts of uninterrupted licking, each of which consisted of a series of rhythmic licks

(**Fig. 1***A*,*B*). Neither the licking frequency (9.15 ± 0.13 Hz for WT vs 9.08 ± 0.18 Hz for L7-PP2B mice) nor the number of licks per bout (5.7 ± 0.6 and 5.4 ± 1.1 licks) differed significantly among genotypes (p = 0.773 and p = 0.841, respectively; **Fig. 1***C*,*D*). In addition, the distributions of interlick intervals within bouts were similar between WT and L7-PP2B mice (p = 0.693, Kolmogorov–Smirnov test; **Fig. 1***D*). These data indicate that the baseline licking performance of freely moving L7-PP2B mice is intact.

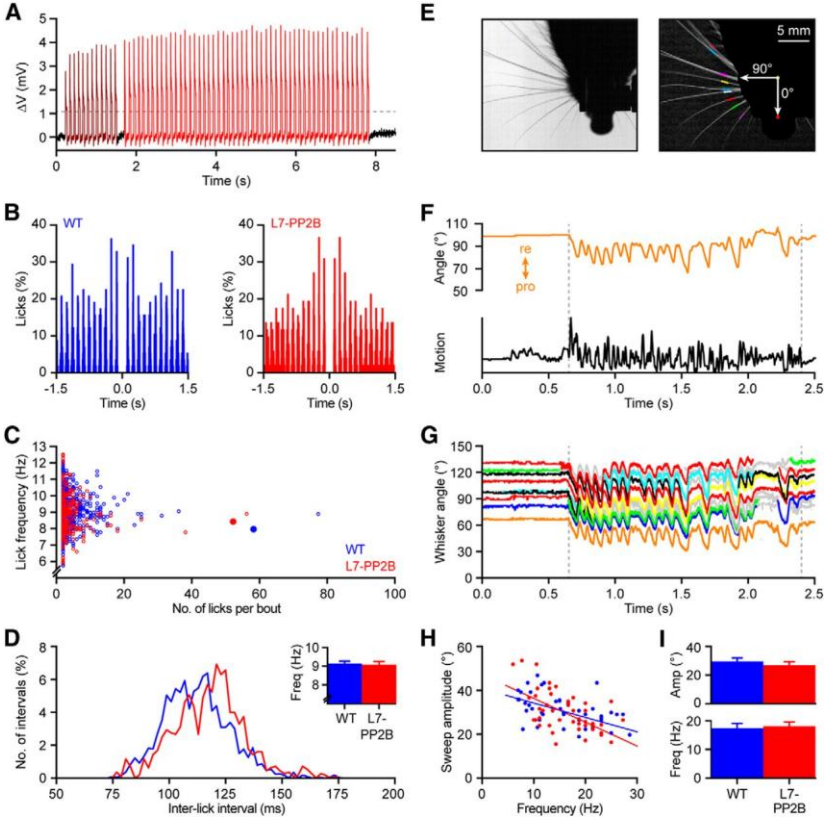

Figure 1. L7-PP2B mice do not have motor deficits preventing normal rhythmic licking and whisking. ***A***, A period of rhythmic licking in a freely moving L7-PP2B mouse. Licks can be seen as positive deflections of the junction potential between

the spout of the drinking bottle and an aluminum floor plate in the home cage. This licking period consisted of two individual licking bouts, as indicated by two colors. The dashed line indicates the threshold used for automated lick detection. ***B***, Auto-correlograms of licking bouts in a WT mouse (left) and an L7-PP2B mouse (right). The right panel is the auto-correlogram of the second licking bout (depicted in red) in ***A***. The bins were normalized with respect to the center bin that was removed to improve visibility. ***C***, Both WT and L7-PP2B mice displayed short and long licking bouts with lick frequencies predominantly between 6 and 12 Hz. Shorter licking bouts tended to vary more in lick frequency than long bouts in both genotypes. The auto-correlograms shown in ***B*** are taken from the bouts that are indicated with larger, filled symbols. ***D***, Histograms of all interlick intervals within licking bouts showed similar distributions in WT and L7-PP2B mice, indicating that L7-PP2B mice had no motor deficits preventing them from licking rhythmically. The histograms were made with a bin size of 2 ms, and the area under the plot was normalized to 100%. Inset, Licking frequency ± SEM averaged per mouse (n = 9 WT mice and 10 L7-PP2B mice; p = 0.773). ***E***, Whisker movements were quantified from high-speed video recordings. In each frame, the proximal parts of the whiskers were tracked with small line segments (colored lines in the right plot). Whisker angles were measured relative to the body axis. ***F***, Whisker motion during a whisking bout was tracked manually (top) and characterized using the motion detection algorithm (bottom; see Materials and Methods). It can be seen that the motion detection reliably captured the duration of the whisker movements. ***G***, The same fragment was subsequently analyzed using automated line detection and subsequent post-processing to detect movements of individual whiskers (see Materials and Methods); tracks with >500 data points are shown with randomly assigned colors, while shorter tracks are shown in gray. The orange trace refers to the same whisker that had been tracked manually (top trace in ***F***). ***H***, There is a clear negative correlation between the frequency and amplitude of a whisker bout: the higher the frequency, the smaller the movements. Linear regression lines of WT mice (n = 47 bouts from 10 mice) and L7-PP2B mice (n = 46 bouts from 11 mice) data were not significantly different from each other (z = 1.579; p = 0.114). ***I***, Neither the amplitude nor the frequency of whisker bouts was significantly different between WT and L7-PP2B mice (p = 0.378 and p = 0.784, respectively).

Free whisking in head-restrained mice

Putative abnormal whisker use could be a cause for deficits in the results of our whisker-based object localization task. Therefore, we quantified the spontaneous whisker movements of 10 untrained WT mice and 11 L7-PP2B littermates during recording sessions in which no whisker stimulation took place (**Fig. 1***E*). To facilitate the automated detection of whisker movements, we first quantified whisker motion (see Materials and Methods). The whisker motion algorithm reliably identified periods with whisker movements, as verified by manual tracking (see Materials and Methods; **Fig. 1***F*). The video fragments containing whisker movement were further analyzed quantitatively using BWTT (Perkon et al. 2011) and post-processed to track traces of individual whiskers over time (**Fig. 1***G*). We confirmed the accuracy of automatically traced tracks with manually traced tracks [**Fig. 1***F*, orange trace (which is derived from the same whisker as the orange/bottom trace in **Fig. 1***G*, but was made from a more distal location, accounting for the sharper peaks)]. We found that all mice showed repetitive periods of whisking. We quantified the movements of individual whiskers during bouts of rhythmic whisking. Within such bouts, neither the amplitude (WT mice: 29.5 ± 2.5°; L7-PP2B mice: 26.9 ± 2.4°; $p = 0.378$) nor the frequency (WT mice: 17.5 ± 1.6 Hz; L7-PP2B mice: 18.1 ± 1.5 Hz; $p = 0.784$) differed significantly between the two groups of mice (**Fig. 1***G–I*). There was a clear inverse correlation between the amplitude and the frequency of a whisker bout (WT mice: $r = 0.503$; $p < 0.001$; L7-PP2B mice: $r = 0.606$; $p < 0.001$; linear regression; **Fig. 1***H*). The regression lines of the WT and the L7-PP2B mice were not significantly different from each other ($z = 1.579$; $p = 0.114$). We conclude that WT and L7-PP2B mice are similar in their range and frequency of free whisking.

General motor performance during the association stage

Since the frequency of licking can depend on the ease of access to water (Weijnen 1998), we also compared the licking behavior in head-restrained mice during the association task when water was available during the 2000 ms RW. Overall, the average number of licks per minute—as calculated over the whole first association session—was comparable

between head-restrained WT (n = 16) and L7-PP2B (n = 14) mice (WT mice: 96 ± 18 licks/min; L7-PP2B mice: 120 ± 24 licks/min; p = 0.535; data not shown). Most mice [14 of 16 (87.5%) WT mice and 14 of 14 (100%) L7-PP2B mice; p = 0.485, Fisher's exact test] licked rhythmically during the RW of the first association session. WT mice had a slightly different licking frequency, but the difference with L7-PP2B mice was not significant (f = 8.3 ± 0.1 Hz and 7.9 ± 0.1 Hz, respectively; p = 0.06). The strength of the rhythmicity was similar (13.0 ± 0.8% and 11.8 ± 0.7%, respectively; p = 0.306; **Fig. 2***B*). As the association training proceeded, rhythmic licking during the RW increased; at the end, the strength of the rhythmicity was 15.1 ± 1.0% and 14.3 ± 0.9%, respectively, for WT and L7-PP2B mice (p = 0.576). The frequency remained at ∼8 Hz for both groups (7.9 ± 0.1 and 7.8 ± 0.1 Hz, respectively; p = 0.624). Moreover, video analyses of the whisker movements showed that WT and L7-PP2B mice were both actively whisking during the association trials. **Figure 2***C* shows an example of whisker movements in a video of a WT and a L7-PP2B mouse during the first session of the association task. Both mice whisked actively and contacted the stimulation bar during the RW of the association task. Thus, as in naive mice, both WT and L7-PP2B mice had similar lick responses and active whisker exploration behavior while being head restrained during the RWs of the association task.

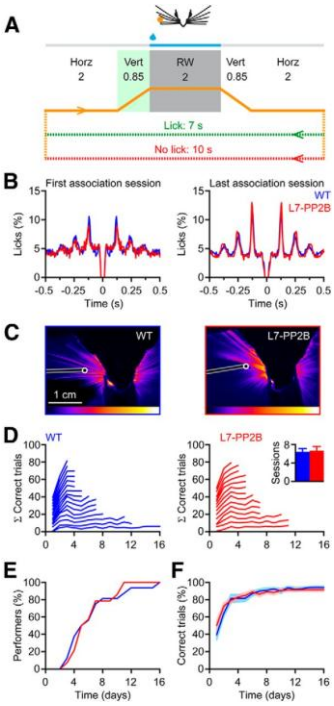

Figure 2. Mice learn to lick after feeling a stimulus bar in their whisker field. ***A***, Learning paradigm. During the association task, mice were subjected only to go trials and learned to lick following whisker contact with a metal bar (orange dot) within a 2000 ms RW. Once the stimulation bar completed the horizontal movement from the (neutral) resting position to the go position, it moved vertically into the whisker field. Whisker contact with the stimulation bar became possible approximately half way through the time interval allotted for the vertical movement. To indicate this, we marked the time period of the vertical movement with a green shading. The RW started after the completion of the vertical movement and is indicated with a gray shading. Correct responses triggered a water reward; incorrect responses postponed the next trial. ***B***, Mice licked rhythmically during the RW of the association phase. Over the sessions, the mice increased their licking rhythmicity, as demonstrated by the increase of the amplitudes of the side peaks at approximately 125 ms [corresponding to a dominant lick frequency of 8 Hz; compare with naive mice (during the first association session) in the left panel and trained mice (during the last association

session) in the right panel]. The auto-correlograms were made with a bin size of 5 ms and were normalized to the center peak (which is not shown to improve clarity). ***C***, SD projection plot showing a representative example of whisker movement during the RW. The color bar at the bottom indicates the amount of movement (black, no change; white, maximal change). It can be seen that both mice moved their whiskers actively during the RW and touched the stimulus bar. ***D***, Summed learning curves during the association phase (see Materials and Methods). The inset shows the average number of sessions required to reach the criterion. Error bars indicate SD. ***E***, Cumulative histogram of the percentage of mice that reached criterion, showing that WT and L7-PP2B mice learned the association task at a similar rate. ***F***, The fraction of correct trials over the sessions. Dark lines show the averages, and the shaded areas cover the average ± SEM.

Association learning

Next, we analyzed the performance of the mice during the association training. We identified a trial as correct when a mouse licked at least once within the RW, independent from its activity outside the RW. On average, both groups had similar percentages of correct trials during the first session when the rod was elevated inside the whisker field (WT mice: 39.4 ± 24.6%; L7-PP2B mice: 50.1 ± 24.2%, mean ± SD; $p = 0.241$). In addition, both genotypes learned equally well during the association task (last session: WT mice, 93.8 ± 5.4%; L7-PP2B, 91.4 ± 7.1%, mean ± SD; $p = 0.238$). WT and L7-PP2B mice required a similar number of sessions to reach criterion (6.6 ± 3.6 and 6.4 ± 2.6 sessions, respectively, mean ± SD; $p = 0.865$; **Fig. 2***D*; see also **Table 1**). The rate at which the mice mastered the task was very similar for WT and L7-PP2B mice ($p = 0.458$, paired *t*test; **Fig. 2***E*). Also, the learning curve, represented as the percentage of correct trials per session, was highly comparable for both types of mice ($p = 0.963$, repeated-measures ANOVA; **Fig. 2***F*). Thus, all mice—regardless of their genotype—learned to lick during the RW of the association test at a similar pace.

General motor performance during localization training

Following completion of the association stage, during which mice only received go trials, they were subjected to the localization learning task, wherein they received both go and no-go trials. During the go trials, the pole was positioned inside the whisker field (as in the association stage), whereas during the no-go trials the pole was raised just in front of their baseline whisker field so they could only detect the rod by means of active forward exploration (**Fig. 3***A*). In contrast to the go trials, when the mice were encouraged to lick, they had to withhold their licking during no-go trials to prevent a long delay for the next trial, postponing potential reinforcement.

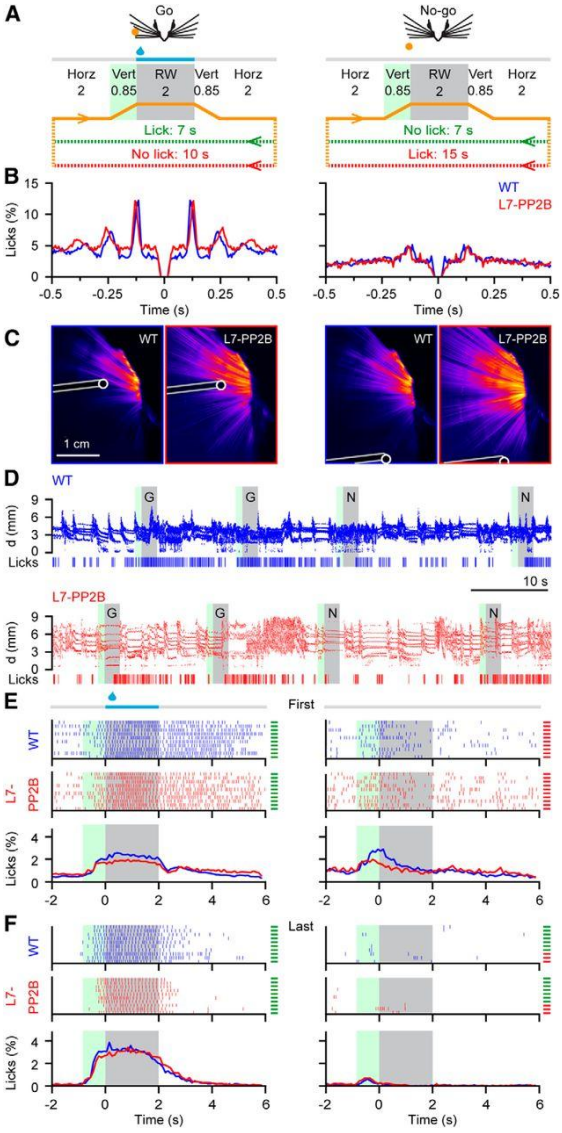

Figure 3. Motor behavior during the object localization task with an RW of 2000 ms. ***A***, Learning paradigm. During the object localization task, mice were subjected

not only to go trials, but also to no-go trials. The mice had to learn to lick during the RW of the go trials, but not during that of the no-go trials. Once the stimulation bar completed the horizontal movement from the (neutral) resting position to the go or the no-go position, it moved vertically into (go) or just in front of (no-go) the whisker field. Whisker contact with the stimulation bar became possible at approximately half way through the time interval allotted for the vertical movement. To indicate this, we marked the time period of the vertical movement with a green shading. The RW started after the completion of the vertical movement and is indicated with a gray shading. Licks during the RW of go trials triggered a water reward; incorrect responses postponed the next trial. ***B***, Mice licked rhythmically during the RW. Rhythmic licking was more prevalent during the go trials, when there was water, than during no-go trials, when there was no water. ***C***, SD projection plots showing representative examples of whisker movement during the RW. It can be seen that both mice moved their whiskers actively during the RW and touched the stimulus bar, in both the go and the no-go trials. ***D***, Whisker movements during the first association phase illustrating that mice of both genotypes whisk often during the task. Plotted are the rostrocaudal positions of the center whiskers at ~3 mm from the snout. Gray areas indicate the RW, and green areas indicate the periods of the preceding vertical movement. Go trials are indicated with a "G," no-go trials with an "N." Longer intertrial intervals indicate incorrect responses. ***E***, Raster plots of lick times showing the first 10 go (left) and no-go trials (right) of representative experiments during the first session of the 2000 ms object localization task. The two top panels show raster plots for a single individual per genotype. The lines at the right border of the plot indicate whether the trial was performed correctly (green) or incorrectly (red). The bottom panel shows the histograms of the relative timing of the licks over all trials averaged for all performers. The green area (850 ms) refers to the interval during which the stimulation bar moved vertically, either into (go trials) or in front of (no-go trials) the resting position of the whisker field. The gray area indicates the response window (2000 ms). ***F***, Same as in ***E*** for the last session of the 2000 ms.

First, we subjected the animals to trials with an RW of 2000 ms, and we analyzed the licking pattern during the RWs of the first localization session. Licking was more rhythmic during the RW of go trials, when the mice received water, than during that of no-go trials, when the mice did not receive water (**Fig. 3***B*). During go trials, the lick rhythm was again ~8 Hz for both genotypes (WT mice: 8.2 ± 0.1 Hz; L7-PP2B mice: 7.9 ± 0.1

Hz; $p = 0.085$), and both genotypes had a similar strength of rhythmic licking (15.6 ± 1.0% and 14.4 ± 0.6%, respectively; $p = 0.304$, *t* test). During no-go trials, the lick rhythm was 8.1 ± 0.2 Hz for WT mice and 7.4 ± 0.2 Hz for mutants ($p = 0.072$), and the amplitudes were 7.9 ± 1.0% and 7.4 ± 0.9%, respectively ($p = 0.710$). Likewise, when we analyzed the whisking behavior during the localization task (from 5 WT and 5 L7-PP2B mice), we found active whisking during both go and no-go trials, regardless of the genotype of the mouse (**Fig. 3***C*,*D*). For this reason, we concluded that, at least initially, the mice were localizing both stimulus positions rather than simply detecting the stimulus during the go trials. Note that the mice could already sense the stimulation bar before it reached the top position. The moment of contact could vary per trial and depended on the actual position of the whiskers. Since mice could contact the stimulation bar as it moved upward into the whisker field, we indicated this period with green shading in **Figures 2**, **3**, and **4**. On average, there were 13.3 ± 5.9 times as many licks during the "green period" of go trials than during that of no-go trials in expert mice ($p < 0.001$, paired *t* test; **Fig. 3***F*). The ratio was higher in WT mice (17.2 ± 7.8) than in L7-PP2B mice (4.3 ± 1.1), but this difference was not significant ($p = 0.147$). Together, this indicates that although there were licks before the start of the RW, these early licks were mainly related to go trials, indicating the presence of whisker contact just before the start of the RW. We found a tendency that WT mice were better able to categorize trials in an early phase of the trial than L7-PP2B mice, since WT mice especially showed many more licks during the early onset of go trials than during that of no-go trials.

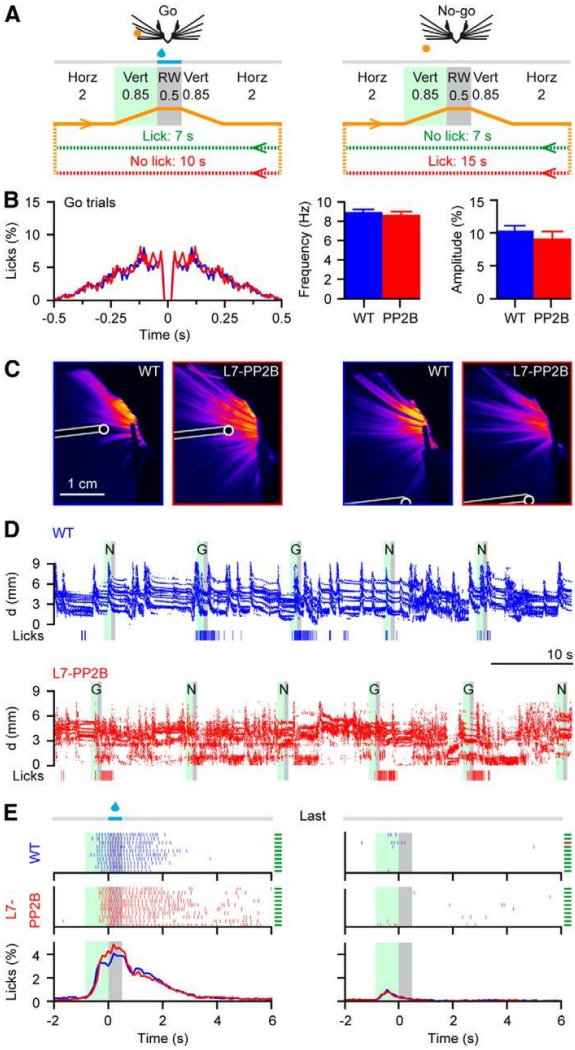

Figure 4. Motor behavior during the object localization task with an RW of 500 ms. ***A***, Learning paradigm. Once the stimulation bar completed the horizontal movement from the (neutral) resting position to the go or the no-go position, it moved vertically into (go) or just in front of (no-go) the whisker field. Whisker contact with the stimulation bar became possible approximately around half way

during the time interval allotted for the vertical movement. To indicate this, we marked the time period of the vertical movement with a green shading. The RW started after the completion of the vertical movement and is indicated with gray shading. Licks during the RW of go trials triggered a water reward; incorrect responses postponed the next trial. ***B***, Mice licked rhythmically during the RW of go trials of the last 500 ms object localization session. At this stage, the mice performed so well that licking during no-go trials was really sparse and that there were not enough licks during the RW of no-go trials to permit quantitative analysis. ***C***, SD projection plot showing a representative example of whisker movement during the RW. It can be seen that both mice moved their whiskers actively during the RW and touched the stimulus bar, both in the go and in the no-go trials. ***D***, Example traces of whisker movements during the last session of the 500 ms object localization task, illustrating that mice of both genotypes whisk often during the task. Plotted are the rostrocaudal positions of the center whiskers at ~3 mm from the snout. Intertrial whisking occurs less often in trained mice than in naive mice (compare Fig. 3*D*). Licks are indicated in the bottom rows. Go trials are indicated with a "G," no-go trials with an "N." A longer intertrial interval indicates an incorrect response. ***E***, Raster plots of lick times showing the last 10 go (left) and no-go trials (right) of representative experiments during the first session of the 500 ms object localization task. The two top panels show raster plots for a single individual per genotype. The lines at the right border of the plot indicate whether the trial was performed correctly (green) or incorrectly (red). The bottom panel shows the histograms of the relative timing of the licks over all trials averaged for all performers. The green area (850 ms) refers to the interval during which the stimulation bar moved vertically, either into (go trials) or in front of (no-go trials) the resting position of the whisker field. The gray area indicates the response window (500 ms).

The mice that performed well during the 2000 ms object localization task were ultimately tested with the same test with an RW of 500 ms (**Fig. 4***A*). During the 500 ms RW of the go trials, mice again licked rhythmically at ~8 Hz (frequency: WT mice, 8.8 ± 0.4 Hz; L7-PP2B mice, 8.5 ± 0.3 Hz; $p = 0.514$; amplitude: WT mice, 10.3 ± 0.8%; L7-PP2B mice, 9.2 ± 1.0%; $p = 0.385$). During this task, high-frequency tongue movements were relatively abundant in both WT and L7-PP2B mice, leading to a similar shape of the auto-correlograms ($p = 0.795$, Kolmogorov–Smirnov test; **Fig. 4***B*). This high-frequency licking was probably due to the shorter

time period of the presence of water at the lickport (500 ms instead of 2 s). Licking during the RW of no-go trials was very sparse in both trained WT and mutant mice (**Fig. 4***E*), precluding a meaningful quantification of lick rhythmicity during the no-go trials. During the last session of the 500 ms object localization task, both WT and L7-PP2B mice whisked actively during both go and no-go trials (**Fig. 4***C*), but, compared with naive mice, both genotypes whisked less during intertrial intervals (compare **Figs. 3***D*, **4***D*).

More WT than L7-PP2B mice learned the localization task

Contrary to the association phase, which could be mastered by all mice, the object localization task with a 2000 ms RW was not learned by all mice. Of the 16 WT mice, 14 reached a success rate of >80% correct trials during two consecutive sessions within 35 daily sessions. Significantly fewer L7-PP2B mice were able to learn this task: only 6 of 14 mice succeeded in obtaining the same criteria (87.5% vs 42.9%; $p = 0.019$, Fisher's exact test; **Fig. 5***A*,*B*, left panels). The mice that did not manage to learn the object localization task with an RW of 2000 ms were considered to be nonperformers and were not tested any further. Mice that did obtain the necessary criteria were considered performers and were moved to the short RW-phase paradigm.

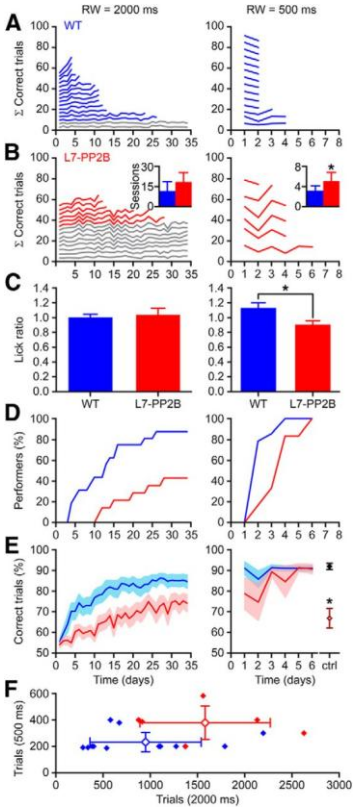

Figure 5. The absence of PP2B in cerebellar Purkinje cells impairs learning of a whisker-based object localization task. ***A***, Summed learning curves of WT mice during the 2000 ms (left) and the 500 ms (right) object localization task across consecutive sessions (*x*-axis). The number of trials per session was normalized to 100% (for details, see Materials and Methods). Upon reaching a success rate of ≥80% during two consecutive sessions, mice continued to the next phase. Performers and nonperformers are indicated in blue and gray, respectively. ***B***, Same as ***A*** for L7-PP2B mice (performers are indicated in red). Insets, Averaged number of sessions ± SD that performers needed to complete the entire object localization task; $*p < 0.017$ (*t* test). ***C***, The fine timing of the lick responses at the end of the 100 ms period preceding the RW and at the first 100 ms period of the RW suggests a cerebellar role in the timing of the decision process to lick. We compared the number of licks during the first 100 ms of the RW and the 100 ms

before the start of the RW, and thus the ratio of licks just after the availability of water and the licks just before the availability of water. This ratio equaled 1 during the last session of the 2000 ms object localization task (left), but was increased in trained WT mice (but not in L7-PP2B mice) during the last 500 ms object localization task (right); *$p < 0.02$. ***D***, Cumulative histograms of the percentage of mice that reached criterion showing that more WT mice were able to learn the object localization task than L7-PP2B and that WT performers were faster than L7-PP2B performers. ***E***, The fraction of correct trials over the sessions. Dark lines show the averages, and the shaded areas cover the average ± SEM. For a control, we clipped the whiskers of 10 mice (8 WT mice and 2 L7-PP2B mice) following successful completion of the 500 ms object localization task. Their performance level during the subsequent session (dark red open symbol) was comparable to that of naive mice and was much lower than that during the last session with intact whiskers (black closed symbol); *$p < 0.001$ (paired *t*test). ***F***, The average numbers of trials the L7-PP2B mice needed to learn the 500 and 2000 ms object localization tasks were significantly greater than those in WT mice ($p < 0.05$).

WT performers learned the localization task faster than L7-PP2B performers

WT performers were faster learners than L7-PP2B mice. For example, the fastest WT mouse took four sessions to master the 2000 ms localization task, whereas the fastest L7-PP2B mouse needed 11 sessions. The complete task including both the 2000 and 500 ms localization tasks was learned significantly faster by WT mice than by L7-PP2B performers [genotype: WT mice ($n = 14$), 17.4 ± 8.7 sessions; L7-PP2B mice ($n = 6$), 24.8 ± 7.7 sessions, mean ± SD; $F_{(1,54)} = 4.395$; $p = 0.041$, two-way ANOVA; **Fig. 5***A*,*B*; **Table 1**, number of trials). With regard to the 2000 ms object localization task only, it took the L7-PP2B mice longer to learn the task than the WT mice, but this difference did not reach statistical significance [WT mice: 11.6 ± 7.0 sessions; L7-PP2B mice: 18.5 ± 6.9 sessions, mean ± SD; $p = 0.090$ (not significant: $\alpha_{corr} = 0.017$; see Materials and Methods), Mann–Whitney test; **Fig. 5***A*,*B*,*D*]. The reduced learning efficiency of the L7-PP2B mice was also reflected in the slower increase of correct responses during the 2000 ms task (genotype: $F_{(1,27)} = 5.098$; $p = 0.032$, repeated-measures ANOVA; **Fig. 5***E*).

WT mice learned to fine-tune the timing of their lick responses better than L7-PP2B mice

When we reduced the RW from 2000 to 500 ms, the L7-PP2B mice required on average significantly more sessions than their WT littermates to reach criterion (WT mice: 2.4 ± 0.7 sessions; L7-PP2B: 3.8 ± 1.3 sessions; $p = 0.010$ [significant: $\alpha_{corr} = 0.017$, Mann–Whitney test); **Fig. 5***A*,*B*; **Table 1**, number of trials]. Thus, while the L7-PP2B mice in general had more difficulties learning the object localization task, the difference with WT mice was especially clear when fast response timing was required.

Further evidence for this claim was indicated by the differences in precise timing of the licks between WT and L7-PP2B mice. We compared the number of licks just before the RW to the number of licks just after the start of the RW in which the water reward became available. The ratio of the licks between 100 ms after and 100 ms before the start of the RW was not significantly different between WT and L7-PP2B mice at the end of the training with the 2000 ms RW (WT mice: 1.01 ± 0.04; L7-PP2B mice: 1.04 ± 0.09; $p = 0.758$). This indicates that the mice did not time their licks very precisely around the onset of the RW. However, at the end of the training with the 500 ms RW, the WT mice showed a clear increase in licking just at the onset of the RW. In contrast, the L7-PP2B mice did not (WT mice: 1.13 ± 0.07; L7-PP2B: 0.91 ± 0.05; $p = 0.019$; **Fig. 5***C*). These data point at reduced sensorimotor timing abilities in L7-PP2B mice that become apparent only under strict timing restraints. Importantly, whisker clipping following training with an RW of 500 ms significantly affected the performance during the object localization task (from 91.9 ± 1.51% to 66.8 ± 4.8%; $n = 10$ mice; $p < 0.001$, paired *t* test; **Fig. 5***E*, right), confirming that mice predominantly used their whiskers to detect the stimulus bar and respond accordingly. However, as the performance level after whisker clipping did not return completely to the 50% chance level (go and no-go trials occurred equally often), we cannot exclude the possibility that some mice also partially used other sensory cues like sound and vibration to facilitate the whisker-based localization task.

Since not all sessions had an equal number of trials, we also compared the number of trials per individual required for the 2000 and 500

ms tasks. This confirmed that WT mice were in general faster in learning than L7-PP2B mice (**Fig. 5***F*; **Table 1**). Moreover, together with the more accurate timing of the licks in WT mice (**Fig. 5***C*), these data indicated that the differences among WT and L7-PP2B mice are more prominent with shorter RWs.

WT mice show a better learning trajectory than L7-PP2B mice

Since we found that the WT and L7-PP2B mice differed in their learning skills during the object localization task, we further investigated the relative contributions of their licks during the go trials and the withholding of their licking during the no-go trials to the overall learning process. First, we plotted for all performers the individual learning curves of the hit rates (i.e., the percentages of go trials during which the mice licked during the RW) and the false alarm rates (i.e., the percentages of no-go trials during which the mice licked during the RW; **Fig. 6***A*,*B*). It can be seen that mice started the object localization training with both high hit rates and false alarm rates, and gradually learned to refrain from licking during the no-go trials. This behavior was further analyzed by plotting the "false alarm" rates vs the "hit" rates for each session of the object localization task. Separate plots of the learning trajectories were constructed in receiver operating characteristic (ROC) space (**Fig. 6***C*). As mentioned before, the mice were trained during the preceding association phase to lick during all trials. Consequently, during the first object localization session (with a 2000 ms RW) they licked very often regardless of the trial type. As a result, they performed at close to the guess rate.

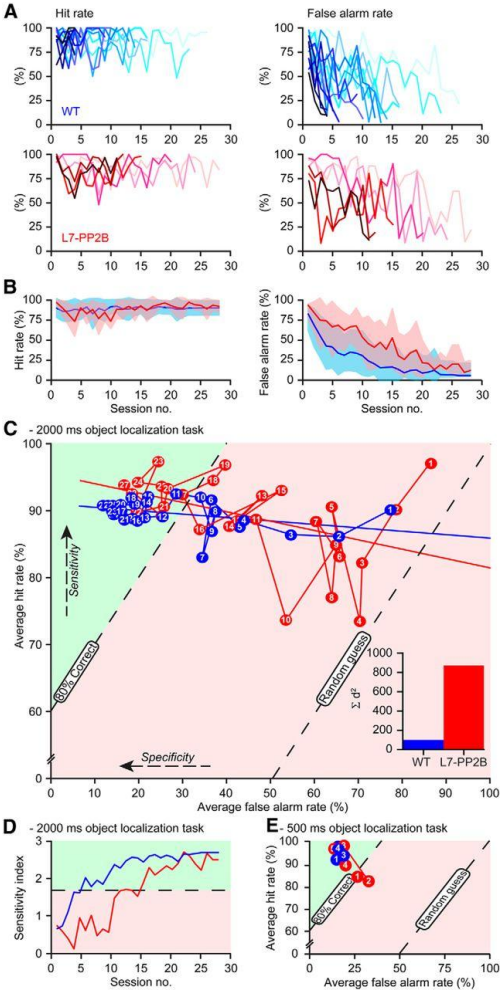

Figure 6. WT mice have more efficient learning trajectories than L7-PP2B mice. ***A***, The hit rates (licking during the RW of go trials; left) and the false alarm rates (licking during the RW of no-go trials; right) of all WT (top) and L7-PP2B (bottom) performers over the sessions of the 2000 ms object localization task. ***B***, Averaged hit (left) and false alarm (right) rates of all performers. Dark lines indicate the average, and the shaded area the average ± SD. ***C***, Average false alarm rates versus average hit rates in ROC space during the 2000 ms object localization

task. Perfect classification of both the go trials and the no-go trials would be 0% false alarms and 100% hits. Successful trials (≥80% correct) can be found in the green area. Plotted are the averages of all WT (blue) and L7-PP2B (red) performers for 28 sessions (the session number is indicated on each symbol), which was the maximum number of sessions required to master the 2000 ms object localization task. Linear regression lines are indicated. Note that the WT mice decrease the number of false alarms from the beginning on, while the L7-PP2B mice first generally reduce the licking responses, regardless of the trial type. The linear regression lines of WT and L7-PP2B mice are not significantly different (z = 1.498; p = 0.134). Inset, Summed least-squares differences between the first 28 sessions and the linear regression lines for WT and L7-PP2B performers during the 2000 ms object localization task. ***D***, The d' of all animals (0 = chance performance; 1.68 = 80% correct trials). ***E***, The same plot as ***C***, but for the 500 ms object localization task. Note that the WT mice are in the green area from the start on, while the L7-PP2B mice initially show a decreased performance relative to the previous phases of the object localization tasks.

During the subsequent sessions, the WT performers markedly and consistently increased accuracy, moving almost along a straight line toward our defined criteria (**Fig. 6***C*, green area). They continued to lick during the go trials, but decreased their licking during no-go trials. Thus, they maintained a high level of sensitivity to go trials, but specifically reduced their response to no-go trials. The WT mouse with the fastest learning capability reached criterion after four sessions, whereas the fastest L7-PP2B mouse reached criterion only after 11 sessions (**Fig. 5***A*,*B*). In contrast to WT mice, the L7-PP2B mice reduced their licking during the first four sessions in a random fashion: they stayed close to the guess rate. The difference between the WT and L7-PP2B mice during these first four sessions was striking. The WT mice kept licking at the same rate during the go trials, but reduced their licking during the no-go trials. In contrast, the L7-PP2B mice initially did not discriminate between go and no-go trials.

In the subsequent sessions, the six L7-PP2B performers also increased their successful licks, but their learning trajectories remained noisier than those of the WT performers. This difference in learning trajectories was particularly evident when comparing the deviations from the linear regression between the WT and L7-PP2B performers (**Fig. 6***C*, inset). The linear regression lines themselves were not significantly

different (z = 1.498; p = 0.134), but the much larger deviations from the regression line in the L7-PP2B mice in combination with the longer time required to reach high performance levels clearly confirmed that learning was affected in L7-PP2B mice. The differences in learning strategies were characterized by the changes in the d' (WT vs L7-PP2B, p = 0.001; **Fig. 6***D*). These curves illustrated the superior ability of WT mice compared with L7-PP2B mutants to discriminate between go and no-go trials, and act accordingly. When the same analysis was performed for the 500 ms localization task, which was rapidly learned, the averages of the WT and L7-PP2B performers were already mostly in the "green area," indicating good performance, from the first session onward (**Fig. 6***E*). Still, here too, the L7-PP2B performers showed a clear drop in performance during the second session of the 500 ms task.

Purkinje cell activity during object localization

If the differences in learning ability for whisker-based object localization between WT and L7-PP2B are indeed due to differences in intrinsic and synaptic potentiation of Purkinje cells, one can expect differences in the activity of these cells among the two genotypes. We therefore recorded the single-unit activity of Purkinje cells at the end of the localization task in ipsilateral crus 1 and crus 2, which are involved both in whisking (Axelrad and Crepel 1977; Bosman et al. 2010) and licking (Bryant et al. 2010). To compare Purkinje cell activity during the trial with baseline activity, we divided the recordings into trial and intertrial periods. We considered the interval between the end of the (second) horizontal movement and the start of the (first) horizontal movement of the next trial the intertrial period, and the interval between the start of the upward vertical movement until the end of the downward vertical movement the trial period (**Fig. 3***A*).

First, we characterized the simple spike firing and the complex spike firing during the intertrial periods. In line with the findings by (Schonewille et al. 2010) for the vestibulocerebellum, the rate of simple spike firing was similar between WT and L7-PP2B Purkinje cells [WT

cells (n = 24): 60.23 ± 4.65 Hz; L7-PP2B cells (n = 25): 55.36 ± 3.31 Hz; p = 0.398), but the local variation in simple spike firing (CV2 WT vs L7-PP2B: 0.490 ± 0.027 vs 0.275 ± 0.026; p < 0.001) as well as the complex spike firing rate (WT vs L7-PP2B: 1.35 ± 0.06 vs 1.00 ± 0.08 Hz; p = 0.002) were significantly reduced in L7-PP2B Purkinje cells (**Fig. 7***C–E*, left panels).

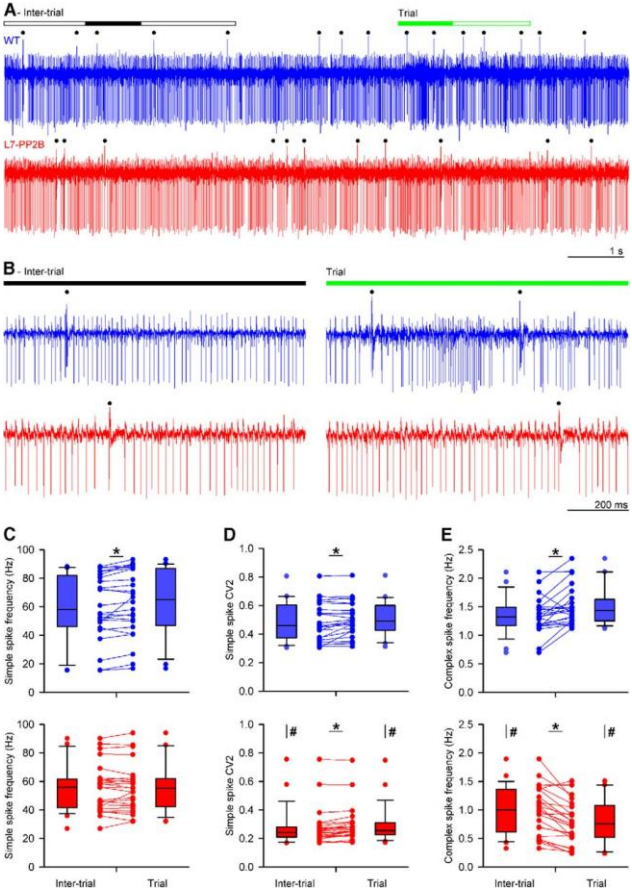

Figure 7. Differential Purkinje cell activity during the object localization task. ***A***, Example single-unit traces of a WT (top) and a L7-PP2B (bottom) Purkinje cell in crus 1/crus 2 area of the cerebellum ipsilateral to the stimulus location in trained mice. The recording was divided into a trial period (consisting of the RW and the flanking periods of vertical movement of the stimulation bar) and an intertrial period (excluding the trial period and the flanking periods of horizontal movement of the stimulation bar; see Fig. 3*A*). The filled lines indicate the periods that are enlarged in ***B***. Complex spikes are indicated with a black dot above the trace. The other downward deflections are the simple spikes. ***C–E***, The firing characteristics of 24 WT and 25 L7-PP2B Purkinje cells are summarized with box plots for the simple spike frequency (***C***), simple spike CV2 (***D***), and complex spike frequency (***E***). Recordings were made after finishing the object localization training. The simple spike frequency was not significantly different between WT and L7-PP2B Purkinje cells. Only in WT Purkinje cells was there a modest, but significant, increase in simple spike frequency during the trial periods compared with the intertrial periods. The local variation (CV2) in simple spike firing was reduced in L7-PP2B compared with WT Purkinje cells. Yet, in both types of Purkinje cells the CV2 was increased during the trial periods. The complex spike frequency was reduced in L7-PP2B compared with WT Purkinje cells. The WT Purkinje cells showed an increase in complex spike firing during trial periods, whereas the L7-PP2B Purkinje cells showed a decrease during trial periods. #$p < 0.05$ (WT vs L7-PP2B); *$p < 0.05$ (trial vs intertrial).

Next, we compared Purkinje cell activity between the trial and intertrial periods. WT Purkinje cells showed a moderate, but consistent, net increase in simple spike firing (intertrial interval: 60.23 ± 4.66 Hz; trial: 62.72 ± 4.74 Hz; $p = 0.004$, Wilcoxon matched-pairs test; **Fig. 7***C*, top). In contrast, L7-PP2B Purkinje cells did not show such an increased simple spike firing (intertrial interval: 55.36 ± 3.31 Hz; trial: 55.54 ± 3.32 Hz; $p = 0.853$, Wilcoxon matched-pairs test; **Fig. 7***C*, bottom). Thus, as might be predicted, the net increase in simple spike firing observed in WT mice is not observed in trained mice in the absence of intrinsic and synaptic potentiation of their Purkinje cells. In line with the occurrence of sensory input, the simple spike CV2 was increased both in WT and in L7-PP2B Purkinje cells, indicating that these Purkinje cells were indeed involved in the behavioral task (WT cells: intertrial interval, 0.490 ± 0.027; trial, 0.507 ± 0.024; $p = 0.021$; L7-PP2B: intertrial interval, 0.275 ± 0.026; trial, 0.292

± 0.025; $p < 0.001$, Wilcoxon matched-pairs tests). The complex spike activity of WT mice and L7-PP2B mutants also both showed prominent changes between trial and intertrial periods, but these changes moved into opposite directions (**Fig. 7***E*). In WT mice, the complex spike firing rate increased (intertrial interval vs trial: 1.35 ± 0.06 vs 1.50 ± 0.07 Hz; $p = 0.002$), whereas in L7-PP2B it decreased (intertrial interval vs trial: 1.00 ± 0.08 vs 0.79 ± 0.08 Hz; $p < 0.001$, Wilcoxon matched-pairs tests). We conclude that Purkinje cells in both WT and L7-PP2B mice were probably involved in the object localization task, since both groups of Purkinje cells showed an increased variability in simple spike firing. Yet, trained WT mice reacted with a net increase in both simple spike and complex spike firing, whereas the L7-PP2B mice did not. We expect that such a difference in Purkinje cell activity, which appears to be well in line with a lack of potentiation in the L7-PP2B mice, may cause changes in the output of the cerebellar nuclei that can in turn affect cerebral cortical processing via the thalamus.

7.4 Discussion

In the current study, we showed that L7-PP2B mice, which suffer from impaired intrinsic plasticity and synaptic potentiation of their Purkinje cells (Schonewille et al. 2010), exhibited learning deficits during a whisker-based object localization task. Not only were fewer L7-PP2B mice able to learn the task at long response windows, the ones that did needed more time, and the fine-tuning of the precise timing of their learned responses was especially deficient at short response windows. Moreover, L7-PP2B mice showed deficits in maintaining the hit rate while reducing false alarms, and their learning trajectory was considerably noisier. Finally, we showed that Purkinje cells in WT mice, but not in L7-PP2B mice, showed a net increase in firing during trials in trained mice, which further substantiates the possibility that the cerebellum is involved in learning of this whisker-based object localization task.

Can the observed learning deficits be explained by motor, sensory, and/or developmental aberrations?

Even though L7-PP2B mice do not show overt signs of motor ataxia (Schonewille et al. 2010), in principle they might suffer from small deficits in motor performance during licking and/or whisking behavior, since both types of behavior have neural correlates in the cerebellum (Bosman et al. 2010; Bryant et al. 2010; Lang et al. 2006). We therefore first investigated licking and whisking behavior of freely moving and head-fixed WT and L7-PP2B mice. In line with the literature (Horowitz et al. 1977; Wiesenfeld et al. 1977; Yamamoto et al. 1982), the licking behavior was dominated by ~8 Hz rhythmic tongue movements for both WT and L7-PP2B. Moreover, the variations in lick rhythmicity, which can depend on contextual parameters (Weijnen 1998) such as those associated with the various stages of learning used here, occurred at an equal level in WT and L7-PP2B mice. Likewise, we recorded free whisking behavior in head-restrained mice and found that WT and L7-PP2B mice showed bouts of rhythmic whisking at comparable frequencies, that both WT and L7-PP2B mice scanned the whole area within reach of their whiskers, and that they both actively whisked during the insertion and presence of the stimulus bar in all trials tested. These control data are particularly relevant as object localization in the horizontal dimension requires active exploratory whisking (Knutsen et al. 2006), which, indeed, has been shown to typically occur in healthy mice at frequencies of 5–15 Hz (Berg and Kleinfeld 2003; Cao et al. 2012).

It is, in principle, also possible that the localization deficits in L7-PP2B mice reflected impairments in cerebellar sensory processing rather than motor or cognitive deficits (Hartmann and Bower 2001). We adapted our paradigm by beginning training of both genotypes with an association task. This allowed a baseline performance measure to test whether both groups not only whisked equally well, but also responded well to sensory stimulation. We found these initial learning curves and responses to stimuli to be similar in both genotypes in this task. Moreover, at the subsequent go and no-go trial testing (**Fig. 4**), L7-PP2B performers were able to reach criteria (albeit more slowly), and showed similar performance levels, indicating an ability to carry out the necessary responses to sensory stimuli.

Finally, since PP2B and Cre expressions are affected from early on in the L7-PP2B mutants, it is possible that their learning deficits in the whisker-based localization task result from aberrations in development rather than acute ongoing defects in cerebellar plasticity. If present at all, these potentially negative effects are probably relatively mild, since developmental compensation usually rescues negative confounders (Wulff et al. 2009), and since our electrophysiological recordings showed that the acute deficits in Purkinje cell activity of adult L7-PP2B mutants are in line with their putative deficits in potentiation and, thereby, in learning deficits. Together, we conclude that L7-PP2B mice do not show overt abnormalities in rhythmicity, frequency, or amplitude either of licking or whisker movements and that their learning deficits in the current whisker-based localization task are in line with the abnormalities in intrinsic plasticity and synaptic plasticity of their Purkinje cells.

Potential role of cerebellum in cognitive tasks

Over the past decade, an active debate has emerged on the potential role of the cerebellum in cognition. Supportive evidence was obtained not only in neuropsychological studies of cerebellar patients, functional imaging studies of human subjects, and tracing experiments in monkeys (Onuki et al. 2015; Schmahmann 2010; Strick et al. 2009; Timmann et al. 2010), but also in behavioral studies of cerebellar cell-specific mutant mice, in which specific aspects of spatial navigation or repetitive behavior were affected (Burguière et al. 2005; Rochefort et al. 2011; Tsai et al. 2012). Yet, it is not directly clear how to neutralize the argument that most of these so-called cognitive effects reflect small aberrations in sensorimotor activity such as the planning of eye movements (Glickstein et al. 2009). Moreover, we recently subjected four different cerebellar cell-specific mouse mutants, including L7-PP2B mice, to various cognitive tasks such as a sociability test, Morris water maze, contextual and cued fear conditioning, and open-field anxiety test, and none of the mutants showed a consistent deficit in any cognitive function (Galliano et al. 2013). However, none of these cognitive tasks included a response window or demanded precise processing in the temporal domain with a resolution of tens to hundreds of milliseconds. Given that the role of cerebellar processing in motor control has been shown to be particularly relevant when precise temporal accuracy

is required (De Zeeuw et al. 2011; Onuki et al. 2015), we reasoned that this facet might also be paramount for its control in cognitive function. We therefore undertook the current whisker-based localization study in which the temporal constraints play a prominent role, while the essential role of cerebral cortex in this task has been established (Aronoff et al. 2010; Brecht 2007; Huber et al. 2012; O'Connor et al. 2010a; O'Connor et al. 2010b; Petreanu et al. 2012; Xu et al. 2012). Several of the present findings support the possibility that the cerebellum contributes to cognitive processing when temporal demands are critical. First, the findings that fewer L7-PP2B mice were able to learn the whisker-based localization task, that they needed more time, and that their learning trajectories were considerably noisier than in WT mice support the possibility of a general contribution of cerebellar processing in this particular cognitive task. Second, the findings that fine-tuning of the precise timing of learned responses of L7-PP2B mutants was especially deficient at short response windows and that the trained WT, but not L7-PP2B, mice showed a well timed increase in licking just at the onset of the 500 ms RW corroborate our hypothesis that the cerebellum contributes to cognitive processing, in particular when temporal demands are engaged.

How may the cerebellum contribute to temporal precision in cognitive functions?

Different parts of the cerebellar cortex may engage different coding schemes varying from pure rate coding to temporal coding (Heck et al. 2013). Given that during trials we observed an increase in both firing rate and variability (CV2) in the simple spike activity of WT Purkinje cells, while the firing rate of their complex spike was also increased, it is likely that both coding mechanisms play a role (De Zeeuw et al. 2011). Indeed, in L7-PP2B animals we did not observe an increase in simple spike or complex spike firing frequency in the transition from intertrial to trial periods, and the irregularity of their simple spike firing was consistently lower than that in WT animals. While changes in rate coding might directly translate into differences in modulation amplitude, and thereby the rate activity of downstream targets (De Zeeuw et al. 1995), those in temporal coding may have a prominent impact on the precise timing of the activity of downstream targets (De Zeeuw et al. 2011; De Zeeuw et al. 2008). Pauses

in simple spike activity, which are reflected in the irregularity of firing, can translate into prominent rebound firing in the cerebellar nuclei, which in turn can trigger the initiation of movements (Witter et al. 2013). Likewise, one could imagine that rebound firing in the nuclei affects well timed initiation of activity as well as spiking coherence in areas downstream of the thalamus that are involved in cognitive tasks. For the whisker-based localization task, these may include not only the barrel cortex and whisker motor cortex (Popa et al. 2013a; Popa et al. 2013b), but also the striatum (Bostan et al. 2010; Hoshi et al. 2005). Conditional discrimination tasks that require goal-directed acts are typically thought to involve the basal ganglia (Hallock et al. 2013; Nishizawa et al. 2012), which may process stop cues for cancelling actions such as during no-go trials (Schmidt et al. 2013). One could hypothesize that the differences in activity in the cerebellar microzones that use rate coding (Heck et al. 2013; Zhou et al. 2014) explain the significant difference between the number of L7-PP2B and WT mice that exhibit successful learning at the long response window phase, whereas those in the cerebellar zones that predominantly use temporal coding may explain the differences and deficits seen at the shorter RW phase and no-go trials.

8. General discussion

The role of the cerebellum in learning and storage of sensory motor information has been widely probed over the years. It is generally assumed that long-term modifications in the strength of the synaptic transmission, in form of potentiation (LTP) or depression (LTD), and in neuronal intrinsic excitability constitute the biological basis for learning in the neuronal circuits. The LTD at parallel fiber-Purkinje cell (PF-PC) synapse, under control of climbing fibers (CFs) teaching signal, was initially suggested to provide the principal mechanism for cerebellar motor learning *(**Albus** 1971b; Marr and D. 1969)*. Following this initial proposal, several forms of synaptic and non-synaptic plasticity have been described in the cerebellar cortex *in vivo* and *in vitro (D'Angelo 2014; Gao et al. 2012)*. However, recent reviews raise the possibility that one form of plasticity at a single synapse is insufficient to explain the cerebellar motor learning which likely emerges from a more complex picture that includes various forms of long-term plasticity not confined to the cerebellar cortex *(D'Angelo et al. 2016a)*. Consistently with experimental data, computational models, embedding plasticity sites at the cerebellar nuclear level, show faster and more stable learning capabilities compared to previous models with only cortical plasticity sites, providing a more realistic reproduction of human-like behavior during cerebellar learning of associative task and shedding light on the crucial role of DCN neurons, previously poorly considered *(Antonietti et al. 2016a)*. Long-term modifications in the synaptic strength (both LTP and LTD) have been described in the inhibitory synapses between PCs and DCN neurons and in the excitatory synapses between MFs and DCN *(Medina and Mauk 1999; Morishita and Sastry 1996; Ouardouz and Sastry 2000; Pugh and Raman 2009; Zhang and Linden 2006)*. Moreover, persistent changes of the intrinsic excitability have been also reported in nuclear neurons *(Zhang et al. 2004)*. Despite plasticity in cerebellar neurons has extensively been studied over the years, to date, whether and how DCN are able to modify their discharge properties in response to patterned sensory stimulation had not been explored. Sensory tactile stimuli organized in theta patterns have been reported to induce long-term changes in cerebellar granule cells *(Roggeri et al. 2008)*, Purkinje cells and molecular layer interneurons *(Ramakrishnan et al. 2016)*

in vivo. This thesis addressed the role of the deep cerebellar nuclei in learning and storage of sensory information. We showed that sensory tactile stimulation evokes several discharge patterns in DCN neurons *in vivo*, likely depending on the synaptic pathways engaged by the stimulation. Moreover, our results provide the first evidence that DCN neurons are able to modify their discharge properties following a patterned sensory stimulation, completing the picture of the theta sensory stimulation impact on cerebellar neurons discharge *in vivo*.

Furthermore, we investigated the potential contribution of the cerebellum to cognition, starting from the considerable amount of studies which provide evidence of the connection between the cerebellum and cerebral associative areas of the brain, such as the medial prefrontal cortex (mPFC). Clinical reports support the hypothesis of a cerebellar role in cognitive function linking cerebellar abnormalities with several cognitive dysfunctions. The integral tractographic reconstruction of the pathways passing through the superior cerebellar peduncle provide a picture of the nature of cerebello-cerebral communication in humans *(Palesi et al. 2015)* which manly involve projections from the deep cerebellar nuclei directed toward the prefrontal cortex. *In vivo* electrophysiological studies in rodents support the same finding, reporting a bidirectional connection between these brain regions *(Watson et al. 2014; Watson et al. 2009)*. Herein, we characterized neuronal responses in the prelimbic region (PrL) of the mPFC, following the electrical stimulation of DCN. Furthermore, using selective dopamine receptors antagonists, we have pharmacologically explored whether and how PrL neurons spontaneous and evoked activities are influenced by the dopaminergic system. Overall our findings show physiological interactions between the cerebellum and the PrL of the mPFC, providing insights of a functional interplay between these two regions and for understanding neuronal correlates underlying dopamine-related cognitive deficits involving the mPFC.

Moreover, *in vivo* extracellular recordings from cerebellar Purkinje cells of L7-PP2B mutants, which suffer from impaired intrinsic plasticity and postsynaptic long-term potentiation at parallel fibers-Purkinje cells synapses, and littermate control mice, both subjected to a decision making task, support the hypothesis of a cerebellar contribution to cognitive task,

on the basis of genotypic, behavioral and electrophysiological differences *(Rahmati et al. 2014)*.

Overall, the findings reported in this thesis provide new insights for understanding DCN role in cerebellar functioning and in driving PrL neurons activity. As reported in chapter 5, DCN neurons are able to modify their responsiveness following sensory stimulation, depending on stimulus-induced oscillatory behavior. These results are relevant not only for understanding cerebellar processing itself, but also to understand cerebellar contribution to higher order cognitive systems. Indeed, the results described in chapter 6 provide strong evidence of a DCN drive over mPFC PrL neuronal activity, also involving the dopaminergic neuromodulatory system. Also considering the results reported in chapter 7 and briefly summarized above, it is more and more evident that cerebellar processing should be considered in a broader picture of general brain (and cortical) processing, including higher order cognitive functions, going beyond its role in the sensori-motor system.

References

Albus J. The theory of cerebellar function. Math. Biosci., 1971a, p. 25-61.

Albus JS. A theory of cerebellar function. *Math Biosci 10, 25-61* 1971b.

Ambrosi G, Flace P, Lorusso L, Girolamo F, Rizzi A, Bosco L, Errede M, Virgintino D, Roncali L, and Benagiano V. Non-traditional large neurons in the granular layer of the cerebellar cortex. *Eur J Histochem* 51 Suppl 1: 59-64, 2007.

Andreasen NC, O'Leary DS, Cizadlo T, Arndt S, Rezai K, Ponto LL, Watkins GL, and Hichwa RD. Schizophrenia and cognitive dysmetria: a positron-emission tomography study of dysfunctional prefrontal-thalamic-cerebellar circuitry. *Proc Natl Acad Sci U S A* 93: 9985-9990, 1996.

Andreasen NC, and Pierson R. The role of the cerebellum in schizophrenia. *Biol Psychiatry* 64: 81-88, 2008.

Ankri L, Husson Z, Pietrajtis K, Proville R, Lena C, Yarom Y, Dieudonne S, and Uusisaari MY. A novel inhibitory nucleo-cortical circuit controls cerebellar Golgi cell activity. *Elife* 4: 2015.

Antonietti A, Casellato C, Garrido JA, Luque NR, Naveros F, Ros E, D' Angelo E, and Pedrocchi A. Spiking Neural Network With Distributed Plasticity Reproduces Cerebellar Learning in Eye Blink Conditioning Paradigms. *IEEE Trans Biomed Eng* 63: 210-219, 2016a.

Antonietti A, Casellato C, Garrido JA, Luque NR, Naveros F, Ros E, E DA, and Pedrocchi A. Spiking Neural Network With Distributed Plasticity Reproduces Cerebellar Learning in Eye Blink Conditioning Paradigms. *IEEE Trans Biomed Eng* 63: 210-219, 2016b.

Apps R, and Hawkes R. Cerebellar cortical organization: a one-map hypothesis. *Nat Rev Neurosci* 10: 670-681, 2009.

Armano S, Rossi P, Taglietti V, and D'Angelo E. Long-term potentiation of intrinsic excitability at the mossy fiber-granule cell synapse of rat cerebellum. *J Neurosci* 20: 5208-5216, 2000.

Aronoff R, Matyas F, Mateo C, Ciron C, Schneider B, and Petersen CC. Long-range connectivity of mouse primary somatosensory barrel cortex. *Eur J Neurosci* 31: 2221-2233, 2010.

Attwell PJE, Rahman S, and Yeo CH. Acquisition of Eyeblink Conditioning Is Critically Dependent on Normal Function in Cerebellar Cortical Lobule HVI. *The Journal of Neuroscience* 21: 5715-5722, 2001.

Axelrad H, and Crepel F. [Selective representation of vibrissa at the level of cerebellar Purkinje cells by way of climbing fibers in rats]. *C R Acad Sci Hebd Seances Acad Sci D* 284: 1321-1324, 1977.

Bagnall MW, Zingg B, Sakatos A, Moghadam SH, Zeilhofer HU, and du Lac S. Glycinergic projection neurons of the cerebellum. *J Neurosci* 29: 10104-10110, 2009.

Barski JJ, Dethleffsen K, and Meyer M. Cre recombinase expression in cerebellar Purkinje cells. *Genesis* 28: 93-98, 2000.

Bengtsson F, Ekerot CF, and Jörntell H. In vivo analysis of inhibitory synaptic inputs and rebounds in deep cerebellar nuclear neurons. *PLoS One* 6: e18822, 2011.

Bengtsson F, and Jorntell H. Ketamine and xylazine depress sensory-evoked parallel fiber and climbing fiber responses. *J Neurophysiol* 98: 1697-1705, 2007.

Bennett MR. Monoaminergic synapses and schizophrenia: 45 years of neuroleptics. *J Psychopharmacol* 12: 289-304, 1998.

Berg RW, and Kleinfeld D. Rhythmic whisking by rat: retraction as well as protraction of the vibrissae is under active muscular control. *J Neurophysiol* 89: 104-117, 2003.

Blaha CD, Yang CR, Floresco SB, Barr AM, and Phillips AG. Stimulation of the ventral subiculum of the hippocampus evokes glutamate receptor-mediated changes in dopamine efflux in the rat nucleus accumbens. *Eur J Neurosci* 9: 902-911, 1997.

Bosman LW, Houweling AR, Owens CB, Tanke N, Shevchouk OT, Rahmati N, Teunissen WH, Ju C, Gong W, Koekkoek SK, and De Zeeuw CI. Anatomical pathways involved in generating and sensing rhythmic whisker movements. *Front Integr Neurosci* 5: 53, 2011.

Bosman LW, Koekkoek SK, Shapiro J, Rijken BF, Zandstra F, van der Ende B, Owens CB, Potters JW, de Gruijl JR, Ruigrok TJ, and De Zeeuw CI. Encoding of whisker input by cerebellar Purkinje cells. *J Physiol* 588: 3757-3783, 2010.

Bostan AC, Dum RP, and Strick PL. The basal ganglia communicate with the cerebellum. *Proc Natl Acad Sci U S A* 107: 8452-8456, 2010.

Bower JM, and Woolston DC. Congruence of spatial organization of tactile projections to granule cell and Purkinje cell layers of cerebellar hemispheres of the albino rat: vertical organization of cerebellar cortex. *J Neurophysiol* 49: 745-766, 1983.
Brecht M. Barrel cortex and whisker-mediated behaviors. *Curr Opin Neurobiol* 17: 408-416, 2007.
Bryant JL, Boughter JD, Gong S, LeDoux MS, and Heck DH. Cerebellar cortical output encodes temporal aspects of rhythmic licking movements and is necessary for normal licking frequency. *Eur J Neurosci* 32: 41-52, 2010.
Buchta WC, Mahler SV, Harlan B, Aston-Jones GS, and Riegel AC. Dopamine terminals from the ventral tegmental area gate intrinsic inhibition in the prefrontal cortex. *Physiol Rep* 5: 2017.
Burguière E, Arleo A, Hojjati M, Elgersma Y, De Zeeuw CI, Berthoz A, and Rondi-Reig L. Spatial navigation impairment in mice lacking cerebellar LTD: a motor adaptation deficit? *Nat Neurosci* 8: 1292-1294, 2005.
Buzsaki G. *Rhythms of the brain*. New York: Oxford University Press US, 2006.
Buzsaki G. Theta rhythm of navigation: link between path integration and landmark navigation, episodic and semantic memory. *Hippocampus* 15: 827-840, 2005.
Caligiore D, Pezzulo G, Baldassarre G, Bostan AC, Strick PL, Doya K, Helmich RC, Dirkx M, Houk J, Jörntell H, Lago-Rodriguez A, Galea JM, Miall RC, Popa T, Kishore A, Verschure PF, Zucca R, and Herreros I. Consensus Paper: Towards a Systems-Level View of Cerebellar Function: the Interplay Between Cerebellum, Basal Ganglia, and Cortex. *Cerebellum* 16: 203-229, 2017.
Canto CB, Witter L, and De Zeeuw CI. Whole-Cell Properties of Cerebellar Nuclei Neurons In Vivo. *PLoS One* 11: e0165887, 2016.
Cantrell AR, Smith RD, Goldin AL, Scheuer T, and Catterall WA. Dopaminergic modulation of sodium current in hippocampal neurons via cAMP-dependent phosphorylation of specific sites in the sodium channel alpha subunit. *J Neurosci* 17: 7330-7338, 1997.
Cao Y, Roy S, Sachdev RN, and Heck DH. Dynamic correlation between whisking and breathing rhythms in mice. *J Neurosci* 32: 1653-1659, 2012.

Carvell GE, and Simons DJ. Biometric analyses of vibrissal tactile discrimination in the rat. *J Neurosci* 10: 2638-2648, 1990.

Casellato C, Antonietti A, Garrido JA, Carrillo RR, Luque NR, Ros E, Pedrocchi A, and D'Angelo E. Adaptive robotic control driven by a versatile spiking cerebellar network. *PLoS One* 9: e112265, 2014.

Casellato C, Antonietti A, Garrido JA, Carrillo RR, Luque NR, Ros E, Pedrocchi A, and D'Angelo E. Distributed cerebellar plasticity implements generalized multiple-scale memory components in real-robot sensorimotor tasks. *Front Comput Neurosci* in press: 2015.

Cheron G, Marquez-Ruiz J, and Dan B. Oscillations, Timing, Plasticity, and Learning in the Cerebellum. *Cerebellum* 15: 122-138, 2016.

Cook JR, and Wiesendanger M. Input from trigeminal cutaneous afferents to neurones of the inferior olive in rats. *Exp Brain Res* 26: 193-202, 1976.

D'Angelo E. The organization of plasticity in the cerebellar cortex: from synapses to control. *Prog Brain Res* 210: 31-58, 2014.

D'Angelo E, Antonietti A, Casali S, Casellato C, Garrido JA, Luque NR, Mapelli L, Masoli S, Pedrocchi A, Prestori F, Rizza MF, and Ros E. Modeling the Cerebellar Microcircuit: New Strategies for a Long-Standing Issue. *Front Cell Neurosci* 10: 176, 2016a.

D'Angelo E, and Casali S. Seeking a unified framework for cerebellar function and dysfunction: from circuit operations to cognition. *Front Neural Circuits* 6: 116, 2012.

D'Angelo E, and De Zeeuw CI. Timing and plasticity in the cerebellum: focus on the granular layer. *Trends Neurosci* 32: 30-40, 2009.

D'Angelo E, Mapelli L, Casellato C, Garrido JA, Luque N, Monaco J, Prestori F, Pedrocchi A, and Ros E. Distributed Circuit Plasticity: New Clues for the Cerebellar Mechanisms of Learning. *Cerebellum* 15: 139-151, 2016b.

De Zeeuw CI, Hoebeek FE, Bosman LW, Schonewille M, Witter L, and Koekkoek SK. Spatiotemporal firing patterns in the cerebellum. *Nat Rev Neurosci* 12: 327-344, 2011.

De Zeeuw CI, Hoebeek FE, and Schonewille M. Causes and consequences of oscillations in the cerebellar cortex. *Neuron* 58: 655-658, 2008.

De Zeeuw CI, Wylie DR, Stahl JS, and Simpson JI. Phase relations of Purkinje cells in the rabbit flocculus during compensatory eye movements. *J Neurophysiol* 74: 2051-2064, 1995.
Dembrow N, and Johnston D. Subcircuit-specific neuromodulation in the prefrontal cortex. *Front Neural Circuits* 8: 54, 2014.
Diwakar S, Lombardo P, Solinas S, Naldi G, and D'Angelo E. Local field potential modeling predicts dense activation in cerebellar granule cells clusters under LTP and LTD control. *PLoS One* 6: e21928, 2011.
Dykstra S, Engbers JD, Bartoletti TM, and Turner RW. Determinants of rebound burst responses in rat cerebellar nuclear neurons to physiological stimuli. *J Physiol* 594: 985-1003, 2016.
Ernst M, Zametkin AJ, Matochik JA, Pascualvaca D, and Cohen RM. Low medial prefrontal dopaminergic activity in autistic children. *Lancet* 350: 638, 1997.
Fatemi SH, Aldinger KA, Ashwood P, Bauman ML, Blaha CD, Blatt GJ, Chauhan A, Chauhan V, Dager SR, Dickson PE, Estes AM, Goldowitz D, Heck DH, Kemper TL, King BH, Martin LA, Millen KJ, Mittleman G, Mosconi MW, Persico AM, Sweeney JA, Webb SJ, and Welsh JP. Consensus paper: pathological role of the cerebellum in autism. *Cerebellum* 11: 777-807, 2012.
Floresco SB, and Magyar O. Mesocortical dopamine modulation of executive functions: beyond working memory. *Psychopharmacology (Berl)* 188: 567-585, 2006.
Floresco SB, Magyar O, Ghods-Sharifi S, Vexelman C, and Tse MT. Multiple dopamine receptor subtypes in the medial prefrontal cortex of the rat regulate set-shifting. *Neuropsychopharmacology* 31: 297-309, 2006.
Gall D, Prestori F, Sola E, D'Errico A, Roussel C, Forti L, Rossi P, and D'Angelo E. Intracellular calcium regulation by burst discharge determines bidirectional long-term synaptic plasticity at the cerebellum input stage. *J Neurosci* 25: 4813-4822, 2005.
Galliano E, Potters JW, Elgersma Y, Wisden W, Kushner SA, De Zeeuw CI, and Hoebeek FE. Synaptic transmission and plasticity at inputs to murine cerebellar Purkinje cells are largely dispensable for standard nonmotor tasks. *J Neurosci* 33: 12599-12618, 2013.
Gao Z, Proietti-Onori M, Lin Z, Ten Brinke MM, Boele HJ, Potters JW, Ruigrok TJ, Hoebeek FE, and De Zeeuw CI. Excitatory Cerebellar

Nucleocortical Circuit Provides Internal Amplification during Associative Conditioning. *Neuron* 89: 645-657, 2016.
Gao Z, van Beugen BJ, and De Zeeuw CI. Distributed synergistic plasticity and cerebellar learning. *Nat Rev Neurosci* 13: 619-635, 2012.
Garrido JA, Luque NR, D'Angelo E, and Ros E. Distributed cerebellar plasticity implements adaptable gain control in a manipulation task: a closed-loop robotic simulation. *Front Neural Circuits* 7: 159, 2013.
Gaspar P, Bloch B, and Le Moine C. D1 and D2 receptor gene expression in the rat frontal cortex: cellular localization in different classes of efferent neurons. *Eur J Neurosci* 7: 1050-1063, 1995.
Giza J, Urbanski MJ, Prestori F, Bandyopadhyay B, Yam A, Friedrich V, Kelley K, D'Angelo E, and Goldfarb M. Behavioral and cerebellar transmission deficits in mice lacking the autism-linked gene islet brain-2. *J Neurosci* 30: 14805-14816, 2010.
Glickstein M, Strata P, and Voogd J. Cerebellum: history. *Neuroscience* 162: 549-559, 2009.
Godaux E, Cheron G, and Mettens P. Ketamine induces failure of the oculomotor neural integrator in the cat. *Neurosci Lett* 116: 162-167, 1990.
Gowen E, and Miall RC. The cerebellum and motor dysfunction in neuropsychiatric disorders. *Cerebellum* 6: 268-279, 2007.
Grishkat HL, and Eisenman LM. Development of the spinocerebellar projection in the prenatal mouse. *J Comp Neurol* 363: 93-108, 1995.
Grodd W, Hülsmann E, Lotze M, Wildgruber D, and Erb M. Sensorimotor mapping of the human cerebellum: fMRI evidence of somatotopic organization. *Hum Brain Mapp* 13: 55-73, 2001.
Gulledge AT, and Jaffe DB. Dopamine decreases the excitability of layer V pyramidal cells in the rat prefrontal cortex. *J Neurosci* 18: 9139-9151, 1998.
Hallock HL, Arreola AC, Shaw CL, and Griffin AL. Dissociable roles of the dorsal striatum and dorsal hippocampus in conditional discrimination and spatial alternation T-maze tasks. *Neurobiol Learn Mem* 100: 108-116, 2013.
Hansel C, Linden DJ, and D'Angelo E. Beyond parallel fiber LTD: the diversity of synaptic and non-synaptic plasticity in the cerebellum. *Nat Neurosci* 4: 467-475, 2001a.

Hansel C, Linden DJ, and D'Angelo E. Beyond parallel fiber LTD: the diversity of synaptic and nonsynaptic plasticity in the cerebellum. *Nature Neuroscience* 4: 467-475, 2001b.
Hara K, and Harris RA. The anesthetic mechanism of urethane: the effects on neurotransmitter-gated ion channels. *Anesth Analg* 94: 313-318, table of contents, 2002.
Hartmann MJ. Active touch, exploratory movements, and sensory prediction. *Integr Comp Biol* 49: 681-690, 2009.
Hartmann MJ, and Bower JM. Tactile responses in the granule cell layer of cerebellar folium crus IIa of freely behaving rats. *J Neurosci* 21: 3549-3563, 2001.
Hayar A, Bryant JL, Boughter JD, and Heck DH. A low-cost solution to measure mouse licking in an electrophysiological setup with a standard analog-to-digital converter. *J Neurosci Methods* 153: 203-207, 2006.
Heck DH, De Zeeuw CI, Jaeger D, Khodakhah K, and Person AL. The neuronal code(s) of the cerebellum. *J Neurosci* 33: 17603-17609, 2013.
Heinricher MM. *Principles of Extracellular Single-Unit Recording*. Thieme Verlagsgruppe, Stuttgart, New York, Delhi, Rio, 2004.
Henze R, Brunner R, Thiemann U, Parzer P, Richterich A, Essig M, Resch F, and Stieltjes B. Gray matter alterations in first-admission adolescents with schizophrenia. *J Neuroimaging* 21: 241-246, 2011.
Hnasko TS, Hjelmstad GO, Fields HL, and Edwards RH. Ventral tegmental area glutamate neurons: electrophysiological properties and projections. *J Neurosci* 32: 15076-15085, 2012.
Hoebeek FE, Witter L, Ruigrok TJ, and De Zeeuw CI. Differential olivo-cerebellar cortical control of rebound activity in the cerebellar nuclei. *Proc Natl Acad Sci U S A* 107: 8410-8415, 2010.
Hoover WB, and Vertes RP. Anatomical analysis of afferent projections to the medial prefrontal cortex in the rat. *Brain Struct Funct* 212: 149-179, 2007.
Horowitz GP, Stephan FK, Smith JC, and Whitney G. Genetic and environmental variability in lick rates of mice. *Physiol Behav* 19: 493-496, 1977.
Hoshi E, Tremblay L, Féger J, Carras PL, and Strick PL. The cerebellum communicates with the basal ganglia. *Nat Neurosci* 8: 1491-1493, 2005.

Houck BD, and Person AL. Cerebellar loops: a review of the nucleocortical pathway. *Cerebellum* 13: 378-385, 2014.
Huber D, Gutnisky DA, Peron S, O'Connor DH, Wiegert JS, Tian L, Oertner TG, Looger LL, and Svoboda K. Multiple dynamic representations in the motor cortex during sensorimotor learning. *Nature* 484: 473-478, 2012.
Ikai Y, Takada M, Shinonaga Y, and Mizuno N. Dopaminergic and non-dopaminergic neurons in the ventral tegmental area of the rat project, respectively, to the cerebellar cortex and deep cerebellar nuclei. *Neuroscience* 51: 719-728, 1992.
Ito M. Cerebellar long-term depression: characterization, signal transduction, and functional roles. *Physiol Rev* 81: 1143-1195, 2001.
Jacobson GA, Rokni D, and Yarom Y. A model of the olivo-cerebellar system as a temporal pattern generator. *Trends Neurosci* 31: 617-625, 2008.
Jirenhed DA, Bengtsson F, and Hesslow G. Acquisition, extinction, and reacquisition of a cerebellar cortical memory trace. *J Neurosci* 27: 2493-2502, 2007.
Kansal K, Yang Z, Fishman AM, Sair HI, Ying SH, Jedynak BM, Prince JL, and Onyike CU. Structural cerebellar correlates of cognitive and motor dysfunctions in cerebellar degeneration. *Brain* 140: 707-720, 2017.
Kehr W, Lindqvist M, and Carlsson A. Distribution of dopamine in the rat cerebral cortex. *J Neural Transm* 38: 173-180, 1976.
Kishore A, Meunier S, and Popa T. Cerebellar influence on motor cortex plasticity: behavioral implications for Parkinson's disease. *Front Neurol* 5: 68, 2014.
Kistler WM, and De Zeeuw CI. Time windows and reverberating loops: a reverse-engineering approach to cerebellar function. *Cerebellum* 2: 44-54, 2003.
Kleinfeld D, and Deschênes M. Neuronal basis for object location in the vibrissa scanning sensorimotor system. *Neuron* 72: 455-468, 2011.
Knutsen PM, Pietr M, and Ahissar E. Haptic object localization in the vibrissal system: behavior and performance. *J Neurosci* 26: 8451-8464, 2006.

Konarski JZ, McIntyre RS, Grupp LA, and Kennedy SH. Is the cerebellum relevant in the circuitry of neuropsychiatric disorders? *J Psychiatry Neurosci* 30: 178-186, 2005.
Kyriakopoulos M, Vyas NS, Barker GJ, Chitnis XA, and Frangou S. A diffusion tensor imaging study of white matter in early-onset schizophrenia. *Biol Psychiatry* 63: 519-523, 2008.
Lang EJ, Sugihara I, and Llinás R. Olivocerebellar modulation of motor cortex ability to generate vibrissal movements in rat. *J Physiol* 571: 101-120, 2006.
Larouche M, Che PM, and Hawkes R. Neurogranin expression identifies a novel array of Purkinje cell parasagittal stripes during mouse cerebellar development. *J Comp Neurol* 494: 215-227, 2006.
Lawyer G, Nesvåg R, Varnäs K, Okugawa G, and Agartz I. Grey and white matter proportional relationships in the cerebellar vermis altered in schizophrenia. *Cerebellum* 8: 52-60, 2009.
LeDoux MS, Hurst DC, and Lorden JF. Single-unit activity of cerebellar nuclear cells in the awake genetically dystonic rat. *Neuroscience* 86: 533-545, 1998.
Li CL, and Parker LO. Effect of dentate stimulation on neuronal activity in the globus pallidus. *Exp Neurol* 24: 298-309, 1969.
Lidow MS, Koh PO, and Arnsten AF. D1 dopamine receptors in the mouse prefrontal cortex: Immunocytochemical and cognitive neuropharmacological analyses. *Synapse* 47: 101-108, 2003.
Llinas R, and Muhlethaler M. An electrophysiological study of the in vitro, perfused brain stem-cerebellum of adult guinea-pig. *J Physiol* 404: 215-240, 1988.
Llinas RR. The intrinsic electrophysiological properties of mammalian neurons: insights into central nervous system function. *Science* 242: 1654-1664, 1988.
Loewenstein Y, Mahon S, Chadderton P, Kitamura K, Sompolinsky H, Yarom Y, and Häusser M. Bistability of cerebellar Purkinje cells modulated by sensory stimulation. *Nat Neurosci* 8: 202-211, 2005.
LORENTE de NO R. A study of nerve physiology. *Stud Rockefeller Inst Med Res Repr* 131: 1-496, 1947.
Luque NR, Garrido JA, Carrillo RR, D'Angelo E, and Ros E. Fast convergence of learning requires plasticity between inferior olive and deep

cerebellar nuclei in a manipulation task: a closed-loop robotic simulation. *Front Comput Neurosci* 8: 97, 2014.
Malenka RC, and Nicoll RA. Dopamine decreases the calcium-activated afterhyperpolarization in hippocampal CA1 pyramidal cells. *Brain Res* 379: 210-215, 1986.
Mapelli J, and D'Angelo E. The spatial organization of long-term synaptic plasticity at the input stage of cerebellum. *J Neurosci* 27: 1285-1296, 2007.
Mapelli L, Pagani M, Garrido JA, and D'Angelo E. Integrated plasticity at inhibitory and excitatory synapses in the cerebellar circuit. *Front Cell Neurosci* 9: 169, 2015a.
Mapelli L, Pagani M, Garrido JA, and D'Angelo E. Integrated plasticity at inhibitory and excitatory synapses in the cerebellar circuit. *Front Cell Neurosci* 9: 2015b.
Marquez-Ruiz J, and Cheron G. Sensory stimulation-dependent plasticity in the cerebellar cortex of alert mice. *PLoS One* 7: e36184, 2012.
Marr, and D. A theory of cerebellar cortex. *J Physiol* 1969.
Marr D. A theory of cerebellar cortex. *J Physiol* 202: 437-470, 1969.
Marshall SP, and Lang EJ. Inferior olive oscillations gate transmission of motor cortical activity to the cerebellum. In: *J Neurosci*. United States: 2004, p. 11356-11367.
Mason CA, and Gregory E. Postnatal maturation of cerebellar mossy and climbing fibers: transient expression of dual features on single axons. *J Neurosci* 4: 1715-1735, 1984.
Maurice N, Deniau JM, Glowinski J, and Thierry AM. Relationships between the prefrontal cortex and the basal ganglia in the rat: physiology of the cortico-nigral circuits. *J Neurosci* 19: 4674-4681, 1999.
Mawhinney LJ, de Rivero Vaccari JP, Alonso OF, Jimenez CA, Furones C, Moreno WJ, Lewis MC, Dietrich WD, and Bramlett HM. Isoflurane/nitrous oxide anesthesia induces increases in NMDA receptor subunit NR2B protein expression in the aged rat brain. *Brain Res* 1431: 23-34, 2012.
Medina JF, Garcia KS, and Mauk MD. A mechanism for savings in the cerebellum. *J Neurosci* 21: 4081-4089, 2001.
Medina JF, and Mauk MD. Computer simulation of cerebellar information processing. *Nat Neurosci* 3 Suppl: 1205-1211, 2000.

Medina JF, and Mauk MD. Simulations of cerebellar motor learning: computational analysis of plasticity at the mossy fiber to deep nucleus synapse. *J Neurosci* 19: 7140-7151, 1999.
Middleton FA, and Strick PL. Anatomical evidence for cerebellar and basal ganglia involvement in higher cognitive function. *Science* 266: 458-461, 1994.
Middleton FA, and Strick PL. Cerebellar projections to the prefrontal cortex of the primate. *J Neurosci* 21: 700-712, 2001.
Middleton FA, and Strick PL. Dentate output channels: motor and cognitive components. *Prog Brain Res* 114: 553-566, 1997.
Mittleman G, Goldowitz D, Heck DH, and Blaha CD. Cerebellar modulation of frontal cortex dopamine efflux in mice: relevance to autism and schizophrenia. *Synapse* 62: 544-550, 2008.
Monaco J, Casellato C, Koch G, and D'Angelo E. Cerebellar theta burst stimulation dissociates memory components in eyeblink classical conditioning. *Eur J Neurosci* 40: 3363-3370, 2014.
Morishita W, and Sastry BR. Postsynaptic mechanisms underlying long-term depression of GABAergic transmission in neurons of the deep cerebellar nuclei. *J Neurophysiol* 76: 59-68, 1996.
Morissette J, and Bower JM. Contribution of somatosensory cortex to responses in the rat cerebellar granule cell layer following peripheral tactile stimulation. *Exp Brain Res* 109: 240-250, 1996.
Muller T, Grosche J, Ohlemeyer C, and Kettenmann H. NMDA-activated currents in Bergmann glial cells. *Neuroreport* 4: 671-674, 1993.
Murray E, Wise S, and and Graham K. The Evolution of Memory Systems. edited by Press OU2017.
Nieoullon A, Cheramy A, and Glowinski J. Release of dopamine in both caudate nuclei and both substantia nigrae in response to unilateral stimulation of cerebellar nuclei in the cat. *Brain Res* 148: 143-152, 1978.
Nishizawa K, Fukabori R, Okada K, Kai N, Uchigashima M, Watanabe M, Shiota A, Ueda M, Tsutsui Y, and Kobayashi K. Striatal indirect pathway contributes to selection accuracy of learned motor actions. *J Neurosci* 32: 13421-13432, 2012.
O'Connor DH, Clack NG, Huber D, Komiyama T, Myers EW, and Svoboda K. Vibrissa-based object localization in head-fixed mice. *J Neurosci* 30: 1947-1967, 2010a.

O'Connor DH, Peron SP, Huber D, and Svoboda K. Neural activity in barrel cortex underlying vibrissa-based object localization in mice. *Neuron* 67: 1048-1061, 2010b.
Ohyama T, Nores WL, and Mauk MD. Stimulus generalization of conditioned eyelid responses produced without cerebellar cortex: implications for plasticity in the cerebellar nuclei. *Learn Mem* 10: 346-354, 2003.
Ohyama T, Nores WL, Medina JF, Riusech FA, and Mauk MD. Learning-induced plasticity in deep cerebellar nucleus. *J Neurosci* 26: 12656-12663, 2006.
Okugawa G, Nobuhara K, Takase K, and Kinoshita T. Cerebellar posterior superior vermis and cognitive cluster scores in drug-naive patients with first-episode schizophrenia. *Neuropsychobiology* 56: 216-219, 2007.
Oldfield CS, Marty A, and Stell BM. Interneurons of the cerebellar cortex toggle Purkinje cells between up and down states. *Proc Natl Acad Sci U S A* 107: 13153-13158, 2010.
Omelchenko N, and Sesack SR. Ultrastructural analysis of local collaterals of rat ventral tegmental area neurons: GABA phenotype and synapses onto dopamine and GABA cells. *Synapse* 63: 895-906, 2009.
Onuki Y, Van Someren EJ, De Zeeuw CI, and Van der Werf YD. Hippocampal-cerebellar interaction during spatio-temporal prediction. *Cereb Cortex* 25: 313-321, 2015.
Otani S, Bai J, and Blot K. Dopaminergic modulation of synaptic plasticity in rat prefrontal neurons. *Neurosci Bull* 31: 183-190, 2015.
Ouardouz M, and Sastry BR. Mechanisms underlying LTP of inhibitory synaptic transmission in the deep cerebellar nuclei. *J Neurophysiol* 84: 1414-1421, 2000.
Palesi F, Tournier JD, Calamante F, Muhlert N, Castellazzi G, Chard D, D'Angelo E, and Wheeler-Kingshott CA. Contralateral cerebello-thalamo-cortical pathways with prominent involvement of associative areas in humans in vivo. *Brain Struct Funct* 220: 3369-3384, 2015.
Palmen SJ, van Engeland H, Hof PR, and Schmitz C. Neuropathological findings in autism. *Brain* 127: 2572-2583, 2004.
Parfitt KD, Gratton A, and Bickford-Wimer PC. Electrophysiological effects of selective D1 and D2 dopamine receptor agonists in the medial

prefrontal cortex of young and aged Fischer 344 rats. *J Pharmacol Exp Ther* 254: 539-545, 1990.

Pedarzani P, and Storm JF. Dopamine modulates the slow Ca(2+)-activated K+ current IAHP via cyclic AMP-dependent protein kinase in hippocampal neurons. *J Neurophysiol* 74: 2749-2753, 1995.

Perkon I, Kosir A, Itskov PM, Tasic J, and Diamond ME. Unsupervised quantification of whisking and head movement in freely moving rodents. *J Neurophysiol* 105: 1950-1962, 2011.

Petreanu L, Gutnisky DA, Huber D, Xu NL, O'Connor DH, Tian L, Looger L, and Svoboda K. Activity in motor-sensory projections reveals distributed coding in somatosensation. *Nature* 489: 299-303, 2012.

Pierce K, and Courchesne E. Evidence for a cerebellar role in reduced exploration and stereotyped behavior in autism. *Biol Psychiatry* 49: 655-664, 2001.

Pirot S, Godbout R, Mantz J, Tassin JP, Glowinski J, and Thierry AM. Inhibitory effects of ventral tegmental area stimulation on the activity of prefrontal cortical neurons: evidence for the involvement of both dopaminergic and GABAergic components. *Neuroscience* 49: 857-865, 1992.

Pockett S. Dopamine changes the shape of action potentials in hippocampal pyramidal cells. *Brain Res* 342: 386-390, 1985.

Popa D, Spolidoro M, Proville RD, Guyon N, Belliveau L, and Léna C. Functional role of the cerebellum in gamma-band synchronization of the sensory and motor cortices. *J Neurosci* 33: 6552-6556, 2013a.

Popa T, Velayudhan B, Hubsch C, Pradeep S, Roze E, Vidailhet M, Meunier S, and Kishore A. Cerebellar processing of sensory inputs primes motor cortex plasticity. *Cereb Cortex* 23: 305-314, 2013b.

Prestori F, Bonardi C, Mapelli L, Lombardo P, Goselink R, De Stefano ME, Gandolfi D, Mapelli J, Bertrand D, Schonewille M, De Zeeuw C, and D'Angelo E. Gating of long-term potentiation by nicotinic acetylcholine receptors at the cerebellum input stage. *PLoS One* 8: e64828, 2013.

Pugh JR, and Raman IM. Mechanisms of potentiation of mossy fiber EPSCs in the cerebellar nuclei by coincident synaptic excitation and inhibition. *J Neurosci* 28: 10549-10560, 2008.

Pugh JR, and Raman IM. Nothing can be coincidence: synaptic inhibition and plasticity in the cerebellar nuclei. *Trends Neurosci* 32: 170-177, 2009.
Pugh JR, and Raman IM. Potentiation of mossy fiber EPSCs in the cerebellar nuclei by NMDA receptor activation followed by postinhibitory rebound current. *Neuron* 51: 113-123, 2006.
Racine RJ, Wilson DA, Gingell R, and Sunderland D. Long-term potentiation in the interpositus and vestibular nuclei in the rat. *Exp Brain Res* 63: 158-162, 1986.
Rahmati N, Owens CB, Bosman LW, Spanke JK, Lindeman S, Gong W, Potters JW, Romano V, Voges K, Moscato L, Koekkoek SK, Negrello M, and De Zeeuw CI. Cerebellar potentiation and learning a whisker-based object localization task with a time response window. *J Neurosci* 34: 1949-1962, 2014.
RALL W. Electrophysiology of a dendritic neuron model. *Biophys J* 2: 145-167, 1962.
Ramakrishnan KB, Voges K, De Propris L, De Zeeuw CI, and D'Angelo E. Tactile Stimulation Evokes Long-Lasting Potentiation of Purkinje Cell Discharge In Vivo. *Front Cell Neurosci* 10: 36, 2016.
Rand S., and Swenson MD. REVIEW OF CLINICAL AND FUNCTIONAL NEUROSCIENCE. 2006.
Rasmussen A, Jirenhed DA, and Hesslow G. Simple and complex spike firing patterns in Purkinje cells during classical conditioning. *Cerebellum* 7: 563-566, 2008.
Ratcheson RA, and Li CL. Effect of dentate stimulation on neuronal activity in the caudate nucleus. *Exp Neurol* 25: 268-281, 1969.
Rinaldi A, Mandillo S, Oliverio A, and Mele A. D1 and D2 receptor antagonist injections in the prefrontal cortex selectively impair spatial learning in mice. *Neuropsychopharmacology* 32: 309-319, 2007.
Rochefort C, Arabo A, André M, Poucet B, Save E, and Rondi-Reig L. Cerebellum shapes hippocampal spatial code. *Science* 334: 385-389, 2011.
Rogers TD, Dickson PE, Heck DH, Goldowitz D, Mittleman G, and Blaha CD. Connecting the dots of the cerebro-cerebellar role in cognitive function: neuronal pathways for cerebellar modulation of dopamine release in the prefrontal cortex. *Synapse* 65: 1204-1212, 2011.

Roggeri L, Rivieccio B, Rossi P, and D'Angelo E. Tactile stimulation evokes long-term synaptic plasticity in the granular layer of cerebellum. *J Neurosci* 28: 6354-6359, 2008.
Rowland NC, and Jaeger D. Coding of tactile response properties in the rat deep cerebellar nuclei. *J Neurophysiol* 94: 1236-1251, 2005.
Rowland NC, and Jaeger D. Responses to tactile stimulation in deep cerebellar nucleus neurons result from recurrent activation in multiple pathways. *J Neurophysiol* 99: 704-717, 2008.
Roy D, Sigala R, Breakspear M, McIntosh AR, Jirsa VK, Deco G, and Ritter P. Using the virtual brain to reveal the role of oscillations and plasticity in shaping brain's dynamical landscape. *Brain Connect* 4: 791-811, 2014.
Sasaki K, Jinnai K, Gemba H, Hashimoto S, and Mizuno N. Projection of the cerebellar dentate nucleus onto the frontal association cortex in monkeys. *Exp Brain Res* 37: 193-198, 1979.
Sawaguchi T, and Goldman-Rakic PS. D1 dopamine receptors in prefrontal cortex: involvement in working memory. *Science* 251: 947-950, 1991.
Schmahmann JD. The role of the cerebellum in cognition and emotion: personal reflections since 1982 on the dysmetria of thought hypothesis, and its historical evolution from theory to therapy. *Neuropsychol Rev* 20: 236-260, 2010.
Schmahmann JD, and Sherman JC. The cerebellar cognitive affective syndrome. *Brain* 121 (Pt 4): 561-579, 1998.
Schmidt R, Leventhal DK, Mallet N, Chen F, and Berke JD. Canceling actions involves a race between basal ganglia pathways. *Nat Neurosci* 16: 1118-1124, 2013.
Schonewille M, Belmeguenai A, Koekkoek SK, Houtman SH, Boele HJ, van Beugen BJ, Gao Z, Badura A, Ohtsuki G, Amerika WE, Hosy E, Hoebeek FE, Elgersma Y, Hansel C, and De Zeeuw CI. Purkinje cell-specific knockout of the protein phosphatase PP2B impairs potentiation and cerebellar motor learning. *Neuron* 67: 618-628, 2010.
Schweighofer N, Doya K, and Kuroda S. Cerebellar aminergic neuromodulation: towards a functional understanding. *Brain Res Brain Res Rev* 44: 103-116, 2004.

Seamans JK, Gorelova N, Durstewitz D, and Yang CR. Bidirectional dopamine modulation of GABAergic inhibition in prefrontal cortical pyramidal neurons. *J Neurosci* 21: 3628-3638, 2001.
Seamans JK, and Yang CR. The principal features and mechanisms of dopamine modulation in the prefrontal cortex. *Prog Neurobiol* 74: 1-58, 2004.
Sesack SR, and Bunney BS. Pharmacological characterization of the receptor mediating electrophysiological responses to dopamine in the rat medial prefrontal cortex: a microiontophoretic study. *J Pharmacol Exp Ther* 248: 1323-1333, 1989.
Shin SL, Hoebeek FE, Schonewille M, De Zeeuw CI, Aertsen A, and De Schutter E. Regular patterns in cerebellar Purkinje cell simple spike trains. *PLoS One* 2: e485, 2007.
Smith MA, Ghazizadeh A, and Shadmehr R. Interacting adaptive processes with different timescales underlie short-term motor learning. *PLoS Biol* 4: e179, 2006.
Snider RS, and Maiti A. Cerebellar contributions to the Papez circuit. *J Neurosci Res* 2: 133-146, 1976.
Snider RS, Maiti A, and Snider SR. Cerebellar pathways to ventral midbrain and nigra. *Exp Neurol* 53: 714-728, 1976.
Solinas S, Forti L, Cesana E, Mapelli J, Schutter ED, and Angelo ED. Fast-reset of pacemaking and theta-frequency resonance patterns in cerebellar Golgi cells : Simulations of their impact in vivo. 1: 1-9, 2007.
Stanzione P, Calabresi P, Mercuri N, and Bernardi G. Dopamine modulates CA1 hippocampal neurons by elevating the threshold for spike generation: an in vitro study. *Neuroscience* 13: 1105-1116, 1984.
Strick PL, Dum RP, and Fiez JA. Cerebellum and nonmotor function. *Annu Rev Neurosci* 32: 413-434, 2009.
Sugihara I, Lang EJ, and Llinas R. Serotonin modulation of inferior olivary oscillations and synchronicity: a multiple-electrode study in the rat cerebellum. *Eur J Neurosci* 7: 521-534, 1995.
Sweeney JE, Lamour Y, and Bassant MH. Arousal-dependent properties of medial septal neurons in the unanesthetized rat. *Neuroscience* 48: 353-362, 1992.

Swenson RS, Kosinski RJ, and Castro AJ. Topography of spinal, dorsal column nuclear, and spinal trigeminal projections to the pontine gray in rats. *J Comp Neurol* 222: 301-311, 1984.
Takeda T, and Maekawa K. Transient direct connection of vestibular mossy fibers to the vestibulocerebellar Purkinje cells in early postnatal development of kittens. *Neuroscience* 32: 99-111, 1989.
Timmann D, Drepper J, Frings M, Maschke M, Richter S, Gerwig M, and Kolb FP. The human cerebellum contributes to motor, emotional and cognitive associative learning. A review. *Cortex* 46: 845-857, 2010.
Timofeev I. Neuronal plasticity and thalamocortical sleep and waking oscillations. *Prog Brain Res* 193: 121-144, 2011.
Trantham-Davidson H, Kröner S, and Seamans JK. Dopamine modulation of prefrontal cortex interneurons occurs independently of DARPP-32. *Cereb Cortex* 18: 951-958, 2008.
Tsai PT, Hull C, Chu Y, Greene-Colozzi E, Sadowski AR, Leech JM, Steinberg J, Crawley JN, Regehr WG, and Sahin M. Autistic-like behaviour and cerebellar dysfunction in Purkinje cell Tsc1 mutant mice. *Nature* 488: 647-651, 2012.
Uusisaari MY, and Knopfel T. Diversity of neuronal elements and circuitry in the cerebellar nuclei. *Cerebellum* 11: 420-421, 2012.
Uusisaari MY, and Knöpfel T. Diversity of neuronal elements and circuitry in the cerebellar nuclei. *Cerebellum* 11: 420-421, 2012.
Vargas DL, Nascimbene C, Krishnan C, Zimmerman AW, and Pardo CA. Neuroglial activation and neuroinflammation in the brain of patients with autism. *Ann Neurol* 57: 67-81, 2005.
Watson TC, Becker N, Apps R, and Jones MW. Back to front: cerebellar connections and interactions with the prefrontal cortex. *Front Syst Neurosci* 8: 4, 2014.
Watson TC, Jones MW, and Apps R. Electrophysiological mapping of novel prefrontal - cerebellar pathways. *Front Integr Neurosci* 3: 18, 2009.
Weijnen JA. Licking behavior in the rat: measurement and situational control of licking frequency. *Neurosci Biobehav Rev* 22: 751-760, 1998.
Whitney ER, Kemper TL, Bauman ML, Rosene DL, and Blatt GJ. Cerebellar Purkinje cells are reduced in a subpopulation of autistic brains: a stereological experiment using calbindin-D28k. *Cerebellum* 7: 406-416, 2008.

Wiesenfeld Z, Halpern BP, and Tapper DN. Licking behavior: evidence of hypoglossal oscillator. *Science* 196: 1122-1124, 1977.
Williams GV, and Goldman-Rakic PS. Modulation of memory fields by dopamine D1 receptors in prefrontal cortex. *Nature* 376: 572-575, 1995.
Witter L, Canto CB, Hoogland TM, de Gruijl JR, and De Zeeuw CI. Strength and timing of motor responses mediated by rebound firing in the cerebellar nuclei after Purkinje cell activation. *Front Neural Circuits* 7: 133, 2013.
Witter L, Rudolph S, Pressler RT, Lahlaf SI, and Regehr WG. Purkinje Cell Collaterals Enable Output Signals from the Cerebellar Cortex to Feed Back to Purkinje Cells and Interneurons. *Neuron* 91: 312-319, 2016.
Wulff P, Schonewille M, Renzi M, Viltono L, Sassoè-Pognetto M, Badura A, Gao Z, Hoebeek FE, van Dorp S, Wisden W, Farrant M, and De Zeeuw CI. Synaptic inhibition of Purkinje cells mediates consolidation of vestibulo-cerebellar motor learning. *Nat Neurosci* 12: 1042-1049, 2009.
Xu NL, Harnett MT, Williams SR, Huber D, O'Connor DH, Svoboda K, and Magee JC. Nonlinear dendritic integration of sensory and motor input during an active sensing task. *Nature* 492: 247-251, 2012.
Yamamoto T, Matsuo R, Fujiwara T, and Kawamura Y. EMG activities of masticatory muscles during licking in rats. *Physiol Behav* 29: 905-913, 1982.
Yue BW, and Huguenard JR. The role of H-current in regulating strength and frequency of thalamic network oscillations. *Thalamus Relat Syst* 1: 95-103, 2001.
Zahrt J, Taylor JR, Mathew RG, and Arnsten AF. Supranormal stimulation of D1 dopamine receptors in the rodent prefrontal cortex impairs spatial working memory performance. *J Neurosci* 17: 8528-8535, 1997.
Zeng H, Chattarji S, Barbarosie M, Rondi-Reig L, Philpot BD, Miyakawa T, Bear MF, and Tonegawa S. Forebrain-specific calcineurin knockout selectively impairs bidirectional synaptic plasticity and working/episodic-like memory. *Cell* 107: 617-629, 2001.
Zhang W, and Linden DJ. Long-term depression at the mossy fiber-deep cerebellar nucleus synapse. *J Neurosci* 26: 6935-6944, 2006.

Zhang W, Shin JH, and Linden DJ. Persistent changes in the intrinsic excitability of rat deep cerebellar nuclear neurones induced by EPSP or IPSP bursts. *J Physiol* 561: 703-719, 2004.
Zheng N, and Raman IM. Synaptic inhibition, excitation, and plasticity in neurons of the cerebellar nuclei. *Cerebellum* 9: 56-66, 2010.
Zhou H, Lin Z, Voges K, Ju C, Gao Z, Bosman LW, Ruigrok TJ, Hoebeek FE, De Zeeuw CI, and Schonewille M. Cerebellar modules operate at different frequencies. *Elife* 3: e02536, 2014.

Acknowledgements

I will go straight to the point, since the considerable amount of people I sincerely must thank. I thank Prof. D'Angelo for opportunities and credits he gave me in these years. I'm grateful and I tried to repay you working harder and harder until the end. Many thanks to Lisa Mapelli for having supervisioned my work and my thesis. I'm extremely grateful Lis. Special thanks to God, because he makes impossible possible, I couldn't go through these years without his support. Furthermore, nothing reported in this thesis would have been done without his benevolence. Thanks to Mohammed Meshkat, you are my best friend, my brother, a special gift that life gave me. Thanks to Laurens Bosman, you are an example for me, I aspire to become like you one day. Many thanks to Vincenzo Romano, despite our endless, funny fights, you are always there for me. Colleagues time! Oh dears, most of you didn't do anything for me : -) and now I have to invent something I shared with you. I am joking, I love you so much and I will miss you so badly. Marialuisa Tognolina, you haven't been just a colleague for me, you and our memories occupy a huge spot in my heart. Teresa Soda, sodissima, we shared many things and played so many stupid jokes... you biking in the lab with my bike will be the way I will picture you in our memories. Giuseppe Gagliano, the best beer-companion I have ever had, try to survive until the end of your PhD too!!! Francesca Prestori I will never forget your funny stories during our lab lunch together! Francesca Locatelli, I will bring with me your vocabulary, full of words ending in –ino, such as cuoricino, rosino... and I will try to introduce these words in the german language. Simona Tritto, well, if you are reading these acknowledgements I am sure you have already found "the hair inside the egg" and you are complaining about the way I wrote something. Ileana Montagna, I have nothing left to teach you, just remember, when you will not see the light at the end of the tunnel (and it will happen often) don't give up but try harder! Thanks to Martina Rizza, Stefano Masoli for the efficient technical support, Stefano Casali for so many things, including the contribution to this work and many thanks to Licia De Propris, my PhD journey started with you, we had a lot of fun upstairs for a while. To Gabriele Ferrari, thank you so much for the technical support, you adapted

the set-up to the most various experimental conditions and you have never looked bad at me despite my absurd requests.

To my reviewers, thank you for your time and advices.

Ai miei genitori ed a mio fratello, non posso ripagarvi per tutto quello che avete fatto per me nel corso degli anni, è troppo. Questa tesi e tutto quello che seguirà nella mia vita è per voi. Vi voglio tanto bene, grazie di tutto.

To me, I am so proud of me.